

Dissertation zur Erlangung des Doktorgrades
der Fakultät für Chemie und Pharmazie der
Ludwig-Maximilians-Universität München

Nitridoaluminate Phosphors for Solid-State Lighting

Peter Jorg Wagatha

aus

Hoffman Estates, Illinois, USA

2019

Erklärung

Diese Dissertation wurde im Sinne von §7 der Promotionsordnung vom 28.11.2011 von Herrn Prof. Dr. Wolfgang Schnick betreut.

Eidesstattliche Versicherung

Diese Dissertation wurde eigenständig und ohne unerlaubte Hilfe erarbeitet.

München, den 13.06.2019

(Peter Wagatha)

Dissertation eingereicht am 13.06.2019

1. Gutachter:	Prof. Dr. Wolfgang Schnick
2. Gutachter:	Prof. Dr. Konstantin Karaghiosoff
Mündliche Prüfung am	17.07.2019

Acknowledgements

Ich möchte mich besonders bei Herrn Prof. Dr. Wolfgang Schnick bedanken. Meine Promotion im "Arbeitskreis der unbegrenzten Möglichkeiten" durchzuführen und meine Dissertation anzufertigen, hat mir zahlreiche Freiheiten und Gestaltungsspielräume gegeben, die keineswegs als selbstverständlich zu erachten sind.

Großer Dank gebührt auch Peter Schmidt und Volker Weiler von Lumileds, ohne deren persönlichen Einsatz viele Projekte nicht umsetzbar gewesen wären. Dazu zählen natürlich alle Artikel aus meiner Feder, aber beispielsweise auch Beschaffung und Aufbau der HIP. Die bei Lumileds gewonnenen Eindrücke über die industrielle Forschung und das nächtliche Aachen sind von großem Wert.

Den Mitgliedern der Prüfungskommission meiner Promotion danke ich für ihre Einsatzbereitschaft und investierte Zeit.

Mein Dank gebührt außerdem einer Vielzahl weiterer Personen. Da ich selbst einige kurze Dankesworte im persönlichen Gespräch deutlich gegenüber der Nennung in einer Danksagung bevorzuge, werde ich an dieser Stelle nichts weiter zu Papier bringen.

Ich widme diese Dissertation meinen Großeltern!

"Nur wer erwachsen wird und ein Kind bleibt, ist ein Mensch"

Erich Kästner

Table of Contents

1. Introduction	1
References	8
2. Hot Isostatic Press (HIP)	11
3. $\text{Ca}_{18.75}\text{Li}_{10.5}[\text{Al}_{39}\text{N}_{55}]:\text{Eu}^{2+}$—Supertetrahedron Phosphor for Solid-State Lighting	15
Abstract	15
Introduction	16
Experimental Section	17
Synthesis	17
Single-Crystal X-ray Diffraction	17
Powder X-ray Diffraction	18
Electron Microscopy	18
EDX Spectroscopy	18
Electron Energy-Loss Spectroscopy (EELS)	18
Luminescence	19
Results and Discussion	19
Synthesis and Chemical Analysis	19
Crystal Structure	20
Powder X-ray Diffraction	23
Luminescence	24
EELS	29
Conclusion	30
Associated Content	31
Supporting Information	31
Author Information	31

Acknowledgements	31
References	31
4. Tunable Red Luminescence in Nitridomagnesoaluminates α-Sr₂[MgAl₅N₇]:Eu²⁺, β-Sr₂[MgAl₅N₇]:Eu²⁺ and Sr₈[LiMg₂Al₂₁N₂₈]:Eu²⁺	35
Abstract	35
Introduction	36
Experimental Section	37
Synthesis	37
Powder X-ray Diffraction	38
Electron Microscopy	38
EDX Spectroscopy	38
Luminescence	38
Results and Discussion	39
Synthesis and Chemical Analysis	39
Crystal Structure	40
β -Sr ₂ [MgAl ₅ N ₇]:Eu ²⁺	44
Luminescence	48
Conclusion	51
Associated Content	52
Supporting Information	52
Author Information	52
Acknowledgements	53
References	53
5. Narrow-Band Red Luminescence in Nitridolithoaluminate CaBa[Li₂Al₆N₈]:Eu²⁺	55
Abstract	55
Introduction	56

Experimental Section	57
Synthesis	57
Powder X-Ray Diffraction	58
Electron Microscopy	58
EDX Spectroscopy	58
Luminescence	58
Results and Discussion	59
Synthesis and Chemical Analysis	59
Crystal Structure	59
Luminescence	64
Conclusion	69
Associated Content	70
Supporting Information	70
Author Information	70
Acknowledgements	70
References	70
6. Conclusion and Outlook	73
Final Remarks	76
References	77
7. Summary	81
Ca _{18.75} Li _{10.5} [Al ₃₉ N ₅₅]:Eu ²⁺ —Supertetrahedron Phosphor for Solid-State Lighting	81
Tunable Red Luminescence in Nitridomagnesoaluminates α-Sr ₂ [MgAl ₅ N ₇]:Eu ²⁺ , β-Sr ₂ [MgAl ₅ N ₇]:Eu ²⁺ , and Sr ₈ [LiMg ₂ Al ₂₁ N ₂₈]:Eu ²⁺	82
Narrow-Band Red Luminescence in Nitridolithoaluminate CaBa[Li ₂ Al ₆ N ₈]:Eu ²⁺	83

Table of Contents

8. Appendix	85
Supporting Information for $\text{Ca}_{18.75}\text{Li}_{10.5}[\text{Al}_{39}\text{N}_{55}]:\text{Eu}^{2+}$ —Supertetrahedron Phosphor for Solid-State Lighting	85
9. Publications	89
List of Publications within this Thesis	89
Other Publications	90
Conference Contributions	91
Deposited Crystallographic Data	91

1. Introduction

Experimental materials chemistry at the junction of fundamental and applied research offers varied opportunities for scientists to advancing mankind's knowledge base and technology. A specific challenge for today's global society is our seemingly insatiable hunger for energy, that is mainly dependent on fossil fuels like mineral oil, black coal and lignite or nuclear power generation. The adverse effects of unrestrained fossil fuel combustion on local and global environments subsumed under the term "climate change", and several catastrophic releases of large amounts of high-level radioactive materials from nuclear power or reprocessing plants since the beginning of the atomic age, clearly show the necessity for curtailing humanity's energy consumption.

Estimations by the United States Department of Energy (DOE) ascribe up to 15% of electrical power usage to lighting.¹ In this context, lighting plays a decisive role in the effort of reducing energy usage. The classical incandescent light bulb, formerly widely used in western countries, converts only about 5% of its power input into visible light. The remainder of energy is emitted as infrared radiation useless for illumination. Because of this pronounced low luminous efficacy—i.e. the normalized ratio of input power to extracted luminous flux—incandescent light bulbs were subject to a stepwise ban from manufacture and sale in important markets like the European Union (EU) initially in the year 2009. While halogen lamps allow higher filament temperatures, thus increasing the luminous efficacy enough to avoid the initial ban, the year 2018 will finally mark the end to inefficient incandescent lighting at least in the EU. Possible alternatives to incandescent lighting are fluorescent lamps, either tubular or compact.

Compared to light bulbs, affordable commercial fluorescent lamps boast greatly increased luminous efficacies at the cost of limited color rendition due to the high-energy UV radiation generated by the mercury-vapor gas discharge being converted to visible light by line emitting phosphors, leaving large gaps in the output spectrum. Another major drawback of fluorescent lamps is their content of toxic mercury, that poses health and environmental hazards if the lamp body is structurally compromised or disposed of inappropriately.

1. Introduction

The second alternative to incandescent lighting is solid-state lighting with LEDs.² Solid-state light generation was first observed by Henry Joseph Round in 1907 when passing an electrical current through a silicon carbide crystal.³ This effect was later rediscovered and described in more detail by Russian scientist and inventor Oleg Lossev,⁴ and led to the invention of the first visible-light emitting diode in 1962 by Nick Holonyak.⁵

In principle, an LED is a semiconductor device exploiting the phenomenon of electroluminescence when applying an electrical current to a junction of p- and n-type doped semiconductor materials. Electrons injected into the conduction band of the n-type material by doping with an electron surplus element radiatively recombine at the p-n junction with the holes created in the valence band of the p-type material by doping with an electron deficient element. The separation between conduction- and valence band—i.e. the band gap—determines the energy of the emitted electromagnetic radiation. A schematic diagram of the working principle of a LED is given in Figure 1.1.

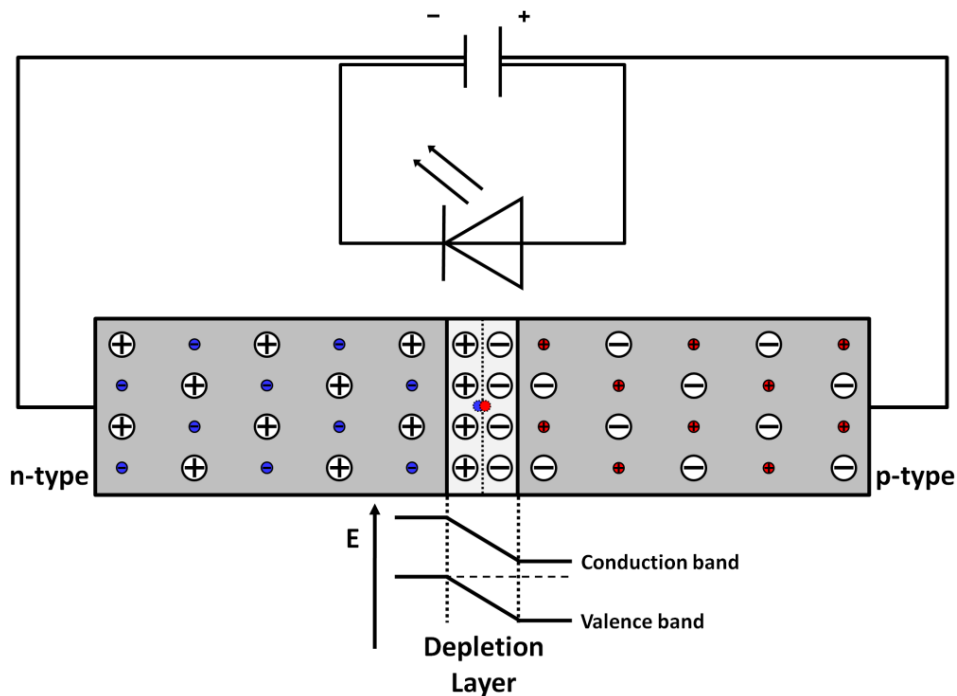


Figure 1.1: Working principle of an LED and schematic of the p-n junction of positively (p) and negatively (n) doped semiconductor materials.

At the time of their invention, LEDs suffered from small light outputs and generally low efficiencies, and as a consequence were never taken into serious consideration for general lighting purposes. Here the target is the generation of white light. Since LEDs are nearly

monochromatic light sources with emission wavelengths corresponding to the semiconductor material's band gap, white light can only be generated by additive color mixing of the primary colors red, green and blue. Two strategies are here possible: Firstly, the combination of three discrete LEDs of appropriate respective color, or secondly the combination of a high-energy LED with suitable light conversion materials, called phosphors. Compared to UV LEDs, blue LEDs offer an inherently higher efficiency for the latter kind of application, due to the smaller Stokes shifts of the necessary phosphors.

While the first violet emitting GaN based LED was developed in 1972 by Herbert Maruska after pioneering vapor deposition of single-crystalline GaN films on sapphire substrate,⁶ it exhibited only very limited light output.⁷⁻⁸ High-brightness (In)GaN blue LEDs, for the development of which the 2014 Nobel Prize in Physics was awarded, emerged in the early 1990s based on work by Isamu Akasaki and Hiroshi Amano,⁹⁻¹¹ and were brought to industrial application by Shuji Nakamura.¹²⁻¹⁶

The base of all blue LEDs are films of InGaN n- and p-type doped with Si and Mg, respectively, and epitaxially grown on either a sapphire or silicon substrate. In a classical device architecture, the substrate remains part of the LED submount and the individual layers are contacted from the top. Since emission is blocked by the contact areas, the thin-film flip-chip architecture displayed in Figure 1.2 was developed. Here, the substrate is removed by etching after deposition of the semiconductor films and the stack of layers is flipped. Contacting of the respective layers in this case is possible from the bottom of the chip, resulting in a larger emission area per chip. Heat generated inside the semiconductor by ohmic resistance and nonradiative recombination of electrons and holes at the p-n junction is conducted to the submount through the electrical contacts and further dissipated from there. On top of the chip, i.e. in place of the substrate for flip-chip architectures, the downconversion materials are placed.

As already mentioned, white light can be generated by additive color mixing as pictured in Figure 1.3. Technically, suitable phosphors partially absorb the blue light and reemit light of lower—and phosphor specific—energy. The blue light of the base LED in conjunction with the emission of the phosphor(s) create the impression of white light. If no higher demands are made on the quality of the output radiation other than its color, white light is most simply produced by combining a blue LED with a single yellow phosphor. Most commonly used in this application is UV–blue excitable, broadband yellow emitting $\text{Y}_3\text{Al}_5\text{O}_{12}:\text{Ce}^{3+}$

1. Introduction

(YAG:Ce).¹⁷ Due to the low emission intensity in the orange–red spectral region, YAG:Ce converted white LEDs (WLEDs) exhibit only low color rendering indices (CRI < 70) and high correlated color temperatures (CCT \approx 4000–8000 K). In contrast to the overall poor illumination quality, luminous efficacies of YAG:Ce converted LEDs are excellent, making it the combination of choice if only brightness and energy efficiency are of importance. For obtaining high quality illumination grade white light, multi-phosphor solutions have proven their superiority. In the latter the base LED is coated with multiple phosphors, but at least with a green and a red one.

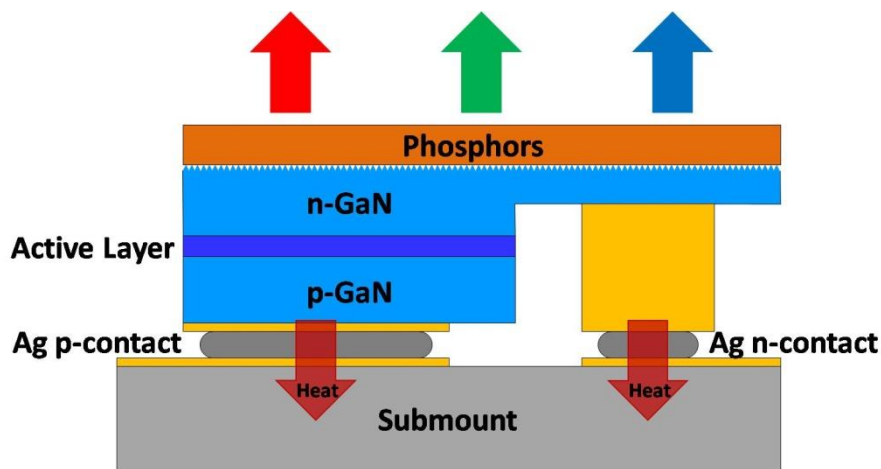


Figure 1.2: Layout of a thin-film flip-chip LED packaged with a ceramic phosphor layer.

Several specific and general requirements for the phosphors to be taken into consideration for industrial application can be identified: The proper emission maximum and full width at half maximum (fwhm), high internal quantum efficiency and emission intensity at operating conditions, chemical and thermal stability. These requirements themselves are dependent on more fundamental properties of the materials, like their crystal structures and chemical compositions, that will be examined later in this work. Industrially, only Ce^{3+} and, even more importantly, Eu^{2+} doped nitride phosphors are of practical relevance in the field of band-emitting luminescent materials.

Due to the great importance of the red-emitting material for the performance of a WLED in terms of color rendition and energy efficiency, great effort has been put into discovering novel red phosphors for application in solid-state lighting. The strong effect of the red emitter on the WLED performance can be easily understood: In sunlight the red spectral region has a high intensity due to the sun being an almost ideal black-body radiation source with a correlated color temperature of \approx 6000 K. Colors with a red component are therefore

only perceived as natural if the illuminating spectrum exhibits a high chromatic saturation in the red spectral region. Generally, colors can only be perceived if they are present in the illuminating spectrum. Adversely, employing a deep-red emitting phosphor in a WLED would strongly decrease its luminous efficacy. Here, the challenge is the combination of these mutually exclusive properties of sufficiently deep-red emission and consequently good color rendition, and high luminous efficacy.

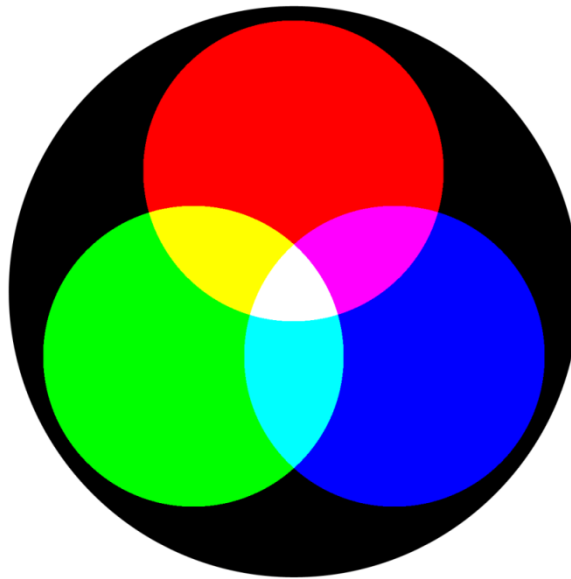


Figure 1.3: Additive color mixing of the three base colors red, green and blue.

The compound class of nitridometallates has proven its potential in producing promising phosphors for application in solid-state lighting (SSL). These materials are structurally derived from silicate chemistry with the anions being N^{3-} instead of O^{2-} . Their crystal structures consist of anionic tetrahedron networks and additional cations for compensation of the network charge. Prominent subclasses of nitridometallates are nitridosilicates, formally the subclass most closely related to oxosilicates. Luminescence in nitridosilicates upon doping with the rare-earth metal Eu was first observed and described for compounds of formula type $M_2Si_5N_8:Eu^{2+}$ ($M = Ca, Sr, Ba, Eu$).¹⁸⁻²²

Solid solutions $Ba_xSr_{2-x}Si_5N_8:Eu^{2+}$, often abbreviated BSSNE, show a distinct amber emission color ideal for indicator- and traffic lights and are therefore widely used in LEDs for the automotive sector. Possibly the most widely used nitridosilicate phosphor is the red emitting $Sr_xCa_{1-x}AlSiN_3:Eu^{2+}$ (SCASN).²³⁻²⁴ Although its emission characteristics are far from optimal—due to the relatively broad emission of the Eu^{2+} emission a significant portion of the red light

1. Introduction

emitted in the non-visible infrared region of the electromagnetic spectrum—it long remained unrivalled. In analogy to naturally occurring silicates, that frequently exhibit mixed occupancy of the network cation position with Si^{4+} and Al^{3+} , SCASN also shows mixed occupancy of Si and Al.

State-of-the-art nitride phosphors often contain no Si at all, but a variety of other network cations like the already mentioned Al^{3+} , Mg^{2+} , Li^+ , Ga^{3+} and Ge^{4+} , or even Be^{2+} . Of special interest for this work is the nitridoaluminate class of materials. While prior to our group taking interest in silicon-free nitridoaluminates only five compounds of this material class had been known,^{25–27} that number could greatly be increased and our research has brought forth several groups of highly-promising host materials. The group with the most representatives to date crystallizes isotypically with the UCr_4C_4 crystal structure or derivatives thereof.²⁸ The obtained materials $M[\text{Mg}_2\text{Al}_2\text{N}_4]:\text{Eu}^{2+}$ ($M = \text{Ca}, \text{Sr}, \text{Ba}, \text{Eu}$; "MMA"),²⁹ $\text{Ca}[\text{LiAl}_3\text{N}_4]:\text{Eu}^{2+}$ ("CLA")³⁰ and $\text{Sr}[\text{LiAl}_3\text{N}_4]:\text{Eu}^{2+}$ ("SLA")³¹ are structurally closely related with a high degree of condensation $\kappa = 1$. The main difference between these compounds is that in MMA the network cations Mg^{2+} and Al^{3+} are statistically distributed over the network cation sites resulting in $(\text{Al},\text{Mg})\text{N}_4$ tetrahedra, while in CLA and SLA the network cations Li^+ and Al^{3+} show ordering with distinguished LiN_4^- and AlN_4 tetrahedra, as displayed in Figure 1.4.

The alkaline-earth counterions are coordinated cube-like by eight N atoms, with uniformly long bond lengths. In conjunction, these structural motifs are correlated with the excellent optical properties of especially SLA. High rigidity of the tetrahedral network and cube-like coordination of the activator site contribute to a small Stokes shift, and consequently a small fwhm, due to suppressing relaxation of the activator in its excited state and structural relaxation in general.

In contrast to statistical disorder, where the varying crystal fields and activator–ligand bond lengths cause strong inhomogeneous line broadening, it is minimized by the ordering of network cations present in SLA. With an emission maximum of $\lambda = 650 \text{ nm}$, an fwhm of $\approx 1180 \text{ cm}^{-1}$ ($\approx 50 \text{ nm}$) and a $\text{QE}_{\text{rel}}(473 \text{ K}) > 95\%$, prototype LEDs employing SLA as red emitting material exhibit excellent color rendition ($Ra_8 = 91$) and luminous efficacies increased by 14% compared to commercially available products.³¹ The luminous efficacy of high-CRI white LEDs could be further increased, if a red-luminescent material with slightly blue-shifted emission at $\lambda_{\text{em}} \approx 630 \text{ nm}$ and $\text{fwhm} \approx 1100\text{--}1200 \text{ cm}^{-1}$ compared to SLA was

available. Recently, nitridooxidoaluminates $\text{Sr}[\text{Li}_2\text{Al}_2\text{O}_2\text{N}_2]:\text{Eu}^{2+}$ with very favorable emission characteristics, was reported on.³² The compound crystallizes in an ordered variant of the already mentioned UCr_4C_4 structure type and emits red light at $\lambda_{\text{em}} = 614 \text{ nm}$ and $\text{fwhm} = 1286 \text{ cm}^{-1}$. Here, the emission peak position on the one hand further reduces IR-spillover compared to SLA, but on the other hand also reduces deep-red chromatic saturation necessary for obtaining excellent color rendition.

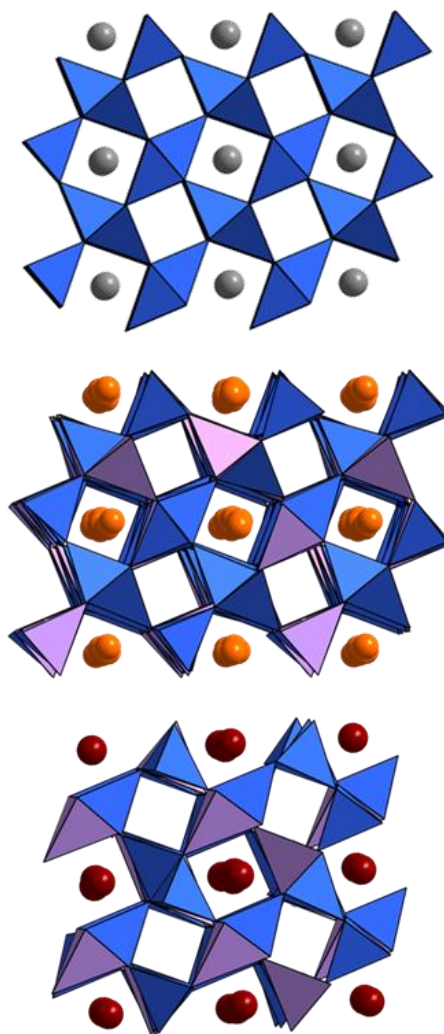


Figure 1.4: Comparison of the crystal structures of $M[\text{Mg}_2\text{Al}_2\text{N}_4]$ ($M = \text{Ca}, \text{Sr}, \text{Ba}, \text{Eu}$) (top), $\text{Ca}[\text{LiAl}_3\text{N}_4]$ (middle) and $\text{Sr}[\text{LiAl}_3\text{N}_4]$ (bottom). In $M[\text{Mg}_2\text{Al}_2\text{N}_4]$ ($M = \text{Ca}, \text{Sr}, \text{Ba}, \text{Eu}$) the tetrahedron centers are statistically occupied by either Mg or Al.

A major challenge when synthesizing novel nitridoaluminates is the thermal stability of the reactant AlN. The high temperatures needed for activating AlN and making a reaction possible often cause significant evaporation or dissociation of other starting materials in the reaction mixture. This is especially the case for magnesium and its relevant compounds, but

1. Introduction

also for example strontium and lithium. During syntheses in the radio-frequency (rf) furnaces at ambient pressures, a fogging of the glass reactor's inner wall with evaporated reactants or intermediates could regularly be observed. Due to the limited mechanical stability of the glass apparatus around the rf furnaces the reactive gas pressure cannot exceed ambient pressures, even though increased gas pressure would help converging the dissociation temperatures of the different metal nitrides used in the reactant mixture and effectively reduce evaporation.

Although combined high-pressure/high-temperature synthesis methods were previously available in our group in the form of ultra-high pressure hydraulically operated multi-anvil presses, synthesis of large-quantity phase-pure samples is close to impossible. The just described starting position prompted intense research efforts for discovering other novel nitridoaluminates. Hot isostatic pressing (hot isostatic press, HIP) of the respective reactants for synthesizing nitridoaluminates has proven its superiority over simple heating in any kind of pressureless furnace. Since the initial startup of the HIP in our group in March 2017, and earlier at Lumileds Phosphor Center Aachen (LPCA), several novel highly promising nitridoaluminate phosphors have been discovered, some of which are part of this work and will be discussed in detail later on.

These materials are united by their method of synthesis using the heterogeneous high-temperature/high-pressure reaction of the metal hydrides and -nitrides (-oxides and -halides for the activator Eu) with N₂ possible in a HIP. Furthermore, other compound classes have been found to be accessible via this approach, e.g. nitridophosphates and nitridoberyllates/-silicates. As the just mentioned compound classes are part of different research projects, the obtained results will not be discussed in this thesis. In the following, the synthesis, crystal structure and physical properties of the nitrido(litho/magneso)aluminates CaBa[Li₂Al₆N₈]:Eu²⁺ (CBLA),³³ α-Sr₈[Li_{2-0.5x}Mg_xAl_{22-0.5x}N₂₈]:Eu²⁺ (x = (0), 2, 4) and β-Sr₂[MgAl₅N₇]:Eu²⁺,³⁴ Ca_{20-x}Li_{8+2x}[Al₃₉N₅₅]:Eu²⁺ (x = 0–2)³⁵ are presented in detail.

References

- (1) *Energy Savings Forecast of Solid-State Lighting in General Illumination Applications*. Building Technologies Office, Energy Efficiency and Renewable Energy, U.S. Department of Energy: Washington, D.C., 2016.

- (2) Pimputkar, S.; Speck, J. S.; Den Baars, S. P.; Nakamura, S., Prospects for LED lighting. *Nat. Photonics* **2009**, *3*, 180–182.
- (3) Round, H. J., A note on carborundum. *Electrical World* **1907**, *49*, 309.
- (4) Lossev, O. V., CII. Luminous carborundum detector and detection effect and oscillations with crystals. *Philos. Mag.* **1928**, *6*, 1024–1044.
- (5) Holonyak, N., Jr.; Bevacqua, S. F., Coherent (visible) Light Emission from Ga(As_{1-x}P_x) Junctions. *Appl. Phys. Lett.* **1962**, *1*, 82–83.
- (6) Maruska, H. P.; Tietjen, J. J., Preparation and properties of vapor-deposited single-crystalline gallium nitride. *Appl. Phys. Lett.* **1969**, *15*, 327–329.
- (7) Maruska, H. P.; Rhines, W. C.; Stevenson, D. A., Preparation of magnesium-doped gallium nitride diodes exhibiting violet electroluminescence. *Mater. Res. Bull.* **1972**, *7*, 777–781.
- (8) Maruska, H. P.; Stevenson, D. A.; Pankove, J. I., Violet luminescence of magnesium-doped gallium nitride. *Appl. Phys. Lett.* **1973**, *22*, 303–305.
- (9) Amano, H.; Sawaki, N.; Akasaki, I.; Toyoda, Y., Metalorganic vapor phase epitaxial growth of a high quality gallium nitride (GaN) film using an aluminum nitride (AlN) buffer layer. *Appl. Phys. Lett.* **1986**, *48*, 353–355.
- (10) Amano, H.; Kito, M.; Hiramatsu, K.; Akasaki, I., P-type conduction in magnesium-doped gallium nitride treated with low-energy electron beam irradiation (LEEBI). *Jpn. J. Appl. Phys.* **1989**, *28*, L2112–L2114.
- (11) Amano, H.; Kito, M.; Hiramatsu, K.; Akasaki, I., UV and blue electroluminescence from aluminum/magnesium-doped gallium nitride/gallium nitride (Al/GaN:Mg/GaN) LED treated with low-energy electron beam irradiation (LEEBI). *Inst. Phys. Conf. Ser.* **1990**, *106*, 725–730.
- (12) Nakamura, S.; Mukai, T.; Senoh, M., High-power gallium nitride P-N junction blue-light-emitting diodes. *Jpn. J. Appl. Phys.* **1991**, *30*, L1998–L2001.
- (13) Nakamura, S.; Senoh, M.; Mukai, T., Highly p-type magnesium doped gallium nitride films grown with GaN buffer layers. *Jpn. J. Appl. Phys.* **1991**, *30*, 1708–1711.
- (14) Nakamura, S.; Mukai, T., High-quality indium gallium nitride films grown on gallium nitride films. *Jpn. J. Appl. Phys.* **1992**, *31*, L1457–L1459.
- (15) Nakamura, S.; Mukai, T.; Senoh, M., Silicon-doped indium gallium nitride films grown on gallium nitride films. *Jpn. J. Appl. Phys.* **1993**, *32*, L16–L19.
- (16) Nakamura, S.; Senoh, M.; Mukai, T., High-power indium gallium nitride/gallium nitride double-heterostructure violet light emitting diodes. *Appl. Phys. Lett.* **1993**, *62*, 2390–2392.
- (17) Blasse, G.; Bril, A., New phosphor for flying-spot cathode-ray tubes for color television. Yellow-emitting cerium-doped yttrium aluminum garnet. *Appl. Phys. Lett.* **1967**, *11*, 53–55.
- (18) Schlieper, T.; Milius, W.; Schnick, W., Nitrido-silicates. II. High-temperature syntheses and crystal structures of Sr₂Si₅N₈ and Ba₂Si₅N₈. *Z. Anorg. Allg. Chem.* **1995**, *621*, 1380–1384.
- (19) Schlieper, T.; Schnick, W., Nitrido silicates. I. High temperature synthesis and crystal structure of Ca₂Si₅N₈. *Z. Anorg. Allg. Chem.* **1995**, *621*, 1037–1041.

1. Introduction

- (20) Huppertz, H.; Schnick, W., $\text{Eu}_2\text{Si}_5\text{N}_8$ and $\text{EuYbSi}_4\text{N}_7$. The first nitridosilicates with a divalent rare earth metal. *Acta Crystallogr. Sect. C* **1997**, *53*, 1751–1753.
- (21) Höpfe, H. A.; Lutz, H.; Morys, P.; Schnick, W.; Seilmeier, A., Luminescence in Eu^{2+} -doped $\text{Ba}_2\text{Si}_5\text{N}_8$: fluorescence, thermoluminescence, and upconversion. *J. Phys. Chem. Solids* **2000**, *61*, 2001–2006.
- (22) Huppertz, H. *Doctoral Thesis*, University of Bayreuth, 1997.
- (23) Uheda, K.; Hirosaki, N.; Yamamoto, H., Host lattice materials in the system $\text{Ca}_3\text{N}_2\text{-AlN-Si}_3\text{N}_4$ for white light emitting diode. *Phys. Status Solidi A* **2006**, *203*, 2712–2717.
- (24) Uheda, K.; Hirosaki, N.; Yamamoto, Y.; Naito, A.; Nakajima, T.; Yamamoto, H., Luminescence properties of a red phosphor, $\text{CaAlSiN}_3\text{:Eu}^{2+}$, for white light-emitting diodes. *Electrochem. Solid-State Lett.* **2006**, *9*, H22–H25.
- (25) Blase, W.; Cordier, G.; Ludwig, M.; Kniep, R., $\text{Sr}_3[\text{Al}_2\text{N}_4]$: A Nitrodoaluminate with Corrugated Tetrahedral Chains $\infty^1[\text{AlN}_{4/2}^{3-}]$. *Z. Naturforsch., B: Chem. Sci.* **1994**, *49*, 501–505.
- (26) Ludwig, M.; Niewa, R.; Kniep, R., Dimers $[\text{Al}_2\text{N}_6]^{12-}$ and chains $\infty^1[\text{AlN}_{4/2}^{3-}]$ in the crystal structures of $\text{Ca}_6[\text{Al}_2\text{N}_6]$ and $\text{Ba}_3[\text{Al}_2\text{N}_4]$. *Z. Naturforsch., B: Chem. Sci.* **1999**, *54*, 461–465.
- (27) Ludwig, M.; Jäger, J.; Niewa, R.; Kniep, R., Crystal Structures of Two Polymorphs of $\text{Ca}_3[\text{Al}_2\text{N}_4]$. *Inorg. Chem.* **2000**, *39*, 5909–5911.
- (28) Behrens, R. K.; Jeitschko, W., Uranium chromium carbide (UCr_4C_4) with filled molybdenum-nickel (MoNi_4) type structure. *Monatsh. Chem.* **1987**, *118*, 43–50.
- (29) Pust, P.; Hintze, F.; Hecht, C.; Weiler, V.; Locher, A.; Zitnanska, D.; Harm, S.; Wiechert, D.; Schmidt, P. J.; Schnick, W., Group (III) Nitrides $M[\text{Mg}_2\text{Al}_2\text{N}_4]$ ($M = \text{Ca}, \text{Sr}, \text{Ba}, \text{Eu}$) and $\text{Ba}[\text{Mg}_2\text{Ga}_2\text{N}_4]$ -Structural Relation and Nontypical Luminescence Properties of Eu^{2+} Doped Samples. *Chem. Mater.* **2014**, *26*, 6113–6119.
- (30) Pust, P.; Wochnik, A. S.; Baumann, E.; Schmidt, P. J.; Wiechert, D.; Scheu, C.; Schnick, W., $\text{Ca}[\text{LiAl}_3\text{N}_4]\text{:Eu}^{2+}$ -A Narrow-Band Red-Emitting Nitridolithoaluminate. *Chem. Mater.* **2014**, *26*, 3544–3549.
- (31) Pust, P.; Weiler, V.; Hecht, C.; Tücks, A.; Wochnik, A. S.; Henss, A.-K.; Wiechert, D.; Scheu, C.; Schmidt, P. J.; Schnick, W., Narrow-band red-emitting $\text{Sr}[\text{LiAl}_3\text{N}_4]\text{:Eu}^{2+}$ as a next-generation LED-phosphor material. *Nat. Mater.* **2014**, *13*, 891–896.
- (32) Hoerder, G. J.; Huppertz, H.; Seibald, M.; Baumann, D.; Schröder, T.; Peschke, S.; Schmid, P. C.; Tyborski, T.; Pust, P.; Stoll, I.; Bergler, M.; Patzig, C.; Reissaus, S.; Krause, M.; Berthold, L.; Hoche, T.; Johrendt, D., $\text{Sr}[\text{Li}_2\text{Al}_2\text{O}_2\text{N}_2]\text{:Eu}^{2+}$ -A high performance red phosphor to brighten the future. *Nat. Comm.* **2019**, *10*, 1824–1833.
- (33) Wagatha, P.; Weiler, V.; Schmidt, P. J.; Schnick, W., Tailoring Emission Characteristics: Narrow-Band Red Luminescence from SLA to $\text{CaBa}[\text{Li}_2\text{Al}_6\text{N}_8]\text{:Eu}^{2+}$. *Chem. Mater.* **2018**, *30*, 7885–7891.
- (34) Wagatha, P.; Weiler, V.; Schmidt, P. J.; Schnick, W., Tunable Red Luminescence in Nitridomagnesoaluminates $\alpha\text{-Sr}_2[\text{MgAl}_5\text{N}_7]\text{:Eu}^{2+}$, $\beta\text{-Sr}_2[\text{MgAl}_5\text{N}_7]\text{:Eu}^{2+}$, and $\text{Sr}_8[\text{LiMg}_2\text{Al}_{21}\text{N}_{28}]\text{:Eu}^{2+}$. *Chem. Mater.* **2018**, *30*, 1755–1761.
- (35) Wagatha, P.; Pust, P.; Weiler, V.; Wochnik, A. S.; Schmidt, P. J.; Scheu, C.; Schnick, W., $\text{Ca}_{18.75}\text{Li}_{10.5}[\text{Al}_{39}\text{N}_{55}]\text{:Eu}^{2+}$ -Supertetrahedron Phosphor for Solid-State Lighting. *Chem. Mater.* **2016**, *28*, 1220–1226.

2. Hot Isostatic Press (HIP)

Aside from the main theme of nitridoaluminates, the aforementioned compounds are united by their method of synthesis. All here presented materials were obtained by a heterogeneous high-temperature/high-pressure reaction of the metal hydrides and -nitrides (-oxides and -halides for the activator Eu) with N₂ in a hot isostatic press (HIP). Traditionally, the process of hot isostatic pressing is associated with ceramics production and powder metallurgy, where it is used for compacting pre-sintered closed-porous parts to final specifications. Open porous work pieces can only be compacted by this method, when the whole part is packaged in a gas proof but flexible container. Otherwise, the internal pressure of the pores adjusts to the external pressure, preventing compression of the pore.

Depending on the type of furnace used and the dimensions of the pressure vessel, maximum temperatures of ≈ 2000 °C and pressures up to ≈ 670 MPa are within the operating envelope. As hot isostatic pressing is generally associated with increased technical complexity and is therefore costly, the method is mainly used for the treatment of small batch series and the production of ceramic parts with increased demand for dimensional accuracy.

In our case, the HIP was used mainly for expanding the operating parameters of our high-temperature syntheses. Several HIP systems were initially considered for acquisition: An EPSI Type HIP 200-77×150 G HIP with graphite furnace ($T_{\max} = 2000$ °C, $\varnothing = 77$ mm, $h = 150$ mm) and a pressure vessel with yoke ($p_{\max} = 200$ MPa, Ar/N₂) and an AIP6-30H HIP with carbon fiber reinforced carbon furnace ($T_{\max} = 2000$ °C, $\varnothing = 70$ mm, $h = 125$ mm) and a threaded pressure vessel ($p_{\max} = 207$ MPa, Ar/N₂/vacuum). Systems from both manufacturers are used at our co-operation partner Lumileds Phosphor Development Center Aachen (LPCA) research and production facilities. Based on the experience gained at LPCA, the AIP system was chosen for purchase since it combined lower cost of acquisition and operation with simple serviceability. Additionally, an identical system is used at LPCA for research purposes, making results easily transferable.

The setup of the machine is pictured in Figure 2.1. Preparations for installing the HIP included finding a location suitable for accommodating a larger machine and its structural

2. Hot Isostatic Press (HIP)

analysis due to the machines considerable weight. Supply of the machine with the necessary media compressed air ($Q \geq 56.6$ L/min, $p_{\max} = 0.7$ MPa), N_2 ($p_{\min} = 5.5$ MPa, $p_{\max} = 19.2$ MPa), Ar ($p_{\min} = 5.5$ MPa/1 MPa, $p_{\max} = 19.2$ MPa) coolant water ($Q \geq 37.8$ L/min, $T_{\min} = \text{ambient}$) and electricity (3 phase, $I_{\max} = 60$ A, U 380/415/480 V) had to be ensured and partially required additional equipment.



Figure 2.1: Fully installed and operational AIP6-30H HIP (center, blue) with pressure booster (top left) and supply lines. The pressure vessel with the crane for lifting the threaded lid and its coolant lines comprise the left side of the machine. The control cabinet on the right houses the control electronics, electrical installation, valves and pumps as well as the main compressor.

A secondary cooling unit ensuring the proper coolant flow and temperature was acquired, because the primary coolant temperature was too low and could have caused condensation within the machine. High-pressure N_2 was supplied with a compressed-air driven two-stage pressure booster (Maximator DLE-5-30-2, $p_{\max} = 60$ MPa) set to an output pressure of 12 MPa and equipped with a relief valve with 18 MPa triggering pressure. The pressure booster volume output was originally specified to exceed the HIP's main compressors intake volume of ≈ 40 L_N/min, making a pressure reservoir that would require periodical inspection obsolete. Presumably due to flow loss, the pressure booster's output volume falls behind expectations, which has to be considered when planning a cycle recipe by allowing extended time of ≈ 30 min/10 MPa for pressure buildup.

The operating envelope of the pressure booster is presented in Figure 2.2. In addition to installing supply lines for the respective media, safety measures for a secure operation of the HIP were implemented. A compartment-air surveillance system constantly measuring the O_2 partial pressure and triggering optical and acoustic alarms when detecting critically low O_2 concentrations was installed following code requirements.

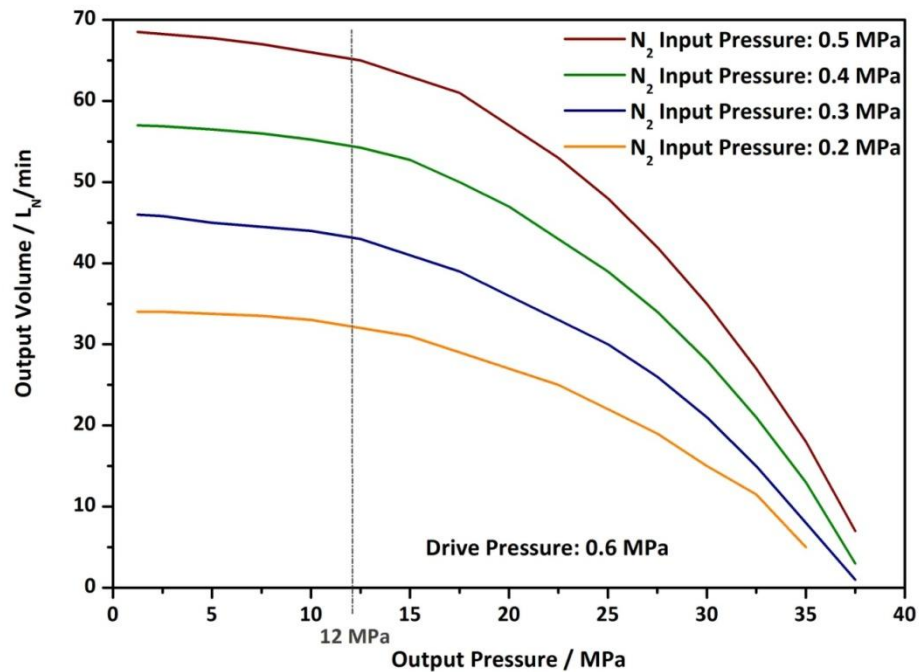


Figure 2.2: Operating envelope of the Maximator DLE-5-30-2 pressure booster at a drive pressure of 0.6 MPa and different N_2 input pressures. The output pressure was set to ≈ 12 MPa for our application.

Secondary to the built in rupture disc preventing overpressurization of the pressure vessel and located in the control cabinet, a pressure relief flap was mounted inside one window frame for preventing overpressurization of the entire room in case of a catastrophic failure of the pressure vessel. Theoretically, at 207 MPa the pressure vessel can hold the equivalent of ≈ 20 m³ unpressurized gas, about the same volume as the room the HIP is located in. Ventilation in the room was increased to 8-fold air exchange per hour, reducing the risk of asphyxiating gas accumulations. Furthermore, the air exhaust port was moved to floor level to prevent hazardous accumulations of higher density gases.

3. $\text{Ca}_{18.75}\text{Li}_{10.5}[\text{Al}_{39}\text{N}_{55}]:\text{Eu}^{2+}$ —Supertetrahedron

Phosphor for Solid-State Lighting

published in: *Chem. Mater.* **2016**, *28*, 1220–1226

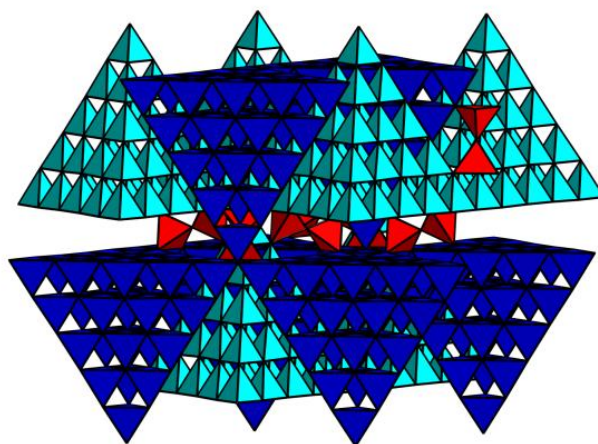
authors: Peter Wagatha, Philipp Pust, Volker Weiler, Angela S. Wochnik,
Peter J. Schmidt, Christina Scheu and Wolfgang Schnick

DOI: 10.1021/acs.chemmater.5b04929

Reprinted with permission from American Chemical Society, Copyright © 2016

Abstract

Highly efficient red-emitting luminescent materials deliver the foundation for next-generation illumination-grade white light-emitting diodes (LEDs). Recent studies demonstrate that the hardly explored class of nitridoaluminates comprises



intriguing phosphor materials, e.g., $\text{Sr}[\text{LiAl}_3\text{N}_4]:\text{Eu}^{2+}$ or $\text{Ca}[\text{LiAl}_3\text{N}_4]:\text{Eu}^{2+}$. Here, we describe the novel material $\text{Ca}_{18.75}\text{Li}_{10.5}[\text{Al}_{39}\text{N}_{55}]:\text{Eu}^{2+}$ with highly efficient narrow-band red emission ($\lambda_{\text{em}} \approx 647 \text{ nm}$, full width at half-maximum, $\text{fwhm} \approx 1280 \text{ cm}^{-1}$). This compound features a rather uncommon crystal structure, comprising sphalerite-like T_5 supertetrahedra that are composed of tetrahedral AlN_4 units that are interconnected by additional AlN_4 moieties. The network charge is compensated by Ca^{2+} and Li^+ ions located between the supertetrahedra. The crystal structure was solved and refined from single-crystal and powder X-ray diffraction data in the cubic space group $\text{Fd} \bar{3}m$ (No. 227) with $a = 22.415(3) \text{ \AA}$ and $Z = 8$. To verify the presence of Li, transmission electron microscopy (TEM) investigations including electron energy-loss spectroscopy (EELS) were performed. Based on the intriguing luminescence properties, we proclaim high potential for application in highpower phosphor-converted white LEDs.

Introduction

With respect to the varied and manifold structural chemistry of sialons (oxonitridoaluminosilicates), nitridoaluminates should exhibit structural similarities to nitridosilicates and thus are expected to show similar materials properties and applications. Basically, nitridoaluminates contain condensed AlN_4 tetrahedra forming silicate-analogous anionic frameworks embedding counterions that compensate the negative formal charge. Since the discovery of Li_3AlN_2 in 1946^{1,2} as the first representative of this compound class, only three further nitridoaluminates have been described prior to 2012, namely, α - and β - $\text{Ca}_3[\text{Al}_2\text{N}_4]$ and $M_3\text{Al}_2\text{N}_4$ ($M = \text{Sr}, \text{Ba}$), as well as $\text{Ca}_6[\text{Al}_2\text{N}_6]$.³⁻⁵ Presumably, the very high thermodynamic stability of binary aluminum nitride AlN impedes synthetic access to less-condensed—and, thus, less-stable—ternary or higher nitridoaluminates. As a typical product of hightemperature synthesis, AlN is often reluctant to react because of kinetic inhibition as well. Recently, several novel nitridoaluminates with remarkable structural features and materials properties have been reported, namely, $\text{Ca}[\text{LiAlN}_2]$, $M[\text{Mg}_2\text{Al}_2\text{N}_4]$ ($M = \text{Ca}, \text{Sr}, \text{Ba}, \text{Eu}$), and $M[\text{LiAl}_3\text{N}_4]$ ($M = \text{Ca}, \text{Sr}$).⁶⁻⁹

As a common feature, these compounds contain highly condensed network structures of vertex- and edge-sharing AlN_4 tetrahedra with partial substitution of Al by Li or Mg. Thus, the degree of condensation (i.e., atomic ratio T:N, where T = Al, Mg, Li) is $\kappa = 1$, corresponding with the value of binary AlN itself. The high stability of these nitridoaluminates may be due to the fact that their anionic network structures can be considered as hypothetical structural variants of AlN with partial substitution of the tetrahedral centers by Li or Mg. Similar to that observed with aluminosilicates, such substitution causes the formation of anionic network structures with a resulting negative formal charge that can be compensated by alkaline-earth metal cations. Upon doping with Eu^{2+} , strong $4f^7 \rightarrow 4f^6 5d^1$ luminescence has been reported for such nitridoaluminates,⁷⁻⁹ which may well find application as lightemitting diode (LED) phosphors like the nitrides $(\text{Ba}, \text{Sr})_2\text{Si}_5\text{N}_8:\text{Eu}^{2+}$ and $\text{CaAlSiN}_3:\text{Eu}^{2+}$.¹⁰⁻¹³ Phosphor-converted LEDs (pc-LEDs) could help reduce the amount of energy used for lighting significantly.

Even for devices with high color rendition indices (CRIs), high luminous efficacies can be achieved when employing next-generation red-emitting materials (e.g., $\text{Sr}[\text{LiAl}_3\text{N}_4]:\text{Eu}^{2+}$).¹⁴ As a variant of the UCr_4C_4 structure type, $\text{Sr}[\text{LiAl}_3\text{N}_4]:\text{Eu}^{2+}$ emerged as an intriguing narrow-band

red-emitting phosphor. The high degree of condensation, cubelike coordination of the activator Eu^{2+} , and ordered distribution of Li and Al tetrahedral centers leads to unprecedented narrow emission in the red spectral region. In this contribution, we present the novel nitridoaluminate $\text{Ca}_{18.75}\text{Li}_{10.5}[\text{Al}_{39}\text{N}_{55}]:\text{Eu}^{2+}$, featuring a highly condensed host lattice. Doped with Eu^{2+} , this novel material shows intense emission in the red spectral region with a narrow full width at half-maximum (fwhm), similar to $\text{Sr}[\text{LiAl}_3\text{N}_4]:\text{Eu}^{2+}$.⁸ However, the structural features unprecedented in nitride chemistry differ fundamentally from the previously described LED phosphors.

Experimental Section

Synthesis

All manipulations were performed under rigorous exclusion of oxygen and moisture in flame-dried glassware on a Schlenk line attached to a vacuum line (10^{-3} mbar) or in an argon-filled glovebox (Unilab, MBraun, Garching, $\text{O}_2 < 1$ ppm, $\text{H}_2\text{O} < 1$ ppm). Synthesis of $\text{Ca}_{18.75}\text{Li}_{10.5}[\text{Al}_{39}\text{N}_{55}]:\text{Eu}^{2+}$ (nominal Eu^{2+} concentration = 0.5 mol %) was carried out in molybdenum-lined corundum crucibles in a hot isostatic press. The starting materials— Li_3N (Sigma-Aldrich, 99.99%), CaH_2 (Cerac, 99.5%), AlN (Tokuyama, 99%), and EuF_3 (Sigma-Aldrich, 99.99%) as a dopant—were premixed in stoichiometric amounts in an agate mortar, followed by fine mixing in a ball mill. The mixture was subsequently filled into the crucibles and heated for 5 h at 1250 °C and a nitrogen pressure of 51.7 MPa. Red octahedral-shaped single crystals of $\text{Ca}_{18.75}\text{Li}_{10.5}[\text{Al}_{39}\text{N}_{55}]:\text{Eu}^{2+}$ were isolated from the yellowish product under a microscope that was integrated in a glovebox. The crystals were enclosed in glass capillaries and sealed under argon. Storage of the powder materials in ambient air for more than 12 months did not lead to noticeable changes in composition.

Single-Crystal X-ray Diffraction

Single-crystal diffraction data were collected on a STOE IPDS I diffractometer (Mo $K\alpha$ radiation, graphite monochromator). The crystal structure was solved using direct methods with SHELXS.¹⁵ The structure was refined by the leastsquares method using SHELXL.¹⁵ Details on the structure investigations may be obtained from the Fachinformationszentrum

3. $\text{Ca}_{18.75}\text{Li}_{10.5}[\text{Al}_{39}\text{N}_{55}]:\text{Eu}^{2+}$ —Supertetrahedron Phosphor for Solid-State Lighting

Karlsruhe, 76344 Eggenstein-Leopoldshafen, Germany (fax: (+49)7247-808-666; e-mail: crysdata@fiz-karlsruhe.de), on quoting the Cambridge Structural Database depository No. CSD-430639.

Powder X-ray Diffraction

Powder X-ray diffraction data were collected on a Huber G670 Guinier imaging plate diffractometer (Cu $K\alpha_1$ radiation, Ge(111) monochromator). Bragg data were simulated based on the single-crystal structural data using the WinXPOW program package.¹⁶ Rietveld refinement was carried out using the TOPAS package.¹⁷

Electron Microscopy

For scanning electron microscopy (SEM) investigations, an SEM microscope system (JEOL, Model JSM-6500F) equipped with a Si/Li energy-dispersive X-ray (EDX) detector (Oxford Instruments, Model 7418) was used. For transmission electron microscopy (TEM) measurements, a TEM microscope system (FEI, Model Titan 80–300) equipped with a post-column energy filter (Gatan, Model GIF Tridiem) and an EDAX EDX detector for analytical characterizations was employed. Diffraction patterns were recorded with a CCD camera (Gatan, Model UltraScan 1000) (2k × 2k) and evaluated using a calibrated camera constant obtained by using a Si standard. The TEM investigations were conducted at an accelerating voltage of 300 kV.

EDX Spectroscopy

To analyze the chemical composition of different crystallites, EDX data were collected with an accelerating voltage of 12 kV. Furthermore, the SEM system was used to collect images for investigating the particle morphology.

Electron Energy-Loss Spectroscopy (EELS)

EELS measurements were performed in diffraction mode in the TEM with a selected area diffraction aperture choosing a circular area of ≈ 150 nm in diameter to avoid beam damage. A 2 mm entrance aperture of the spectrometer and a camera length of 130 mm were applied resulting in a collector angle of 13.5 mrad. Dispersions of 0.3 eV/channel were used, leading to a fwhm of ≈ 0.9 –1.2 eV of the zero loss peak. The acquisition time for the Li K-

edge and Al L_{2,3}-edge was 10 s. The obtained data were corrected for dark current and channel-to-channel gain variation. The pre-edge background was approximated by a firstorder-log-polynomial function and subtracted from the original data.¹⁸

Luminescence

Luminescence investigations were performed on a luminescence microscope consisting of a Horiba Fluorimax4 spectrofluorimeter system that was attached to an Olympus Model BX51 microscope via fiber optics. Single crystals were measured in glass capillaries. Bulk samples were investigated in PTFE sample holders. The excitation wavelength was set to 450 nm with a spectral width of 10 nm. The emission spectra were measured in the wavelength range between 460 nm and 800 nm with a step size of 1 nm. Excitation spectra were measured in the wavelength range between 350 nm and 570 nm with a step size of 1 nm, using a monitor wavelength of 650 nm.

Results and Discussion

Synthesis and Chemical Analysis

The synthesis described above enabled access to the system $\text{Ca}_{(20-x)}\text{Li}_{(8+2x)}[\text{Al}_{39}\text{N}_{55}]:\text{Eu}^{2+}$ in which the phase $\text{Ca}_{18.75}\text{Li}_{10.5}[\text{Al}_{39}\text{N}_{55}]:\text{Eu}^{2+}$ could be isolated as single crystals (Figure 3.1).

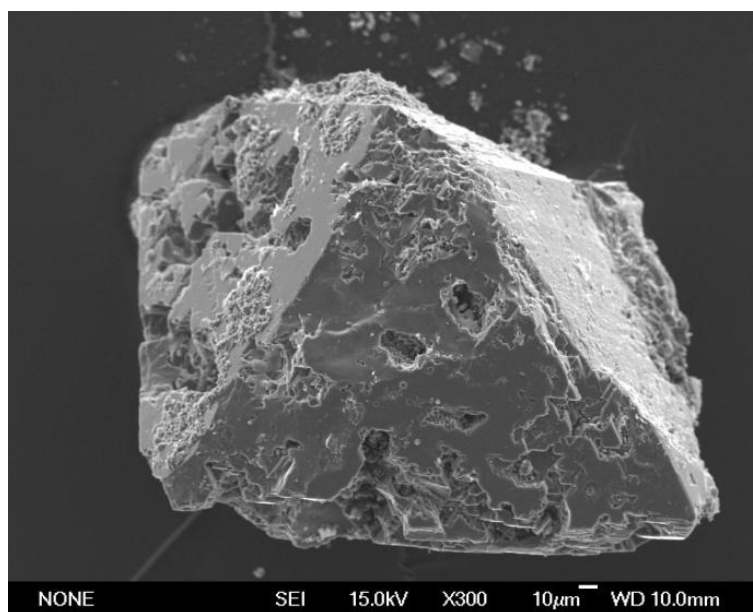


Figure 3.1. SEM image of $\text{Ca}_{18.75}\text{Li}_{10.5}[\text{Al}_{39}\text{N}_{55}]:\text{Eu}^{2+}$.

3. $\text{Ca}_{18.75}\text{Li}_{10.5}[\text{Al}_{39}\text{N}_{55}]:\text{Eu}^{2+}$ —Supertetrahedron Phosphor for Solid-State Lighting

SEM/EDX investigations (five measurements on different crystals) show a Ca:Al:N atomic ratio of 1:2.1:4.0, which is in good accordance with the sum formula. However, a slight overestimation of nitrogen is observed. Eu was not detected in SEM/EDX because of the low accelerating voltage of 12 kV. The oxygen content is zero within the estimated standard deviations.

Crystal Structure

The crystal structure of $\text{Ca}_{18.75}\text{Li}_{10.5}[\text{Al}_{39}\text{N}_{55}]$ was solved and refined in the cubic space group $\text{Fd}\bar{3}\text{m}$ (No. 227) with $a = 22.415(3)$ Å and $Z = 8$. The crystallographic data are summarized in Table 3.1. The atomic coordinates, isotropic displacement parameters, Wyckoff positions, and site occupancy factors (SOF) are specified in the Supporting Information (Table S8.1). Anisotropic displacement parameters are listed in the Supporting Information (Table S8.2). Selected interatomic distances are listed in the Supporting Information (Table S8.3). Eu^{2+} was neglected during structure refinement due to the small amounts of dopant concentration and, therefore, the insignificant scattering density. $\text{Ca}_{18.75}\text{Li}_{10.5}[\text{Al}_{39}\text{N}_{55}]:\text{Eu}^{2+}$ is built up by a network of vertexsharing supertetrahedra with an edge length of five individual AlN_4 tetrahedra-denominated T_5 , each consisting of 35 AlN_4 units (Figure 3.2a). The AlN_4 tetrahedra share common corners as well and form a section of a sphalerite-type network. The supertetrahedra can thus be described as building blocks of cubic AlN .

By vertex sharing, the T_5 supertetrahedra form a diamond-type network with all (super)tetrahedra pointing in one direction (e.g., up). The voids of this superstructure are filled with a second diamond-type network of T_5 supertetrahedra. In the latter structure, all (super)tetrahedra point in the opposite direction (e.g., down). These two superstructures interpenetrate each other and thus represent a hierarchical variant of the NaTl structure type.^{19,20} Furthermore, the T_5 supertetrahedra are cross-linked by additional AlN_4 moieties, resulting in a high overall degree of condensation ($\kappa = 0.71$). The nitridosilicate Li_2SiN_2 exhibits a remotely similar crystal structure formed by two noncondensed interpenetrating cristobalite-type networks of all-vertex sharing Si_4N_{10} T_2 supertetrahedra.²¹

The main difference between the two structures, other than the supertetrahedron size (T_5 vs T_2), is that, in Li_2SiN_2 , the adamantane-type Si_4N_{10} T_2 supertetrahedral networks are not condensed with each other. Thus, in $\text{Ca}_{18.75}\text{Li}_{10.5}[\text{Al}_{39}\text{N}_{55}]:\text{Eu}^{2+}$, the supertetrahedra themselves form diamond-type T_5 -supertetrahedra of infinite order in what can be described

in terms of a hierarchical structure. Other than in Li_2SiN_2 , supertetrahedra are not often encountered as structural motifs in nitride chemistry.

Table 3.1. Crystallographic Data of the Single-Crystal Structure Determination of $\text{Ca}_{18.75}\text{Li}_{10.5}[\text{Al}_{39}\text{N}_{55}]^a$

sum formula	$\text{Ca}_{18.75}\text{Li}_{10.5}[\text{Al}_{39}\text{N}_{55}]$
crystal system	cubic
space group	$\text{Fd}\bar{3}\text{m}$ (No. 227)
lattice parameters	$a = 22.415(3) \text{ \AA}$
cell volume	$11263(2) \text{ \AA}^3$
formula units/unit cell	8
density	$3.123 \text{ g}\cdot\text{cm}^{-3}$
μ	2.432 mm^{-1}
T	$293(2) \text{ K}$
diffractometer	Stoe IPDS I
radiation	$\text{Mo K}\alpha$ ($\lambda = 0.71073 \text{ \AA}$), graphite monochromator
$F(000)$	10389.9
profile range	$2.57^\circ \leq \theta \leq 30.35^\circ$
index ranges	$-29 \leq h \leq 29$
	$-31 \leq k \leq 31$
	$-31 \leq l \leq 31$
number of independent reflections	854 [$R(\text{int}) = 0.0845$]
number of refined parameters	74
goodness of fit	0.991
$R1$ (all data); $R1$ ($F^2 > 2\sigma(F^2)$)	0.0414, 0.0257
$wR2$ (all data); $wR2$ ($F^2 > 2\sigma(F^2)$)	0.0604, 0.0569
$\Delta\rho_{\text{max}}, \Delta\rho_{\text{min}}$	$0.616 \text{ e}\cdot\text{\AA}^{-3}, -0.475 \text{ e}\cdot\text{\AA}^{-3}$

^ae.s.d.s in parentheses

Isolated T_2 supertetrahedra were found in the nitridophosphate $\text{Li}_{10}\text{P}_4\text{N}_{10}$ ²² and low-degree-of-condensation Si_5N_{16} supertetrahedra occur in the nitridosilicate $\text{Ca}_3\text{M}_3[\text{Si}_9\text{N}_{17}]$ ($M = \text{Sm}, \text{Yb}$),²³ but most reports, especially of large supertetrahedra, have been found in the compound class of main-group and transition-metal chalcogenides.^{24–29} The structures range from isolated supertetrahedra to one-dimensional (1D) chains and three-dimensional (3D) networks of vertex-sharing supertetrahedra.^{24,30} The open pore structures and less

3. $\text{Ca}_{18.75}\text{Li}_{10.5}[\text{Al}_{39}\text{N}_{55}]:\text{Eu}^{2+}$ —Supertetrahedron Phosphor for Solid-State Lighting

condensed phases are commonly stabilized by sterically demanding counterions for charge compensation.^{27–29,31}

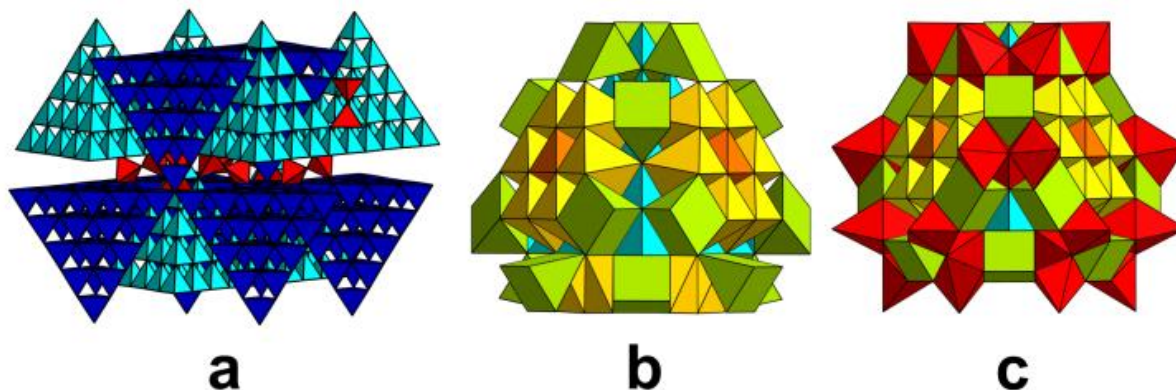


Figure 3.2. Sketched structure of $\text{Ca}_{18.75}\text{Li}_{10.5}[\text{Al}_{39}\text{N}_{55}]:\text{Eu}^{2+}$ showing the characteristic structural feature of T_5 supertetrahedra: (a) AlN_4 -tetrahedra network, (b) three different Ca sites (Ca1, yellow; Ca2, green; Ca3, orange), and (c) two Li sites (red).

In $\text{Ca}_{18.75}\text{Li}_{10.5}[\text{Al}_{39}\text{N}_{55}]:\text{Eu}^{2+}$, the counterions Ca^{2+} and Li^+ fill the interstitial spaces between the T_5 supertetrahedra frameworks (Figure 3.2a). Ca occupies three different sites (Figure 3.2b) with Ca1 and Ca3 showing trigonal antiprismatic (distorted octahedral) coordination by N and Ca–N distances, ranging from 2.39 Å to 2.73 Å. Ca2 shows trigonal prismatic coordination with Ca–N distances from 2.49 Å to 2.73 Å. Structural refinement of single-crystal and powder XRD data revealed a partial occupation for Ca2 (SOF = 0.375). Resulting from a split refinement, Li occupies two positions forming rings around the N1 position (Figure 3.2c). Li–N distances range from 1.94 Å to 2.52 Å. The Ca–N and Li–N distances observed here are in good agreement with the sums of the ionic radii and bond lengths known from other nitridoaluminates or lithium nitrides.^{5,21,32–34}

The nitridoaluminate $\text{Ca}_{18.75}\text{Li}_{10.5}[\text{Al}_{39}\text{N}_{55}]$ is structurally related to the manganate $\text{Na}_{26}\text{Mn}_{39}\text{O}_{55}$.³⁵ Both compounds exhibit similar structural motifs. However, the coordination of the Ca2 site in $\text{Ca}_{18.75}\text{Li}_{10.5}[\text{Al}_{39}\text{N}_{55}]$ differs from the corresponding Na site in $\text{Na}_{26}\text{Mn}_{39}\text{O}_{55}$. In the latter compound, the respective Na^+ occupies Wyckoff position 96g and is coordinated by five N forming quadratic pyramids. In $\text{Ca}_{18.75}\text{Li}_{10.5}[\text{Al}_{39}\text{N}_{55}]$, Ca2 is located at Wyckoff position 48f, which is centered between the Na atoms (Figure 3.3). Therefore, both compounds can be described as homeotypic.

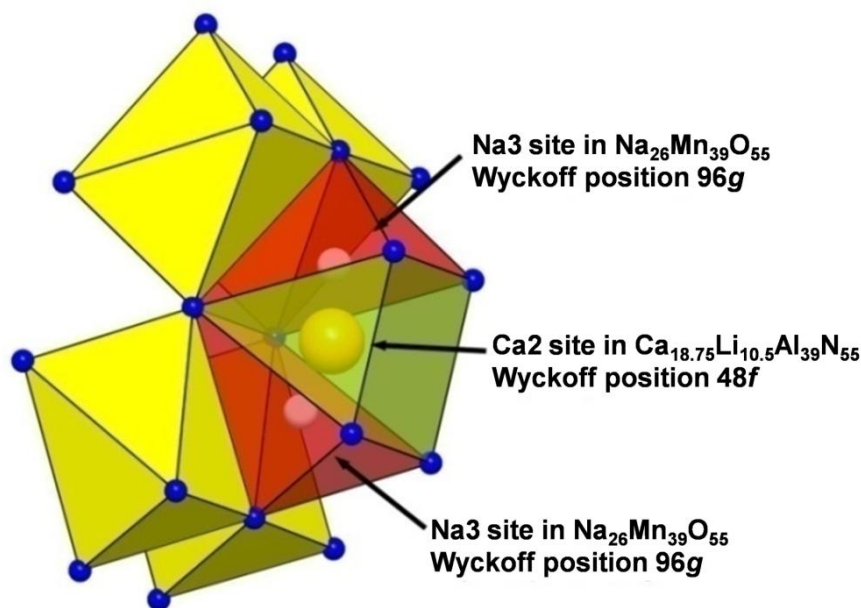


Figure 3.3. Detail of the $\text{Ca}_{18.75}\text{Li}_{10.5}[\text{Al}_{39}\text{N}_{55}]$ crystal structure showing the Ca2 site (Wyckoff position 48f) coordinated trigonally by N (light green polyhedron) which is different from the Na coordination in $\text{Na}_{26}\text{Mn}_{39}\text{O}_{55}$ (red polyhedra). Trigonal antiprismatic Ca1–N6 coordination spheres are depicted as solid yellow polyhedra.

Powder X-ray Diffraction

Rietveld refinement of powder X-ray diffraction (XRD) data based on the structural model obtained from single-crystal XRD is in good accordance with the observed diffraction pattern. Crystallographic data from Rietveld refinement are summarized in the Supporting Information (Table S8.4). The crystal structure of the bulk material $\text{Ca}_{18.75}\text{Li}_{10.5}[\text{Al}_{39}\text{N}_{55}]$ could thus be proven to be identical to that of isolated single crystals (see Figure 3.4). The side phase (AlN) was quantified to ≈ 40 wt% from Rietveld refinement. Whether the observed AlN remained nonreacted from the starting materials or formed anew, because of decomposition of the title compound during synthesis, is unclear at this point. At very high temperatures, several nitridoaluminates show a tendency to decompose over time under the formation of binary AlN. Efforts to reduce or eliminate the impurity phase are the subject to ongoing research.

3. $\text{Ca}_{18.75}\text{Li}_{10.5}[\text{Al}_{39}\text{N}_{55}]:\text{Eu}^{2+}$ —Supertetrahedron Phosphor for Solid-State Lighting

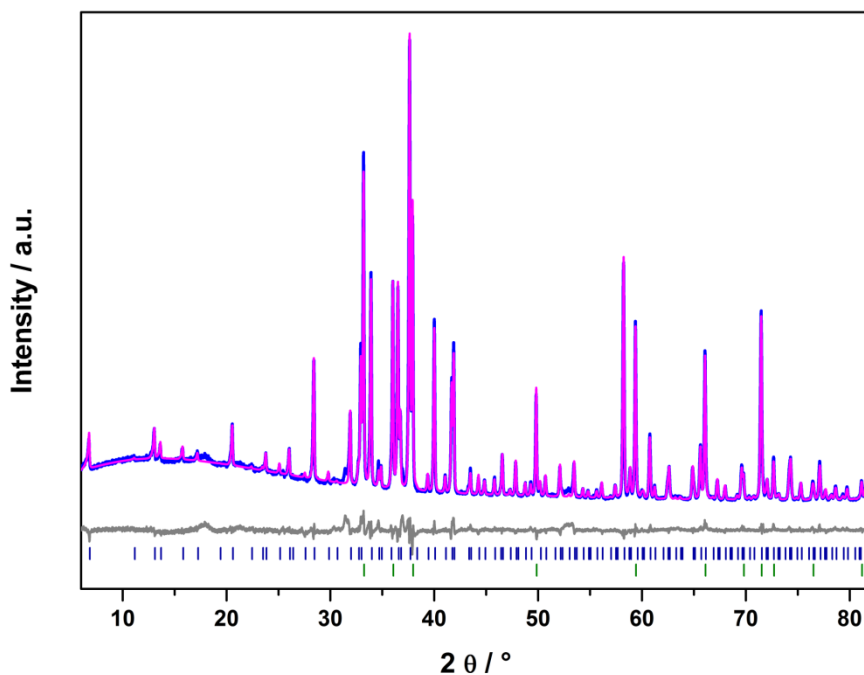


Figure 3.4. Observed (blue) and calculated (red) XRD patterns, as well as a difference profile of the Rietveld refinement of $\text{Ca}_{18.75}\text{Li}_{10.5}[\text{Al}_{39}\text{N}_{55}]$ (gray). The vertical blue bars indicate possible peak positions of the title compound; green bars indicate the peak positions of the side phase (AlN).

Luminescence

Eu^{2+} -doped samples of the title compound exhibit intense red luminescence when irradiated with ultraviolet (UV) to green light. Luminescence investigations were performed on single crystals sealed in silica glass capillaries and on bulk samples in polytetrafluoroethylene (PTFE) sample holders. Both methods deliver similar results; therefore, only measurements of bulk samples with 0.2–1 mol% Eu (nominal composition) are discussed here. Since $\text{Ca}_{18.75}\text{Li}_{10.5}[\text{Al}_{39}\text{N}_{55}]:\text{Eu}^{2+}$ is only one representative in the solid-solution series $\text{Ca}_{(20-x)}\text{Li}_{(8+2x)}[\text{Al}_{39}\text{N}_{55}]:\text{Eu}^{2+}$ ($x = 0$ – 2), tunability of the luminescence properties is expected by modifying the atomic ratio Ca:Li. Therefore, several nominal host lattice compositions ($x = 0, 1.25, 2$) were examined.

Excitation of the title compound ($x = 1.25$) at 450 nm yields an emission band with a maximum at 647 nm and a remarkably narrow fwhm of 1280 cm^{-1} ($\approx 54 \text{ nm}$), with an internal quantum efficiency (IQE) of 11% (see Figure 3.5). Peak emission and fwhm values are in the range of recently published $\text{Sr}[\text{LiAl}_3\text{N}_4]:\text{Eu}^{2+}$ ($\lambda_{\text{em}} \approx 650 \text{ nm}$, $\text{fwhm} \approx 1180 \text{ cm}^{-1}$),⁸ which is a narrow-band red-emitting material with high industrial relevance.

3. $\text{Ca}_{18.75}\text{Li}_{10.5}[\text{Al}_{39}\text{N}_{55}]:\text{Eu}^{2+}$ —Supertetrahedron Phosphor for Solid-State Lighting

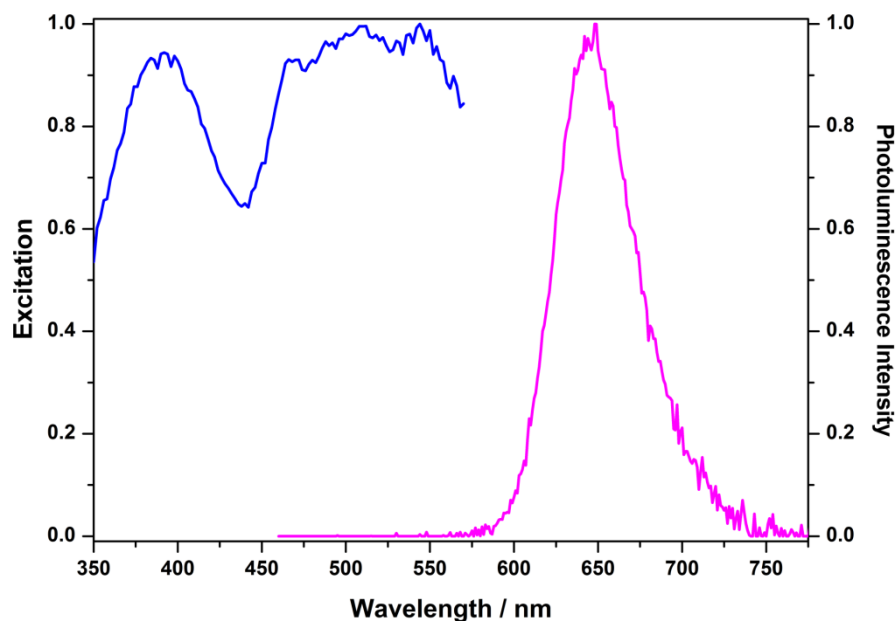


Figure 3.5. Excitation (blue, monitored at 650 nm) and emission (red, $\lambda_{\text{exc}} = 450$ nm) spectra of $\text{Ca}_{18.75}\text{Li}_{10.5}[\text{Al}_{39}\text{N}_{55}]:\text{Eu}^{2+}$ bulk material with a dopant concentration of 0.5 mol% Eu (nominal composition).

The excitation spectrum shows two bands: one in the UV to blue range, peaking at ≈ 380 nm, and another broader band in the blue to green spectral region (see Figure 3.5, blue line).

Table 3.2. Luminescence Data of the Solid-Solution Series $\text{Ca}_{(20-x)}\text{Li}_{(8+2x)}[\text{Al}_{39}\text{N}_{55}]:\text{Eu}^{2+}$

	$x = 0$	$x = 1.25$	$x = 2$
internal quantum efficiency			
($\lambda_{\text{exc}} = 390$ nm)	0.04		
($\lambda_{\text{exc}} = 450$ nm)	0.03	0.11	0.14
($\lambda_{\text{exc}} = 500$ nm)	0.09		0.24
chromaticity			
x	0.391	0.699	0.699
y	0.308	0.300	0.301
lumen equivalents	124	103	93
λ_{max}	640 nm	645 nm	648 nm
fwhm ($\lambda_{\text{exc}} = 500$ nm)	61 nm	58 nm	56 nm

The high and low x -values of the solid-solution series ($x = 0, 2$) yield comparable results (see Table 3.2 and Figure 3.6). The excitation maximum is located at 525 nm. Because of these two excitation maxima and a local minimum in excitation sensitivity at 450 nm, additional

3. $\text{Ca}_{18.75}\text{Li}_{10.5}[\text{Al}_{39}\text{N}_{55}]:\text{Eu}^{2+}$ —Supertetrahedron Phosphor for Solid-State Lighting

photoluminescence spectra were recorded at excitation wavelengths of 390 and 500 nm. In pc-LEDs, such broad excitation bands can lead to reabsorption of green–yellow light by Eu^{2+} -activated red-emitting materials. This is a common problem that is not restricted to $\text{Ca}_{(20-x)}\text{Li}_{(8+2x)}[\text{Al}_{39}\text{N}_{55}]:\text{Eu}^{2+}$. It can be addressed by layering the phosphors, with the red emitter being placed directly onto the LED chip. Thus, only backscattered light from the green–yellow-emitting components can be reabsorbed by the red phosphor.

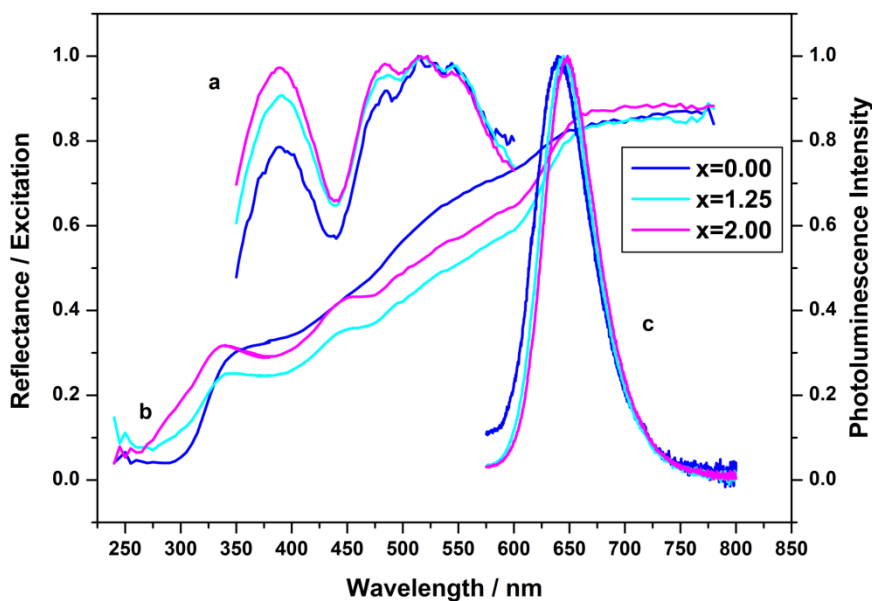


Figure 3.6. (a) Excitation, (b) reflectance, and (c) emission ($\lambda = 390$ nm) spectra of $\text{Ca}_{(20-x)}\text{Li}_{(8+2x)}[\text{Al}_{39}\text{N}_{55}]:\text{Eu}^{2+}$ ($x = 0-2$).

A slight shift of the emission maximum toward lower energies for lower Ca contents can be observed. This shift is accompanied by increasing IQEs but also decreasing lumen equivalents, because of the longer emission wavelengths. The observed increase in IQE for excitation at 390 nm, compared to excitation at 450 nm, results from $\text{Ca}_{(20-x)}\text{Li}_{(8+2x)}[\text{Al}_{39}\text{N}_{55}]:\text{Eu}^{2+}$ exhibiting a local absorption minimum at 450 nm. Because of the longer optical path length needed for absorption at 450 nm, in comparison to both longer and shorter wavelengths, processes such as absorption at defects and side phases become more likely. Excitation at more readily absorbed wavelengths and samples with significantly reduced amounts of side phase should therefore lead to higher QEs.

Thermal behavior of the emission (Figure 3.7) shows strong thermal quenching. Relative quantum efficiencies ($\lambda_{\text{exc}} = 450$ nm) at room temperature range from 45% for $x = 0$, to 53% for $x = 1.25$, to 65% for $x = 2$. At 423 K, relative quantum efficiencies drop below 10% for all

compositions. A negative influence of the AlN side phase on the thermal behavior of the emission seems unlikely, since AlN itself is optically inactive. Eu^{2+} -doped samples of AlN show blue luminescence only in conjunction with either codoping by Si (<9%)³⁶ or partial substitution of Al by Ga.³⁷ Here, AlN is merely an additional scattering material. Still, a hypothetical nonradiative energy transfer from $\text{Ca}_{18.75}\text{Li}_{10.5}[\text{Al}_{39}\text{N}_{55}]:\text{Eu}^{2+}$ to $\text{AlN}:\text{Eu}^{2+}$ and subsequent dissipation cannot be totally excluded.

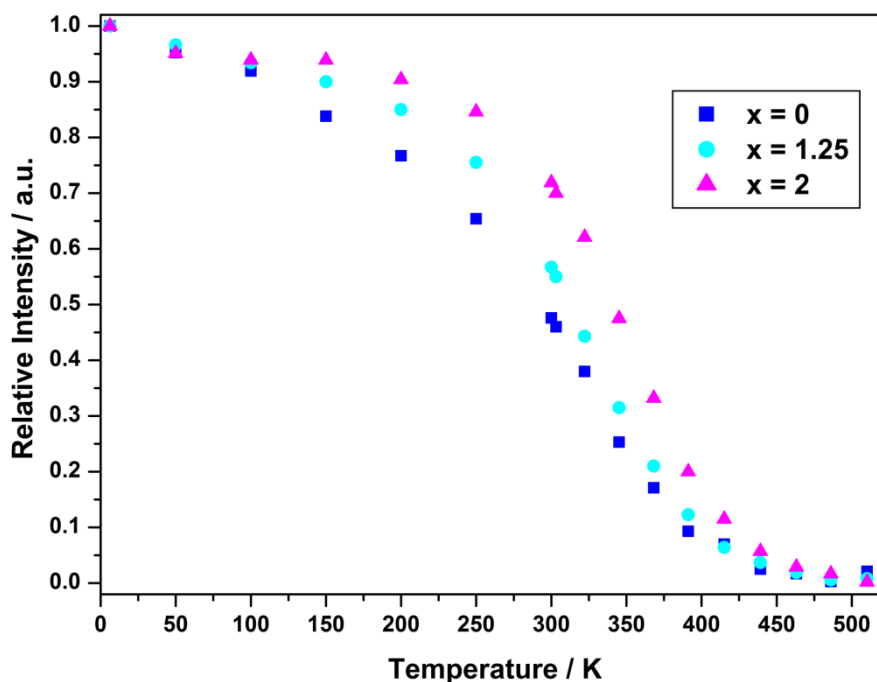


Figure 3.7. Thermal behavior of the emission of $\text{Ca}_{(20-x)}\text{Li}_{(8+2x)}[\text{Al}_{39}\text{N}_{55}]:\text{Eu}^{2+}$.

Compared to other red LED phosphor materials, such as $(\text{Ba,Sr})_2\text{Si}_5\text{N}_8:\text{Eu}^{2+}$ ($\lambda_{\text{em}} \approx 590\text{--}625$ nm, $\text{fwhm} \approx 2050\text{--}2600$ cm^{-1})^{10,11,38} or $(\text{Ca,Sr})\text{SiAlN}_3:\text{Eu}^{2+}$ ($\lambda_{\text{em}} \approx 610\text{--}660$ nm, $\text{fwhm} \approx 2100\text{--}2500$ cm^{-1}),^{12,39} $\text{Ca}_{18.75}\text{Li}_{10.5}[\text{Al}_{39}\text{N}_{55}]:\text{Eu}^{2+}$ shows a remarkably reduced fwhm. This very narrow emission is probably due to the highly symmetric coordination of the Ca sites on which Eu^{2+} is believed to be located as well. Such a narrow band emission in a Eu^{2+} -doped system is typically obtained only when several requirements for the host lattice are fulfilled. On one hand, the linked sphalerite-type T_5 supertetrahedra result in a framework with a high degree of condensation ($\kappa = 0.71$), which is expected to be beneficial for minimizing structural relaxation around the activator site in its excited state. On the other hand, the highly symmetric coordination spheres (2× trigonal antiprismatic, 1× trigonal prismatic) of the three Ca sites may lead to a small Stokes shift. This assumption is

3. $\text{Ca}_{18.75}\text{Li}_{10.5}[\text{Al}_{39}\text{N}_{55}]:\text{Eu}^{2+}$ —Supertetrahedron Phosphor for Solid-State Lighting

corroborated by other experimental observations, suggesting that a high activator site symmetry enables smaller Stokes shifts and therefore reduces emission bandwidth.⁴⁰ Similarly, this effect is observed in other Eu^{2+} phosphors, such as $M[\text{LiAl}_3\text{N}_4]:\text{Eu}^{2+}$ ($M = \text{Ca}, \text{Sr}$) or $\text{BaSi}_2\text{O}_2\text{N}_2:\text{Eu}^{2+}$.^{8,9,41,42}

As mentioned previously, there are three crystallographically independent sites for Ca^{2+} or Eu^{2+} available in $\text{Ca}_{18.75}\text{Li}_{10.5}[\text{Al}_{39}\text{N}_{55}]:\text{Eu}^{2+}$. However, this fact is not in good agreement with the observed narrow-band emission. Different chemical environments around multiple activator sites usually cause broadened composed emission bands. Because of the dense packing of the host framework, an occupation of interstitial positions by Eu^{2+} seems unlikely. We presume that Eu^{2+} is present at all Ca sites, but favors the partially occupied trigonal prismatic coordinated Ca2 site. The larger average Ca2–N distances of 2.65 Å are in better agreement with the sum of the ionic radii of Eu^{2+} and N^{3-} (2.68 Å), according to Baur,³² than the average Ca1–N distances of 2.45 Å and Ca3–N distances of 2.42 Å. However, the obtained data suggest that emission occurs from Ca sites with the lowest lying absorption bands, which are most likely the 6-fold coordinated sites with the shortest Ca–N contacts (trigonal antiprismatic coordinated sites Ca1 and Ca3).

The already-mentioned increase in QE with decreasing Ca content may be explained by simultaneously higher Eu^{2+} occupancy of the Ca1 and Ca3 sites, which is favorable for luminescence. When irradiated with blue–green light ($\lambda_{\text{exc}} = 500 \text{ nm}$), $\text{Ca}_{(20-x)}\text{Li}_{(8+2x)}[\text{Al}_{39}\text{N}_{55}]:\text{Eu}^{2+}$ shows its strongest photoluminescence and highest quantum efficiencies (Table 3.2). In conjunction with the strong absorption in the UV region (Figure 3.6b), the experimental observations indicate that the 5d levels of Eu^{2+} of the nonluminescent site are located within the conduction band, because of the larger energetic separation of the Eu^{2+} 4f and 5d states. This assumption is supported by the low-temperature emission measurements down to 6 K that do not show additional emission bands or broadening of the emission band. Thus, UV light is most likely absorbed by multiple Eu^{2+} sites but emission is partly quenched by photoionization, i.e., excitation of the respective electron into the conduction band, which explains the low overall QE values.⁴⁷ Low-energy excitation in the green spectral range mainly leads to absorption by the emitting sites and, thus, higher QE values, without a significant change of the emission band position and shape.

EELS

To confirm the presence of Li in the crystal structure, EELS measurements were performed in a TEM with an accelerating voltage of 300 kV. The Li K-edge in Figure 3.8 occurs at ≈ 56.5 eV and has a maximum at 61.6 eV.

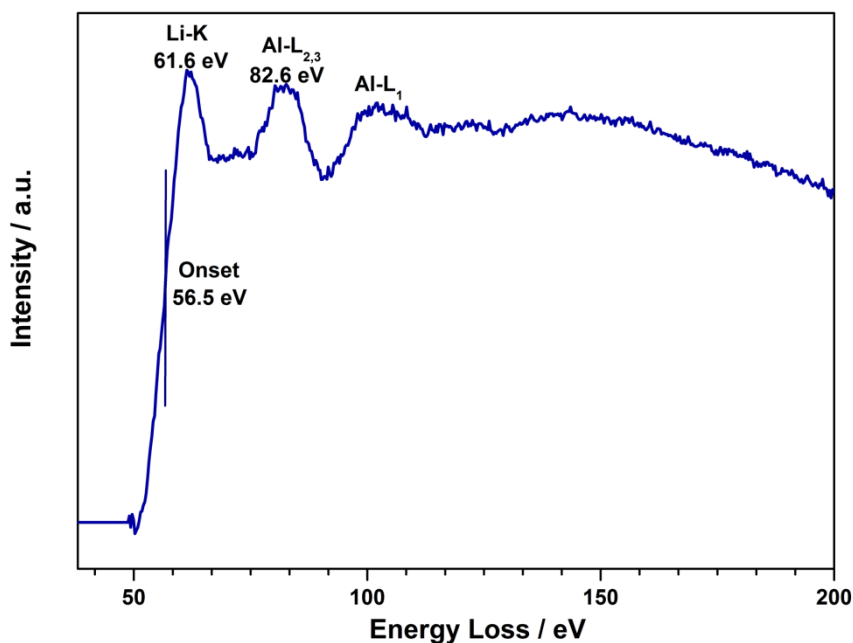


Figure 3.8. EELS spectrum of $\text{Ca}_{18.75}\text{Li}_{10.5}[\text{Al}_{39}\text{N}_{55}]:\text{Eu}^{2+}$. The energy loss region of the Li K-edge, the Al $L_{2,3}$ -edge, and the Al L_1 -edge is shown. The background to the left of the Li K-edge has been subtracted.

The Al $L_{2,3}$ edge and Al L_1 edge can be seen in the spectrum, but they overlap with the higher energy loss region of the Li K-edge. The onset values of the Al edges cannot be determined exactly, because of overlapping. However, the Al $L_{2,3}$ -edge shows a maximum peak at 82.6 eV. The value of the Li K-edge shows a slight deviation, compared to data obtained from the literature (for example, Li_xTiP ($x = 2-11$), $\text{Li}_2\text{CaSi}_2\text{N}_4$, or $\text{Li}_2\text{SrSi}_2\text{N}_4$, which is a result of different bonding types).^{43,44} The shape and maximum peak of the Al $L_{2,3}$ -edge are in good accordance with data published in the literature.^{18,45} The EELS investigations clearly confirm the presence of Li and Al being integrated in the structure.

Conclusion

In this contribution, we have reported on the new nitridoaluminate $\text{Ca}_{18.75}\text{Li}_{10.5}[\text{Al}_{39}\text{N}_{55}]:\text{Eu}^{2+}$ with an exceptional crystal structure and intriguing luminescence properties. The compound was synthesized by a heterogeneous high-temperature/high-pressure reaction. Its crystal structure consists of two interpenetrating diamond-type networks of vertex-sharing T_5 supertetrahedra connected by bridging AlN_4 tetrahedra. Ca and Li fill the interstitial space between the T_5 supertetrahedra network structure. Formally, the structure consists of $\approx 54\%$ cubic AlN by volume, accounting for its thermal stability and chemical inertness. The structural model was refined from single-crystal and powder X-ray diffraction (XRD) data. Furthermore, the presence of Li in the crystal structure was confirmed by EELS spectroscopy. Luminescence investigations on Eu^{2+} -doped samples of $\text{Ca}_{18.75}\text{Li}_{10.5}[\text{Al}_{39}\text{N}_{55}]$ show intense red emission peaking at 647 nm when irradiated with UV to green light. The fwhm of $\approx 1280 \text{ cm}^{-1}$ ($\approx 56 \text{ nm}$) is exceptionally narrow for Eu^{2+} phosphors.

These values are close to other recently published narrow-band red-emitting materials of the nitridosilicate or nitridoaluminate compound class, such as $\text{Sr}[\text{LiAl}_3\text{N}_4]:\text{Eu}^{2+}$ or $\text{Sr}[\text{Mg}_3\text{SiN}_4]:\text{Eu}^{2+}$, which are being intensively discussed as possible next-generation phosphors.^{8,46} However, the uncommon crystal structure of our material demonstrates that narrow-band Eu^{2+} emission is not limited to derivatives of the UCr_4C_4 structure type and cubelike coordination of the heavy atom. In fact, we could show that trigonal (anti)prismatic or octahedral coordination are also suitable for narrow emission bands in Eu^{2+} -doped condensed nitride materials.

In this context, the synthesis of the Sr analogue $\text{Sr}_{(20-x)}\text{Li}_{(8+x)}[\text{Al}_{39}\text{N}_{55}]:\text{Eu}^{2+}$ would be specifically interesting. Substitution of Ca for Sr could lead to energetically lowered $4f$ and $5d$ states within the host lattice band gap and thus higher quantum efficiencies.⁴⁷ Consequently, we claim that $\text{Ca}_{18.75}\text{Li}_{10.5}[\text{Al}_{39}\text{N}_{55}]:\text{Eu}^{2+}$ widens the group of intriguing red-emitting materials and has the potential for application in pc-LEDs. Because of the exceptional crystal structure and the regardless remarkably narrow red emission, we claim that $\text{Ca}_{18.75}\text{Li}_{10.5}[\text{Al}_{39}\text{N}_{55}]:\text{Eu}^{2+}$ is a key material with regard to further comprehending the principles of narrow-band Eu^{2+} emission.

Associated Content

Supporting Information

The Supporting Information is available free of charge on the ACS Publications website at DOI: 10.1021/acs.chemmater.5b04929.

Atomic coordinates and isotropic displacement parameters of $\text{Ca}_{18.75}\text{Li}_{10.5}[\text{Al}_{39}\text{N}_{55}]$ (Table S8.1), Anisotropic displacement parameters of $\text{Ca}_{18.75}\text{Li}_{10.5}[\text{Al}_{39}\text{N}_{55}]$ (Table S8.2), selected bond lengths in $\text{Ca}_{18.75}\text{Li}_{10.5}[\text{Al}_{39}\text{N}_{55}]$ (Table S8.3), and crystallographic data of the Rietveld refinement of $\text{Ca}_{18.75}\text{Li}_{10.5}[\text{Al}_{39}\text{N}_{55}]$ (Table S8.4). This material is also available in Chapter 8: Appendix of this thesis.

Crystallographic data for calcium lithium nitridoaluminate $\text{Ca}_{18.75}\text{Li}_{10.5}[\text{Al}_{39}\text{N}_{55}]$

Author Information

Corresponding Author

*E-mail: wolfgang.schnick@uni-muenchen.de

Present Address

[§]Max-Planck-Institut für Eisenforschung GmbH, Max-Planck-Straße 1, 40237 Düsseldorf, Germany

Notes

The authors declare no competing financial interest.

Acknowledgements

The authors thank Thomas Miller for collecting the singlecrystal data and Christian Minke for the EDX measurements. Financial support by the Fonds der Chemischen Industrie (FCI) is gratefully acknowledged.

References

- (1) Juza, R.; Hund, F. Metal Amides and Metal Nitrides. XVII. The Ternary Nitrides Li_3AlN_2 and Li_3GaN_2 . *Z. Anorg. Chem.* **1948**, *257*, 13–25.

3. $\text{Ca}_{18.75}\text{Li}_{10.5}[\text{Al}_{39}\text{N}_{55}]:\text{Eu}^{2+}$ —Supertetrahedron Phosphor for Solid-State Lighting

- (2) Juza, R.; Hund, F. The Crystal Structures of LiMgN , LiZnN , Li_3AlN_2 , and Li_3GaN_2 . *Naturwissenschaften* **1946**, *33*, 121–122.
- (3) Blase, W.; Cordier, G.; Ludwig, M.; Kniep, R. $\text{Sr}_3[\text{Al}_2\text{N}_4]$: A Nitridoaluminate with Corrugated Tetrahedral Chains $\varpi[\text{AlN}_{4/2}^{3-}]$. *Z. Naturforsch., B: Chem. Sci.* **1994**, *49*, 501–505.
- (4) Ludwig, M.; Jäger, J.; Niewa, R.; Kniep, R. Crystal Structures of Two Polymorphs of $\text{Ca}_3[\text{Al}_2\text{N}_4]$. *Inorg. Chem.* **2000**, *39*, 5909–5911.
- (5) Ludwig, M.; Niewa, R.; Kniep, R. Dimers $[\text{Al}_2\text{N}_6]^{12-}$ and chains $\varpi[\text{AlN}_{4/2}^{3-}]$ in the crystal structures of $\text{Ca}_6[\text{Al}_2\text{N}_6]$ and $\text{Ba}_3[\text{Al}_2\text{N}_4]$. *Z. Naturforsch., B: Chem. Sci.* **1999**, *54*, 461–465.
- (6) Pust, P.; Pagano, S.; Schnick, W. $\text{Ca}[\text{LiAlN}_2]$: A Quaternary Nitridoaluminate. *Eur. J. Inorg. Chem.* **2013**, *2013*, 1157–1160.
- (7) Pust, P.; Hintze, F.; Hecht, C.; Weiler, V.; Locher, A.; Zitnanska, D.; Harm, S.; Wiechert, D.; Schmidt, P. J.; Schnick, W. Group (III) Nitrides $M[\text{Mg}_2\text{Al}_2\text{N}_4]$ ($M = \text{Ca}, \text{Sr}, \text{Ba}, \text{Eu}$) and $\text{Ba}[\text{Mg}_2\text{Ga}_2\text{N}_4]$ —Structural Relation and Nontypical Luminescence Properties of Eu^{2+} Doped Samples. *Chem. Mater.* **2014**, *26*, 6113–6119.
- (8) Pust, P.; Weiler, V.; Hecht, C.; Tücks, A.; Wochnik, A. S.; Henß, A.-K.; Wiechert, D.; Scheu, C.; Schmidt, P. J.; Schnick, W. Narrowband red-emitting $\text{Sr}[\text{LiAl}_3\text{N}_4]:\text{Eu}^{2+}$ as a next-generation LED phosphor material. *Nat. Mater.* **2014**, *13*, 891–896.
- (9) Pust, P.; Wochnik, A. S.; Baumann, E.; Schmidt, P. J.; Wiechert, D.; Scheu, C.; Schnick, W. $\text{Ca}[\text{LiAl}_3\text{N}_4]:\text{Eu}^{2+}$ —A Narrow-Band Red-Emitting Nitridolithoaluminate. *Chem. Mater.* **2014**, *26*, 3544–3549.
- (10) Höpfe, H. A.; Lutz, H.; Morys, P.; Schnick, W.; Seilmeier, A. Luminescence in Eu^{2+} -doped $\text{Ba}_2\text{Si}_5\text{N}_8$: fluorescence, thermoluminescence, and upconversion. *J. Phys. Chem. Solids* **2000**, *61*, 2001–2006.
- (11) Müller-Mach, R.; Müller, G.; Krames, M. R.; Hoeppe, H. A.; Stadler, F.; Schnick, W.; Jüstel, T.; Schmidt, P. Highly efficient all-nitride phosphor-converted white light emitting diode. *Phys. Status Solidi A* **2005**, *202*, 1727–1732.
- (12) Uheda, K.; Hirosaki, N.; Yamamoto, Y.; Naito, A.; Nakajima, T.; Yamamoto, H. Luminescence properties of a red phosphor, $\text{CaAlSiN}_3:\text{Eu}^{2+}$, for white light-emitting diodes. *Electrochem. Solid-State Lett.* **2006**, *9*, H22–H25.
- (13) Zeuner, M.; Schmidt, P. J.; Schnick, W. One-Pot Synthesis of Single-Source Precursors for Nanocrystalline LED Phosphors $M_2\text{Si}_5\text{N}_8:\text{Eu}^{2+}$ ($M = \text{Sr}, \text{Ba}$). *Chem. Mater.* **2009**, *21*, 2467–2473.
- (14) Pust, P.; Schnick, W.; Schmidt, P. J. A revolution in lighting. *Nat. Mater.* **2015**, *14*, 454–458.
- (15) Sheldrick, G. M. A short history of SHELX. *Acta Crystallogr., Sect. A: Found. Crystallogr.* **2008**, *64*, 112–122.
- (16) WINXPOW, v2.21; Stoe & Cie GmbH: Darmstadt, Germany, 2007.
- (17) Coelho, A. TOPAS—Academic; Coelho Software: Brisbane, Australia, 2007.
- (18) Egerton, R. F. *Electron Energy-Loss Spectroscopy in the Electron Microscope*. 3rd Edition; Springer: New York, 2011.
- (19) O’Keeffe, M.; Eddaoudi, M.; Li, H.; Reineke, T.; Yaghi, O. M. Frameworks for Extended Solids: Geometrical Design Principles. *J. Solid State Chem.* **2000**, *152*, 3–20.
- (20) Zintl, E.; Dullenkopf, W. Metals and Alloys. IV. Lattice Structure of Sodium Thallide and its Relation to Structures of the beta-Brass Type. *Z. Phys. Chem. B* **1932**, *16*, 195–205.

3. $\text{Ca}_{18.75}\text{Li}_{10.5}[\text{Al}_{39}\text{N}_{55}]:\text{Eu}^{2+}$ —Supertetrahedron Phosphor for Solid-State Lighting

- (21) Pagano, S.; Zeuner, M.; Hug, S.; Schnick, W. Single-Crystal Structure Determination and Solid-State NMR Investigations of Lithium Nitridosilicate Li_2SiN_2 Synthesized by a Precursor Approach Employing Amorphous “ $\text{Si}(\text{CN}_2)_2$ ”. *Eur. J. Inorg. Chem.* **2009**, 2009, 1579–1584.
- (22) Schnick, W.; Berger, U. $\text{Li}_{10}\text{P}_4\text{N}_{10}$ – A Lithium Phosphorous(V) Nitride Containing the New Complex Anion $\text{P}_4\text{N}_{10}^{10-}$. *Angew. Chem.* **1991**, 103, 857–858; *Angew. Chem., Int. Ed. Engl.* **1991**, 30, 830–831.
- (23) Huppertz, H.; Oeckler, O.; Lieb, A.; Glaum, R.; Johrendt, D.; Tegel, M.; Kaindl, R.; Schnick, W. $\text{Ca}_3\text{Sm}_3[\text{Si}_9\text{N}_{17}]$ and $\text{Ca}_3\text{Yb}_3[\text{Si}_9\text{N}_{17}]$ Nitridosilicates with Interpenetrating Nets that Consist of Star-Shaped $[\text{N}^{4-}(\text{SiN}_3)_4]$ Units and $[\text{Si}_5\text{N}_{16}]$ Supertetrahedra. *Chem.—Eur. J.* **2012**, 18, 10857–10864.
- (24) Döch, M.; Hammerschmidt, A.; Pütz, S.; Krebs, B. Isolated $\text{B}_{10}\text{Se}_{20}$ -Macrotetrahedra in the Novel Quaternary Selenoborate $\text{Li}_{6-2x}\text{Sr}_{2+x}\text{B}_{10}\text{Se}_{20}$ ($x \approx 0.7$). *Phosphorus, Sulfur Silicon Relat. Elem.* **2004**, 179, 933–935.
- (25) Li, H.; Kim, J.; Groy, T. L.; O’Keeffe, M.; Yaghi, O. M. 20 \AA $\text{Cd}_4\text{In}_{16}\text{S}_{35}^{14-}$ Supertetrahedral T4 Clusters as Building Units in Decorated Cristobalite Frameworks. *J. Am. Chem. Soc.* **2001**, 123, 4867–4868.
- (26) Wang, C.; Bu, X.; Zheng, N.; Feng, P. Nanocluster with One Missing Core Atom: A Three-Dimensional Hybrid Superlattice Built from Dual-Sized Supertetrahedral Clusters. *J. Am. Chem. Soc.* **2002**, 124, 10268–10269.
- (27) Wang, C.; Li, Y.; Bu, X.; Zheng, N.; Zivkovic, O.; Yang, C.-S.; Feng, P. Three-Dimensional Superlattices Built from $(\text{M}_4\text{In}_{16}\text{S}_{33})^{10-}$ ($\text{M} = \text{Mn}, \text{Co}, \text{Zn}, \text{Cd}$) Supertetrahedral Clusters. *J. Am. Chem. Soc.* **2001**, 123, 11506–11507.
- (28) Wang, L.; Wu, T.; Bu, X.; Zhao, X.; Zuo, F.; Feng, P. Coassembly between the Largest and Smallest Metal Chalcogenide Supertetrahedral Clusters. *Inorg. Chem.* **2013**, 52, 2259–2261.
- (29) Wang, L.; Wu, T.; Zuo, F.; Zhao, X.; Bu, X.; Wu, J.; Feng, P. Assembly of Supertetrahedral T_5 Copper-Indium Sulfide Clusters into a Super-Supertetrahedron of Infinite Order. *J. Am. Chem. Soc.* **2010**, 132, 3283–3285.
- (30) Hammerschmidt, A.; Hebel, P. z.; Hiltmann, F.; Krebs, B. Synthesis and Crystal Structures of $\text{Li}_{4-2x}\text{Sr}_{2+x}\text{B}_{10}\text{S}_{19}$ ($x \approx 0.27$) and $\text{Na}_6\text{B}_{10}\text{S}_{18}$, Two Novel Thioborates with Highly Polymeric Macrotetrahedral Networks. *Z. Anorg. Allg. Chem.* **1996**, 622, 76–84.
- (31) Li, H.; Laine, A.; O’Keeffe, M.; Yaghi, O. M. Supertetrahedral sulfide crystals with giant cavities and channels. *Science* **1999**, 283, 1145–1147.
- (32) Baur, W. H. Effective Ionic Radii in Nitrides. *Crystallogr. Rev.* **1987**, 1, 59–83.
- (33) Slater, J. C. Atomic Radii in Crystals. *J. Chem. Phys.* **1964**, 41, 3199–3204.
- (34) Schmiechen, S.; Nietschke, F.; Schnick, W. Structural Relationship between the Mg-Containing Nitridosilicates $\text{Ca}_2\text{Mg}[\text{Li}_4\text{Si}_2\text{N}_6]$ and $\text{Li}_2\text{Ca}_2[\text{Mg}_2\text{Si}_2\text{N}_6]$. *Eur. J. Inorg. Chem.* **2015**, 2015, 1592–1597.
- (35) Möller, A.; Amann, P.; Kataev, V.; Schittner, N. The First T_5 -Supertetrahedron in Oxide Chemistry: $\text{Na}_{26}\text{Mn}_{39}\text{O}_{55}$. *Z. Anorg. Allg. Chem.* **2004**, 630, 890–894.
- (36) Dierre, B.; Yuan, X. L.; Inoue, K.; Hirosaki, N.; Xie, R.-J.; Sekiguchi, T. Role of Si in the Luminescence of $\text{AlN}:\text{Eu},\text{Si}$ Phosphors. *J. Am. Ceram. Soc.* **2009**, 92, 1272–1275.
- (37) Yin, L.-J.; Chen, G.-Z.; Zhou, Z.-Y.; Jian, X.; Xu, B.; He, J.-H.; Tang, H.; Luan, C.-H.; Xu, X.; van Ommen, J. R.; Hintzen, H. T. Improved Blue-Emitting $\text{AlN}:\text{Eu}^{2+}$ Phosphors by Alloying with GaN. *J. Am. Ceram. Soc.* **2015**, 98, 3897–3904.

3. $\text{Ca}_{18.75}\text{Li}_{10.5}[\text{Al}_{39}\text{N}_{55}]:\text{Eu}^{2+}$ —Supertetrahedron Phosphor for Solid-State Lighting

- (38) Krames, M.; Mueller, G. O.; Mueller-Mach, R.; Bechtel, H.; Schmidt, P. J. Wavelength conversion for producing white light from high power blue led, *PCT Int. Appl. WO 2010131133 A1*, 2010.
- (39) Uheda, K.; Hirosaki, N.; Yamamoto, H. Host lattice materials in the system $\text{Ca}_3\text{N}_2\text{-AlN-Si}_3\text{N}_4$ for white light emitting diode. *Phys. Status Solidi A* **2006**, *203*, 2712–2717.
- (40) Dirksen, G. J.; Blasse, G. Luminescence in the Pentaborate $\text{LiBa}_2\text{B}_5\text{O}_{10}$. *J. Solid State Chem.* **1991**, *92*, 591–593.
- (41) Kechele, J. A.; Oeckler, O.; Stadler, F.; Schnick, W. Structure elucidation of $\text{BaSi}_2\text{O}_2\text{N}_2$ - A host lattice for rare-earth doped luminescent materials in phosphor-converted (pc)-LEDs. *Solid State Sci.* **2009**, *11*, 537–543.
- (42) Seibald, M.; Rosenthal, T.; Oeckler, O.; Schnick, W. Highly Efficient pc-LED Phosphors $\text{Sr}_{1-x}\text{Ba}_x\text{Si}_2\text{O}_2\text{N}_2:\text{Eu}^{2+}$ ($0 \leq x \leq 1$) - Crystal Structures and Luminescence Properties Revisited. *Crit. Rev. Solid State Mater. Sci.* **2014**, *39*, 215–229.
- (43) Mauchamp, V.; Moreau, P.; Monconduit, L.; Doublet, M.-L.; Boucher, F.; Ouvrard, G. Determination of Lithium Insertion Sites in Li_xTiP_4 ($x = 2\text{--}11$) by Electron Energy-Loss Spectroscopy. *J. Phys. Chem. C* **2007**, *111*, 3996–4002.
- (44) Zeuner, M.; Pagano, S.; Hug, S.; Pust, P.; Schmiechen, S.; Scheu, C.; Schnick, W. $\text{Li}_2\text{CaSi}_2\text{N}_4$ and $\text{Li}_2\text{SrSi}_2\text{N}_4$ —A Synthetic Approach to Three-Dimensional Lithium Nitridosilicates. *Eur. J. Inorg. Chem.* **2010**, *2010*, 4945–4951.
- (45) Scheu, C.; Dehm, G.; Muellejans, H.; Brydson, R.; Ruehle, M. Electron Energy-Loss Near-Edge Structure of Metal–Alumina Interfaces. *Microsc., Microanal., Microstruct.* **1995**, *6*, 19–31.
- (46) Schmiechen, S.; Schneider, H.; Wagatha, P.; Hecht, C.; Schmidt, P. J.; Schnick, W. Toward New Phosphors for Application in Illumination-Grade White pc-LEDs: The Nitridomagnesosilicates $\text{Ca}[\text{Mg}_3\text{SiN}_4]:\text{Ce}^{3+}$, $\text{Sr}[\text{Mg}_3\text{SiN}_4]:\text{Eu}^{2+}$, and $\text{Eu}[\text{Mg}_3\text{SiN}_4]$. *Chem. Mater.* **2014**, *26*, 2712–2719.
- (47) Dorenbos, P. Thermal quenching of Eu^{2+} 5d–4f luminescence in inorganic compounds. *J. Phys.: Condens. Matter* **2005**, *17*, 8103–8111

4. Tunable Red Luminescence in

Nitridomagnesoaluminates α - $\text{Sr}_2[\text{MgAl}_5\text{N}_7]:\text{Eu}^{2+}$,

β - $\text{Sr}_2[\text{MgAl}_5\text{N}_7]:\text{Eu}^{2+}$ and $\text{Sr}_8[\text{LiMg}_2\text{Al}_{21}\text{N}_{28}]:\text{Eu}^{2+}$

published in: *Chem. Mater.* **2018**, *30*, 1755–1761

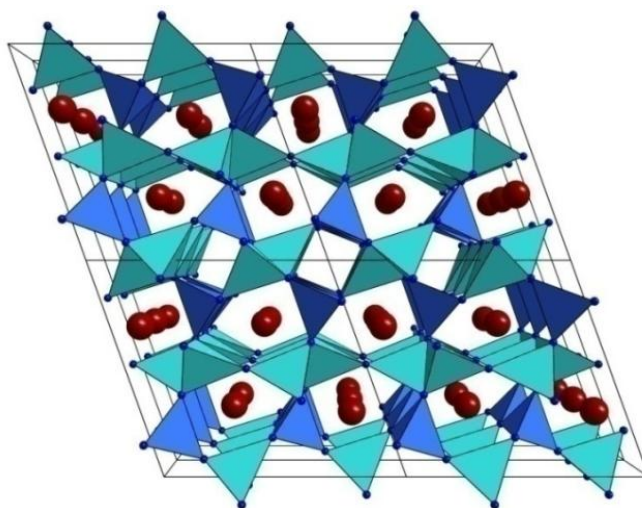
authors: Peter Wagatha, Volker Weiler, Peter J. Schmidt and Wolfgang Schnick

DOI: 10.1021/acs.chemmater.8b00106

Reprinted with permission from American Chemical Society, Copyright © 2018

Abstract

Red-emitting phosphors with the general sum formula $\text{Sr}_8[\text{Li}_{(2-0.5x)}\text{Mg}_x\text{Al}_{(22-0.5x)}\text{N}_{28}]:\text{Eu}^{2+}$ for application in warm-white illumination grade light emitting diodes were obtained by reacting the metals, hydrides, and nitrides in molybdenum crucibles in a hot



isostatic press. Upon irradiation with blue light (440 nm), the materials exhibit red luminescence (emission maximum: 633–665 nm; full width at half-maximum (fwhm): 1736–1964 cm^{-1} , 78–82 nm) tunable by adjusting the compositional variable x (here, 2 and 4) as well as the activator concentration (here, 0.075–1 atom-% Eu^{2+}). The materials show promising thermal behavior of the emission with relative quantum efficiencies, compared to room temperature, of 66% ($x = 0$) and 84% ($x = 2$) at 200 °C. α - $\text{Sr}_8[\text{Li}_{(2-0.5x)}\text{Mg}_x\text{Al}_{(22-0.5x)}\text{N}_{28}]:\text{Eu}^{2+}$ ($x = 2$ and 4) crystallizes isotypically with $\text{Sr}_4[\text{LiAl}_{11}\text{N}_{14}]:\text{Eu}^{2+}$ in the orthorhombic space group $Pn\bar{m}$ (no. 58) with unit cell parameters $a = 10.51818(5)$ – $10.54878(6)$, $b = 10.44513(5)$ – $10.48253(6)$, and $c = 3.25704(1)$ – $3.272752(15)$ Å. β - $\text{Sr}_2[\text{MgAl}_5\text{N}_7]:\text{Eu}^{2+}$ ($x = 4$) crystallizes in the monoclinic space group $C2/m$ (no. 12) with unit

4. Tunable Red Luminescence in Nitridomagnesoaluminates



cell parameters $a = 11.12874(11)$, $b = 3.27289(3)$, $c = 10.54530(11)$ Å, and $\beta = 109.8939(7)^\circ$ and is obtained as side phase (≤ 40 wt%) in syntheses with $x = 4$. The crystal structure of $\beta\text{-Sr}_2[\text{MgAl}_5\text{N}_7]:\text{Eu}^{2+}$ consists of a network of vertex- and edge-sharing Al(/Mg)N₄ tetrahedra with four- and five-membered ring channels along [010]. The Sr²⁺ ions are located within the five-membered ring channels and are coordinated cube-like by eight N atoms.

Introduction

Solid state lighting solutions have become increasingly popular over the past decade. Be it for automotive applications, public lighting, and general illumination, light emitting diodes (LEDs) claim an ever expanding market share. Especially, white LEDs for general illumination exhibit superior properties compared to conventional incandescent or fluorescent light sources. Long lifetime and reliability combined with high luminous efficacy and energy efficiency result in improved environmental friendliness.

In general, white LEDs are manufactured by combining a blue LED with one or more downconversion phosphors. Traditionally, broadband yellow emitting Y₃Al₅O₁₂:Ce³⁺ (YAG:Ce) is used as phosphor material. Such LEDs exhibit high luminous efficacies, but applications are limited due to the low color rendering indices (CRI < 70) and high correlated color temperatures (CCT \approx 4000–8000 K). For high-CRI illumination-grade white LEDs, the red-emitting phosphor is of great importance. A commonly used red luminescent material, e.g., is Sr_{1-x}Ca_xAlSiN₃:Eu²⁺ (SCASN). A major drawback of this material is the relatively broad emission band (fwhm \approx 2100–2500 cm⁻¹) resulting in limited luminous efficacy.^{1,2} In the (deep)red spectral region, narrow-band emission with little IR spillover is critical for achieving the high chromatic saturation necessary for excellent color rendition while preserving a high luminous efficacy.³ Here, the nitridolithoaluminate Sr[LiAl₃N₄]:Eu²⁺ (SLA) emerged as a highly promising red phosphor material for efficient white LEDs with excellent color rendition properties. Exhibiting narrow band deep red emission at $\lambda_{\text{em}} = 650$ nm and fwhm = 1180 cm⁻¹, prototype high-CRI white LEDs show a luminous efficacy increase of 14% compared to commercially available products.⁴

The discovery of Sr[LiAl₃N₄]:Eu²⁺ and its superior luminescence properties have sparked strong interest in the nitridoaluminate compound class. Prior to SLA, only few nitridoaluminates were known and had been investigated concerning their optical

4. Tunable Red Luminescence in Nitridomagnesoaluminates α -Sr₂[MgAl₅N₇]:Eu²⁺, β -Sr₂[MgAl₅N₇]:Eu²⁺ and Sr₈[LiMg₂Al₂₁N₂₈]:Eu²⁺

properties. Kniep and co-workers contributed mainly to the early research but did not report on luminescence upon doping with Eu.⁵⁻⁷ No luminescence was observed in Ca[LiAlN₂],⁸ but almost simultaneously to the discovery of SLA, the structurally closely related red luminescent materials M [Mg₂Al₂N₄]:Eu²⁺ ($M = \text{Ca, Sr, Ba, Eu}$) and Ca[LiAl₃N₄]:Eu²⁺ were found.^{9,10} More recently described materials include Ca[Mg₂AlN₃] exhibiting activator-free orange defect luminescence,¹¹ narrow-red emitting Ca_{18.75}Li_{10.5}[Al₃₉N₅₅]:Eu²⁺ with its unusual supertetrahedroncontaining crystal structure,¹² and Mg₃Al _{n} N _{$n+2$} ($n = 1, 2, 3$) showing either red Eu³⁺ or yellow Eu²⁺ luminescence.¹³ Of special interest for this work was the very recent discovery of deep-red emitting Sr₄[LiAl₁₁N₁₄]:Eu²⁺ with $\lambda_{\text{em}} = 670 \text{ nm}$ and $\text{fwhm} = 1880 \text{ cm}^{-1}$.¹⁴

As high color rendition and high luminous efficacy ultimately are mutually exclusive properties, optimal values for both emission maximum and fwhm can be defined. Compared to white LEDs with SLA, a further increase in luminous efficacy by 14% could be achieved by using a red emitting material with $\lambda_{\text{em}} \approx 630 \text{ nm}$ and $\text{fwhm} \approx 1180 \text{ cm}^{-1}$. Because of its high sensitivity to moisture and low quantum efficiency at room temperature, nitridomagnesosilicate Sr[Mg₃SiN₄]:Eu²⁺ is not industrially used despite its nearly optimal emission characteristics.¹⁵ Here, we present the novel phosphors α - and β -Sr₂[MgAl₅N₇]:Eu²⁺ as well as Sr₈[LiMg₂Al₂₁N₂₈]:Eu²⁺, their preparation, crystal-structure determination, and luminescence properties, as well as their potential for application in high color rendition white LEDs for general lighting.

Experimental Section

Synthesis

All reagents and samples were handled under the exclusion of moisture and oxygen in an Ar-filled glovebox (Unilab, MBraun, Garching, O₂ < 1 ppm, H₂O < 1 ppm). Representatives of the solid-solution series with the general sum formula Sr₈[Li_(2-0.5x)Mg_xAl_(22-0.5x)N₂₈]:Eu²⁺ (nominal Eu concentration: 0.075–1 mol %) were synthesized in molybdenum crucibles in a hot isostatic press. The starting materials SrH₂ (Materion, 99.5%), Li₃N (Materion, 99.5%), Mg (Alfa Aesar, 99.8%), AlN (H.C. Starck, grade B), and Eu₂O₃ (Neo, 99.99%) were mixed in stoichiometric amounts by ball milling. Subsequently, the mixture was transferred into the

4. Tunable Red Luminescence in Nitridomagnesoaluminates

α -Sr₂[MgAl₅N₇]:Eu²⁺, β -Sr₂[MgAl₅N₇]:Eu²⁺ and Sr₈[LiMg₂Al₂₁N₂₈]:Eu²⁺

crucible and heated at 1550 °C for 5 h in a nitrogen atmosphere. Nitrogen pressure was maintained at 50 MPa during the synthesis. α -Sr₂[MgAl₅N₇]:Eu²⁺ (compositional variable $x = 4$) and Sr₈[LiMg₂Al₂₁N₂₈]:Eu²⁺ ($x = 2$) were obtained as finely crystalline, powdery products with orange body color and red luminescence upon irradiation with blue to green light. β -Sr₂[MgAl₅N₇]:Eu²⁺ was obtained as side phase (≤ 40 wt %) in some syntheses that yielded a powdery gray product.

Powder X-ray Diffraction

Powder X-ray diffraction data were collected on a STOE Stadi P diffractometer with CuK α ₁ radiation ($\lambda = 1.5406$ Å) in parafocusing Debye-Scherrer geometry with a Ge(111) monochromator and a Mythen 1K detector. Samples were loaded into glass capillaries with 0.3 mm diameter and 0.01 mm wall thickness (Hilgenberg, Germany). The TOPAS-Academic V4.1 software package, applying the fundamental parameters approach (direct convolution of source emission profiles, axial instrument contributions, crystallite size, and microstrain effects), was used for Rietveld refinement.^{16–19} Absorption effects were corrected using the calculated absorption coefficient. Preferred orientation was handled with the spherical harmonics model of fourth/sixth order. Details on the structure investigation may be obtained from the Cambridge Crystallographic Data Centre on quoting the depository no. CCDC 1813230.

Electron Microscopy

A Dualbeam Helios Nanolab G3 UC (FEI) scanning electron microscope (SEM), equipped with an X-Max 80 SDD (Oxford Instruments) energy-dispersive X-ray (EDX) detector, was used for electron microscope investigations.

EDX Spectroscopy

The chemical composition of the samples and individual crystallites was determined by EDX spectroscopy at an acceleration voltage of 5 kV.

Luminescence

Luminescence measurements on powder samples in PTFE sample holders were conducted on an in-house built system based on a 5.3 in. integrating sphere and a spectrofluorimeter

4. Tunable Red Luminescence in Nitridomagnesoaluminates

α - $\text{Sr}_2[\text{MgAl}_5\text{N}_7]:\text{Eu}^{2+}$, β - $\text{Sr}_2[\text{MgAl}_5\text{N}_7]:\text{Eu}^{2+}$ and $\text{Sr}_8[\text{LiMg}_2\text{Al}_{21}\text{N}_{28}]:\text{Eu}^{2+}$

equipped with a 150 W Xe lamp, two 500 mm Czerny-Turner monochromators, 1800 1/mm lattices, and 250/500 nm lamps, with a spectral range from 230 to 820 nm.

Results and Discussion

Synthesis and Chemical Analysis

The above-mentioned synthesis yielded access to the solid solution series $\text{Sr}_8[\text{Li}_{(2-0.5x)}\text{Mg}_x\text{Al}_{(22-0.5x)}\text{N}_{28}]:\text{Eu}^{2+}$ ($0 \leq x \leq 4$). α - $\text{Sr}_2[\text{MgAl}_5\text{N}_7]:\text{Eu}^{2+}$ ($x = 4$) and $\text{Sr}_8[\text{LiMg}_2\text{Al}_{21}\text{N}_{28}]:\text{Eu}^{2+}$ ($x = 2$) were obtained as finely crystalline powders with bright orange body color and intense red luminescence upon irradiation with blue to green light.

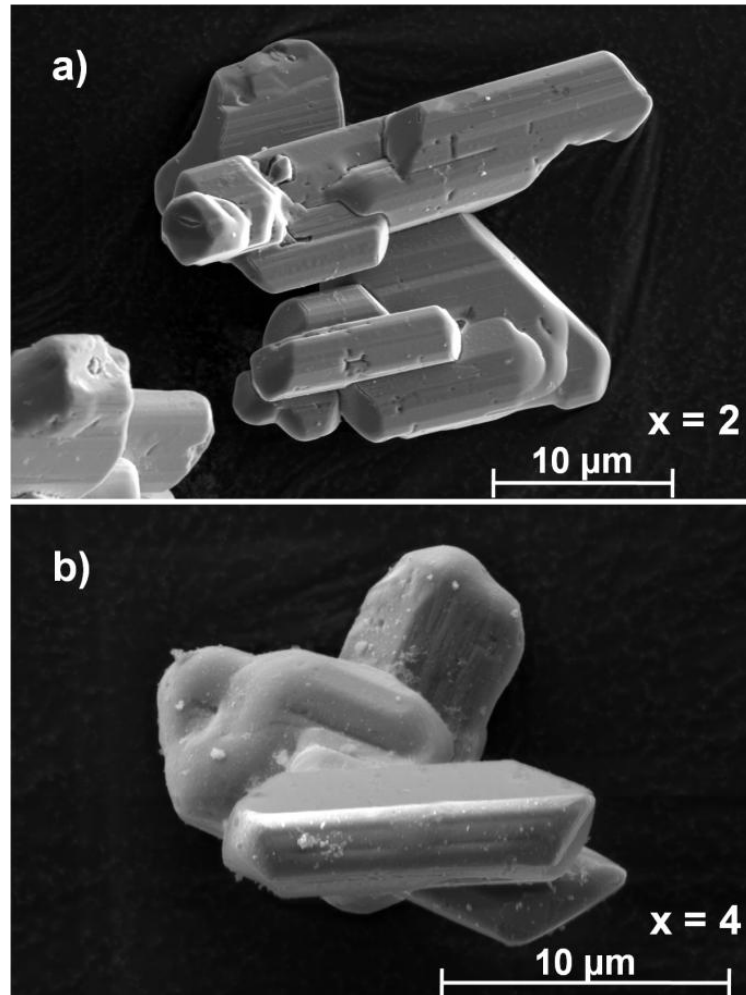


Figure 4.1. SEM images of (a) $\text{Sr}_8[\text{LiMg}_2\text{Al}_{21}\text{N}_{28}]:\text{Eu}^{2+}$ and (b) $\text{Sr}_2[\text{MgAl}_5\text{N}_7]:\text{Eu}^{2+}$.

Atomic ratios of Sr:Mg:Al:N of 2:1.1:4.4:7 ($x = 4$) and 8:2.1:18.8:25.6 ($x = 2$) were determined by EDX measurements on several crystallites. These atomic ratios correspond well with the

4. Tunable Red Luminescence in Nitridomagnesoaluminates



sum formulas (2:1:5:7, $x = 4$; 4:1:10.5:14, $x = 2$). The typical morphology of crystals of the solid-solution series is shown in Figure 4.1. Measured nitrogen concentrations are lower than expected due to surface hydrolyzation of the materials and the surface sensitivity of EDX spectroscopy especially at the low acceleration voltages used.

Crystal Structure

$\alpha\text{-Sr}_2[\text{MgAl}_5\text{N}_7]$ (and $\text{Sr}_8[\text{LiMg}_2\text{Al}_{21}\text{N}_{28}]$) crystallizes isotypically with $\text{Sr}_4[\text{LiAl}_{11}\text{N}_{14}]$ in the orthorhombic space group $Pn\bar{m}$ (no. 58) with unit-cell parameters $a = 10.5489(2)$ (10.44519(16)), $b = 10.4824(2)$ (10.51822(16)), $c = 3.27276(1)$ Å (3.25706(9) Å) and $V = 361.894(3)$ Å³ (357.831(3) Å³). For Rietveld refinement, the structural model of $\text{Sr}_4[\text{LiAl}_{11}\text{N}_{14}]$ reported by Wilhelm et al. from single-crystal X-ray diffraction data was modified and used.¹⁴ Due to its low content of ≤ 1 mol % and the therefore negligible additional scattering power compared to Sr, Eu was disregarded during the refinement. Crystallographic data from the Rietveld refinements are given in Table 4.1. Similar to $\text{Sr}_4[\text{LiAl}_{11}\text{N}_{14}]$, the Al1/Mg1 site in $\alpha\text{-Sr}_2[\text{MgAl}_5\text{N}_7]$ is statistically occupied by Al³⁺ and Mg²⁺ in an atomic ratio of 0.58:0.42.

Due to the observed elongated Al–N distances of the Al3 site, a statistical occupation with Mg was assumed, with an atomic ratio from Rietveld refinement of 0.92:0.08. Naturally, Mg and Al cannot be reliably distinguished by X-ray diffraction due to their virtually identical number of electrons. In this case, the results from XRD data were accepted because of their conformity with the atomic ratios from EDX measurements. Both relative occupancies were refined constrained due to the demand for electroneutrality, resulting in a total Al:Mg ratio of 5:1. A plot of the Rietveld refinement of $\alpha\text{-Sr}_2[\text{MgAl}_5\text{N}_7]:\text{Eu}^{2+}$ is shown in Figure 4.2. In $\text{Sr}_8[\text{LiMg}_2\text{Al}_{21}\text{N}_{28}]:\text{Eu}^{2+}$, the atomic ratios on the mixed occupancy Al1/Mg1/Li1 site are 0.613:0.274:0.113 according to the XRD data. The refinement was restrained to allow only electroneutral sum formulas, i.e., a total Al/Mg/Li ratio of 20.9:2.2:0.9. Like in $\text{Sr}_2[\text{MgAl}_5\text{N}_7]:\text{Eu}^{2+}$, a statistical disorder of the Al3/Mg3/Li3 site can be taken into consideration for explaining the slightly elongated Al3–N distances observed. A plot of the Rietveld refinement of $\text{Sr}_8[\text{LiMg}_2\text{Al}_{21}\text{N}_{28}]:\text{Eu}^{2+}$ is shown in Figure 4.3.

Table 4.1. Crystallographic Data of the Rietveld Refinement of α -Sr₂[MgAl₅N₇]:Eu²⁺ and Sr₈[LiMg₂Al₂₁N₂₈]:Eu²⁺

sum formula	α -Sr ₂ [MgAl ₅ N ₇]	Sr ₈ [LiMg ₂ Al ₂₁ N ₂₈]
crystal system		orthorhombic
space group		<i>Pnnm</i> (no. 58)
lattice parameters		
<i>a</i> /Å	10.54878(6)	10.51818(5)
<i>b</i> /Å	10.48253(6)	10.44513(5)
<i>c</i> /Å	3.272752(15)	3.25704(1)
<i>V</i> /Å ³	361.894(3)	357.831(3)
formula units/cell		1
calculated density/gcm ⁻¹	3.96905(14)	3.9834(10)
<i>T</i> /K		273
diffractometer		STOE Stadi P
radiation		CuK α_1 (λ = 1.54056 Å)
range/deg.		4.0 \leq 2 θ \leq 100.5
background function		Chebychev polynomial (12 parameters)
	<i>R_p</i> = 0.0390	<i>R_p</i> = 0.0409
<i>R</i> values	<i>R_{wp}</i> = 0.0532	<i>R_{wp}</i> = 0.0547
	<i>R_{Bragg}</i> = 0.0225	<i>R_{Bragg}</i> = 0.0245
goodness of fit	3.99	1.85

The crystal structure is homeotypic to the oxozincate K₂Zn₆O₇ and consists of a three-dimensional network of vertex- and edge-sharing distorted tetrahedra with two types of channels in the [001] direction (see Figure 4.4).²⁰ The AlN₄ tetrahedra form *einer* double chains along [001].²¹ Four of these chains are condensed to *achter* rings via common vertices with the opposing chains pointing either inward or outward. Each inward facing *einer* double chain of one *achter* ring is the outward facing *einer* double chain of the adjacent *achter* ring. This kind of arrangement leads to empty *vierer* ring channels between the *achter* rings. The *achter* rings are each subdivided into two *fünfer* rings by two bridging vertex-sharing *einer* single chains of AlN₄ tetrahedra with opposing directions of travel that share common edges with the outward facing *einer* double chains.

4. Tunable Red Luminescence in Nitridomagnesoaluminates

α - $\text{Sr}_2[\text{MgAl}_5\text{N}_7]:\text{Eu}^{2+}$, β - $\text{Sr}_2[\text{MgAl}_5\text{N}_7]:\text{Eu}^{2+}$ and $\text{Sr}_8[\text{LiMg}_2\text{Al}_{21}\text{N}_{28}]:\text{Eu}^{2+}$

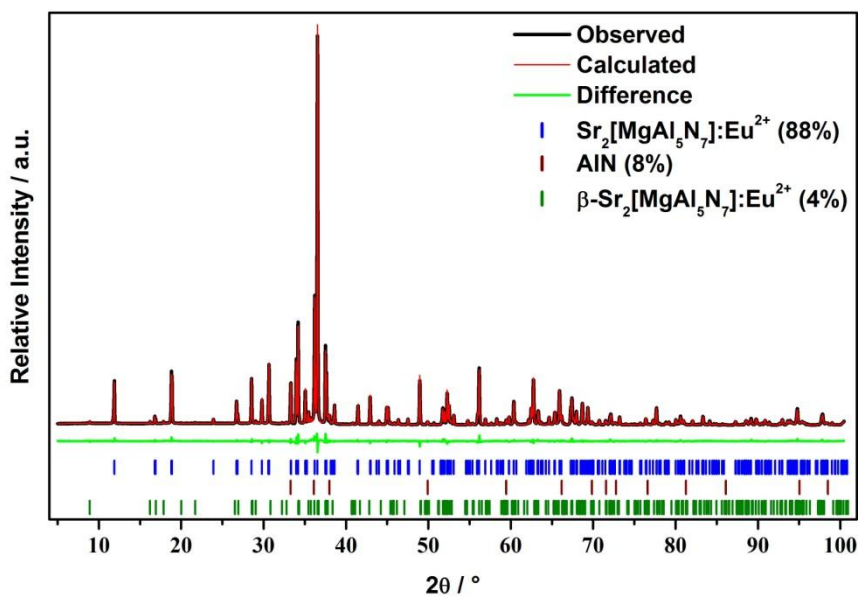


Figure 4.2. Rietveld fit of PXRD data of α - $\text{Sr}_2[\text{MgAl}_5\text{N}_7]:\text{Eu}^{2+}$ ($\text{CuK}\alpha_1$, $\lambda = 1.54056 \text{ \AA}$). The side phases AIN (8 wt %) and β - $\text{Sr}_2[\text{MgAl}_5\text{N}_7]:\text{Eu}^{2+}$ (4 wt %) were identified.

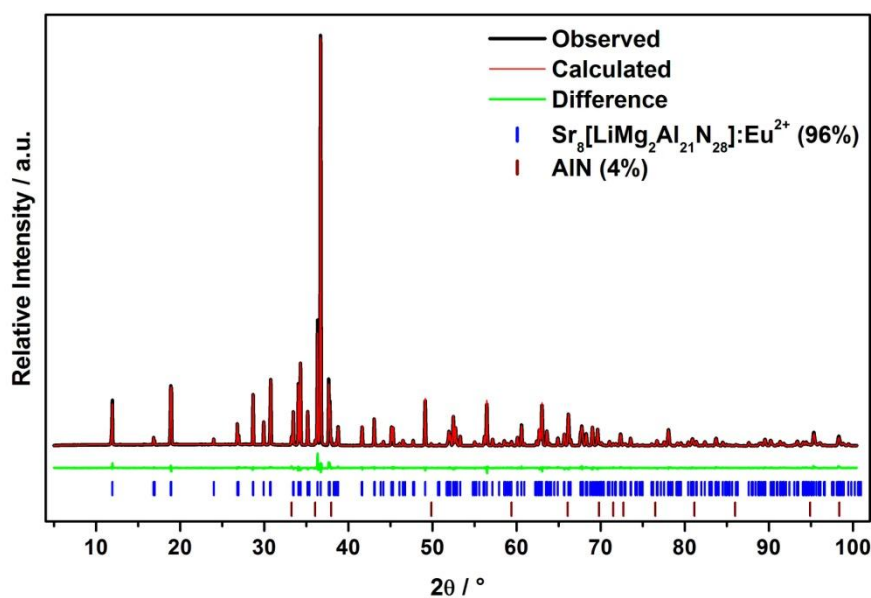


Figure 4.3. Rietveld fit of PXRD data of $\text{Sr}_8[\text{LiMg}_2\text{Al}_{21}\text{N}_{28}]:\text{Eu}^{2+}$ ($\text{CuK}\alpha_1$, $\lambda = 1.54056 \text{ \AA}$). The side-phase AIN (4 wt %) was identified.

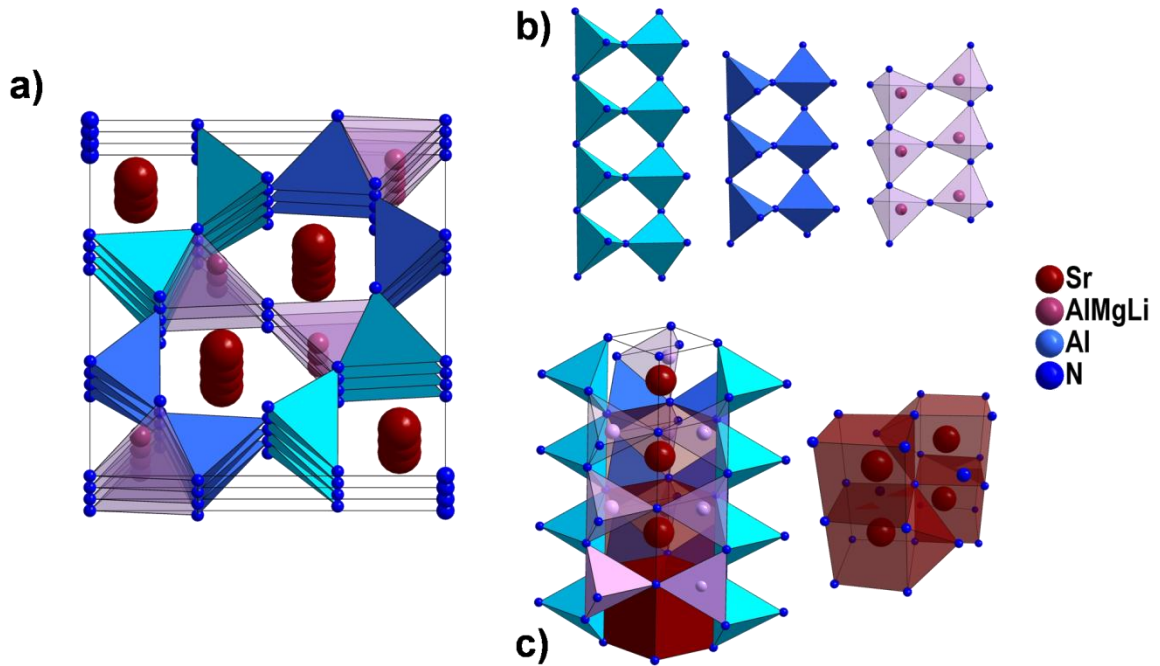


Figure 4.4. Crystal-structure representation of $\text{Sr}_8[\text{Li}_{(2-0.5x)}\text{Mg}_x\text{Al}_{(22-0.5x)}\text{N}_{28}]:\text{Eu}^{2+}$. Alternating inward- and outward-facing *einer* double chains colored blue and light blue, bridging *einer* single chains colored purple, $\text{SrN}_{8(+1)}$ polyhedra chains colored red. (a) View of a stack of three unit cells along [001]. (b) Types of chains formed by $(\text{Al/Mg/Li})\text{N}_4$ tetrahedra. (c) Coordination sphere of Sr and $\text{SrN}_{8(+1)}$ polyhedra.

In total, the high degree of condensation $\kappa = 0.857$ promises a rigid network preferable for use as Eu doped host lattice. A different description of the same network can be found in the literature.¹⁴

The Sr^{2+} counterions are located within these *fünfer* rings. They are coordinated cube-like by eight N atoms, with one polyhedron face capped by a ninth N atom located at a 17% increased distance. Since the distance to the ninth N atom is larger than to the nearest Al/Mg atoms, it is not considered part of the anionic coordination sphere. The SrN_8 -polyhedra share faces forming infinite strands in the [001] direction, with two of these strands being linked via common edges. Bond lengths in $\text{Sr}_2[\text{MgAl}_5\text{N}_7]$ and $\text{Sr}_8[\text{LiMg}_2\text{Al}_{21}\text{N}_{28}]$ are in good agreement with other nitrido(litho)magnesoaluminates.

4. Tunable Red Luminescence in Nitridomagnesoaluminates

α - $\text{Sr}_2[\text{MgAl}_5\text{N}_7]:\text{Eu}^{2+}$, β - $\text{Sr}_2[\text{MgAl}_5\text{N}_7]:\text{Eu}^{2+}$ and $\text{Sr}_8[\text{LiMg}_2\text{Al}_{21}\text{N}_{28}]:\text{Eu}^{2+}$

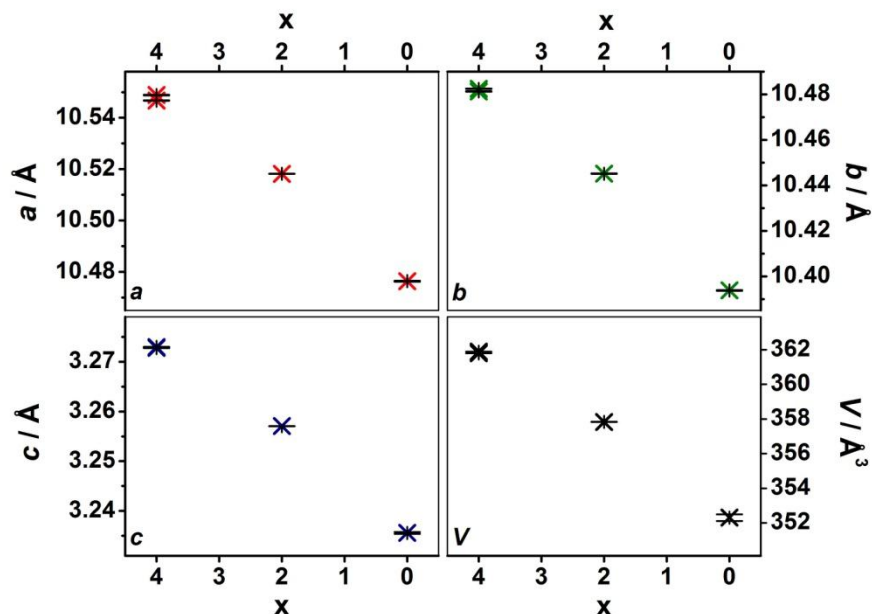


Figure 4.5. Comparison of the orthorhombic unit-cell parameters (a , b , c , V) of $\text{Sr}_8[\text{Li}_{(2-0.5x)}\text{Mg}_x\text{Al}_{(22-0.5x)}\text{N}_{28}]:\text{Eu}^{2+}$ with $x = 0, 2$, and 4 . Values for $x = 0$ were taken from the literature.¹⁴

In $\text{Sr}_2[\text{MgAl}_5\text{N}_7]$ and $\text{Sr}_8[\text{LiMg}_2\text{Al}_{21}\text{N}_{28}]$, Al–N distances are 1.823(6)–1.939(3) Å, values well within the range given in the literature (e.g., $\text{Sr}[\text{LiAl}_3\text{N}_4]$: 1.87–2.00 Å;⁴ $\text{Ca}_{18.75}\text{Li}_{10.5}[\text{Al}_{39}\text{N}_{55}]$: 1.8086(14)–1.9805(14) Å).¹² Al/Mg(Li)–N distances vary from 1.823(6) to 2.182(6) Å (2.125(4) Å) corresponding with the average of Al–N, Mg–N, and Li–N distances reported in $\text{Sr}_3\text{Al}_2\text{N}_4$ (1.86–1.96 Å), CaMg_2N_2 (2.13–2.30 Å), and $\text{Ca}[\text{LiAl}_3\text{N}_4]$ (2.043(3)–2.278(7) Å), respectively.^{5,10,22} Sr–N bond lengths (2.644(1)–2.970(5) Å for the cube-like coordination) are close to the reported values for $\text{Sr}_4[\text{LiAl}_{11}\text{N}_{14}]$ (2.617(1)–2.928(2) Å) and other Sr-nitridoaluminates.^{4,14} A comparison of the experimental unit-cell parameters of $\text{Sr}_8[\text{Li}_{(2-0.5x)}\text{Mg}_x\text{Al}_{(22-0.5x)}\text{N}_{28}]:\text{Eu}^{2+}$ ($x = 0, 2, 4$) is shown in Figure 4.5. The observed linear dependence of all parameters on the Mg concentration is in good accordance with Vegard’s rule for unlimited miscibility and strongly supports the denomination as solid solution series.

β - $\text{Sr}_2[\text{MgAl}_5\text{N}_7]:\text{Eu}^{2+}$

β - $\text{Sr}_2[\text{MgAl}_5\text{N}_7]:\text{Eu}^{2+}$ was obtained as side phase with ≤ 40 wt % during syntheses of α - $\text{Sr}_2[\text{MgAl}_5\text{N}_7]:\text{Eu}^{2+}$. It crystallizes in the monoclinic space group $C2/m$ (no. 12) with unit-cell parameters $a = 11.12874(11)$, $b = 3.27289(3)$, $c = 10.54530(11)$ Å, $\beta = 109.8939(7)^\circ$, and $V = 361.173(7)$ Å³. Crystallographic data from the Rietveld refinement is presented in

4. Tunable Red Luminescence in Nitridomagnesoaluminates
 α -Sr₂[MgAl₅N₇]:Eu²⁺, β -Sr₂[MgAl₅N₇]:Eu²⁺ and Sr₈[LiMg₂Al₂₁N₂₈]:Eu²⁺

Table 4.2; atomic coordinates, isotropic displacement parameters, and site occupancy factors (SOF) are in Table 4.3.

Table 4.2. Crystallographic Data of the Rietveld Refinement of β -Sr₂[MgAl₅N₇]:Eu²⁺

sum formula	β -Sr ₂ [MgAl ₅ N ₇]
crystal system	monoclinic
space group	<i>C2/m</i> (no. 12)
lattice parameters	
<i>a</i> /Å	11.12874(11)
<i>b</i> /Å	3.27289(3)
<i>c</i> /Å	10.54530(11)
β /°	109.8939(7)
<i>V</i> /Å ³	361.173(7)
formula units/cell	1
calculated density/gcm ⁻³	3.97696(7)
<i>T</i> /K	273
diffractometer	STOE Stadi P
radiation	CuK α_1 (λ = 1.54056 Å)
range/deg.	4.0 ≤ 2 θ ≤ 100.5
background function	Chebychev polynomial (18 parameters)
	<i>R</i> _p = 0.0508
<i>R</i> values	<i>R</i> _{wp} = 0.0693
	<i>R</i> _{Bragg} = 0.0249
goodness of fit	4.27

A plot of the Rietveld refinement is shown in Figure 4.6. Two of the three Al sites show mixed occupancy with Mg, namely, the Al1(/Mg1) and Al2(/Mg2) sites. Each site was refined to 25% Mg occupancy.

4. Tunable Red Luminescence in Nitridomagnesoaluminates

α - $\text{Sr}_2[\text{MgAl}_5\text{N}_7]:\text{Eu}^{2+}$, β - $\text{Sr}_2[\text{MgAl}_5\text{N}_7]:\text{Eu}^{2+}$ and $\text{Sr}_8[\text{LiMg}_2\text{Al}_{21}\text{N}_{28}]:\text{Eu}^{2+}$

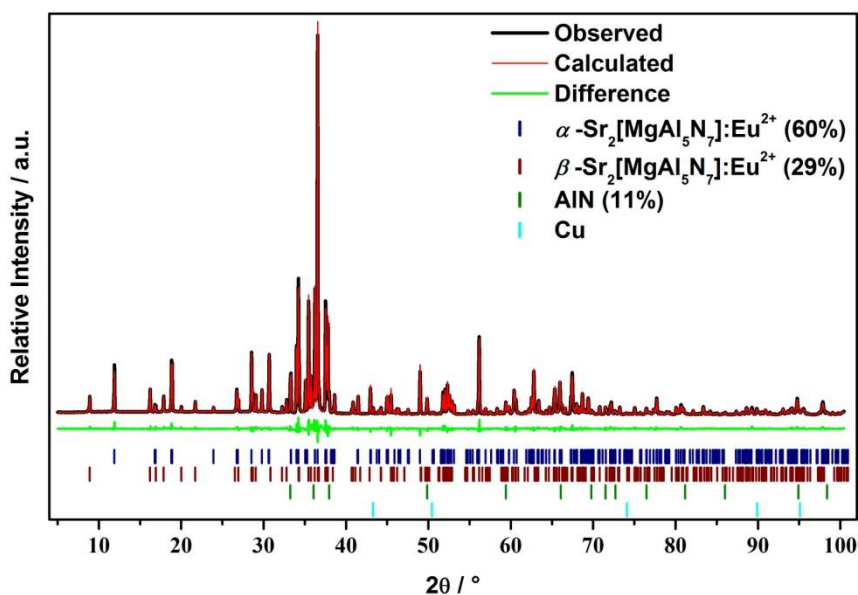


Figure 4.6. Rietveld fit of PXRD data of α - and β - $\text{Sr}_2[\text{MgAl}_5\text{N}_7]:\text{Eu}^{2+}$. β - $\text{Sr}_2[\text{MgAl}_5\text{N}_7]:\text{Eu}^{2+}$ was quantified to ≈ 29 wt %, with side phase AlN (11 wt %) and traces of Cu.

Table 4.3. Atomic Coordinates, Isotropic Displacement Parameters, and Site Occupancy Factors (SOF) of β - $\text{Sr}_2[\text{MgAl}_5\text{N}_7]:\text{Eu}^{2+a}$

atom	Wyckoff position	x	y	z	$U_{\text{iso}}/\text{\AA}^2$	SOF
Sr1	4i	0.6279(2)	1/2	0.69632(16)	0.0210(8)	1
Al1	4i	0.6450(5)	0	0.4457(5)	0.026(2)	0.75
Mg1	4i	0.6450(5)	0	0.4457(5)	0.026(2)	0.25
Al2	4i	0.3520(5)	0	0.0165(5)	0.023(2)	0.75
Mg2	4i	0.3520(5)	0	0.0165(5)	0.023(2)	0.25
Al3	4i	0.8987(5)	0	0.8013(6)	0.023(2)	1
N1	4i	0.6909(13)	1/2	0.0819(12)	0.029(4)	1
N2	4i	0.3061(12)	1/2	0.6212(11)	0.024(4)	1
N3	4i	0.5062(11)	0	0.1815(12)	0.020(4)	1
N4	2d	1/2	0	1/2	0.025(6)	1

^aStandard deviations in parentheses.

Al/Mg–N bond lengths are in the range of 1.887(6)–2.129(16) Å. Al–N bond lengths range from 1.827(13) to 1.924(8) Å. For a more detailed discussion of the bond lengths, please refer to the structure description of α - $\text{Sr}_2[\text{MgAl}_5\text{N}_7]:\text{Eu}^{2+}$. The crystal structures of α - and

4. Tunable Red Luminescence in Nitridomagnesoaluminates

α - $\text{Sr}_2[\text{MgAl}_5\text{N}_7]:\text{Eu}^{2+}$, β - $\text{Sr}_2[\text{MgAl}_5\text{N}_7]:\text{Eu}^{2+}$ and $\text{Sr}_8[\text{LiMg}_2\text{Al}_{21}\text{N}_{28}]:\text{Eu}^{2+}$

β - $\text{Sr}_2[\text{MgAl}_5\text{N}_7]:\text{Eu}^{2+}$ exhibit similar building units in a slightly different arrangement. A comparison of the crystal structures is presented in Figure 4.7.

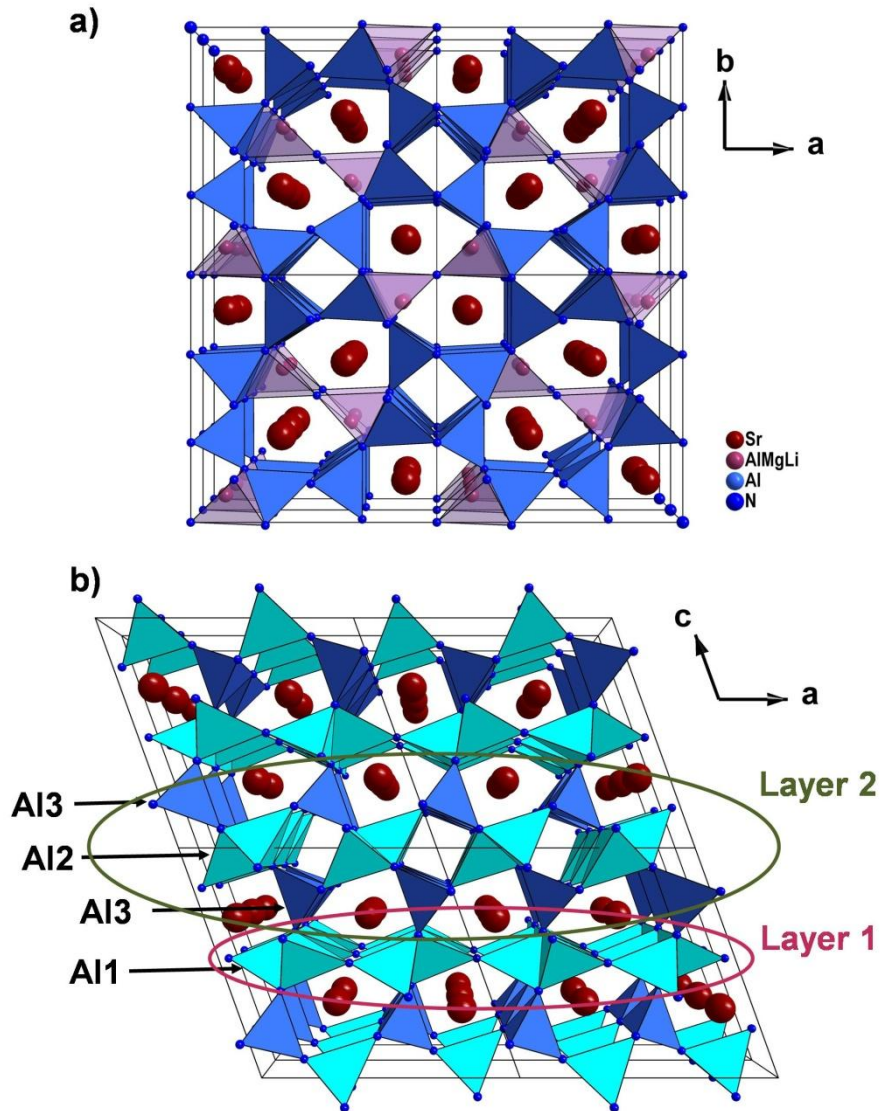


Figure 4.7. Comparison of the crystal structures of α - and β - $\text{Sr}_2[\text{MgAl}_5\text{N}_7]:\text{Eu}^{2+}$. (a) View of α - $\text{Sr}_2[\text{MgAl}_5\text{N}_7]:\text{Eu}^{2+}$ along [001]. (b) View of β - $\text{Sr}_2[\text{MgAl}_5\text{N}_7]:\text{Eu}^{2+}$ along [010]. The layers formed by the tetrahedra of the different Al/(Mg) sites are highlighted.

Both crystal structures exhibit similar channels in different crystallographical directions, i.e., [001] for α - and [010] for β - $\text{Sr}_2[\text{MgAl}_5\text{N}_7]:\text{Eu}^{2+}$. The three-dimensional network of Al/(Mg) N_4 tetrahedra is composed of two different layers. Layer 1 is formed by the alternating edge- and vertex-sharing Al1/Mg1 N_4 tetrahedra resulting in the motif of bow-tie units connected to each other by common vertices. Double strands of edge-sharing tetrahedra in

4. Tunable Red Luminescence in Nitridomagnesoaluminates

α -Sr₂[MgAl₅N₇]:Eu²⁺, β -Sr₂[MgAl₅N₇]:Eu²⁺ and Sr₈[LiMg₂Al₂₁N₂₈]:Eu²⁺

α -Sr₂[MgAl₅N₇]:Eu²⁺ are separated by one all-vertex-sharing tetrahedron but directly condensed in β -Sr₂[MgAl₅N₇]:Eu²⁺. The edge-sharing Al₂/Mg₂N₄ tetrahedra form strands that are bridged on both sides by Al₃N₄ tetrahedra via common vertices constituting layer 2. Layers 1 and 2 are linked via common vertices.

Similar to α -Sr₂[MgAl₅N₇]:Eu²⁺, the Sr²⁺ ions are coordinated cube-like by eight N atoms. One polyhedron face is capped by a ninth N atom located at a larger distance than the nearest Al(/Mg) atoms and is therefore not considered part of the anionic coordination sphere. The SrN₈ polyhedra share common faces forming strands along [010]. Two of these strands are linked by common vertices, respectively. For a more detailed discussion of bond lengths, please refer to the structure description of α -Sr₂[MgAl₅N₇]:Eu²⁺.

Luminescence

Eu-doped samples of the title compound (α -)Sr₈[Li_(2-0.5x)Mg_xAl_(22-0.5x)N₂₈] exhibit red luminescence upon irradiation with blue–green light. Photoluminescence investigations were performed on bulk powder samples in PTFE sample holders. Excitation, emission, and reflectance spectra of α -Sr₂[MgAl₅N₇]:Eu²⁺ at different activator concentrations are shown in Figure 4.8. The materials exhibit an excitation minimum at 380 nm and a broad absorption band at lower energies peaking at \approx 470 nm. Increasing dopant concentrations shift the emission maximum toward lower energies (see Table 4.4). With reference to the excitation spectra exhibiting strong absorption in the red spectral region and significant broadening with increased dopant concentrations, the emission red shift is largely attributed to photon reabsorption effects although resonance type energy transfer mechanisms cannot be excluded.²³ The exhibited narrowing of the emission bands with increasing activator concentrations can also be attributed to reabsorption on the high-energy side of the spectrum. In general, the smallest possible activator concentration with still sufficient absorption is to be considered as optimal for Eu²⁺ activated phosphors since saturation under high drive conditions reduces the quantum efficiency.²⁴

By partially exchanging the network cations Al³⁺ and Mg²⁺ with Li⁺, the emission maximum of (α -)Sr₈[Li_(2-0.5x)Mg_xAl_(22-0.5x)N₂₈]:Eu²⁺ is also shifted toward lower energies (see Table 4.4). The exchange of Mg²⁺ for Li⁺ results in slightly shorter Sr(Eu)–N bond lengths (2.644(1)–2.970(5) Å (without Li)/2.617(1)–2.928(2) Å (without Mg)) indicating a higher crystal field strength around the activator ion and consequently a red shift of the emission.

4. Tunable Red Luminescence in Nitridomagnesoaluminates

α - $\text{Sr}_2[\text{MgAl}_5\text{N}_7]:\text{Eu}^{2+}$, β - $\text{Sr}_2[\text{MgAl}_5\text{N}_7]:\text{Eu}^{2+}$ and $\text{Sr}_8[\text{LiMg}_2\text{Al}_{21}\text{N}_{28}]:\text{Eu}^{2+}$

Photoluminescence for β - $\text{Sr}_2[\text{MgAl}_5\text{N}_7]:\text{Eu}^{2+}$ was not observed separately from α - $\text{Sr}_2[\text{MgAl}_5\text{N}_7]:\text{Eu}^{2+}$ since the β material could not be obtained phase pure.

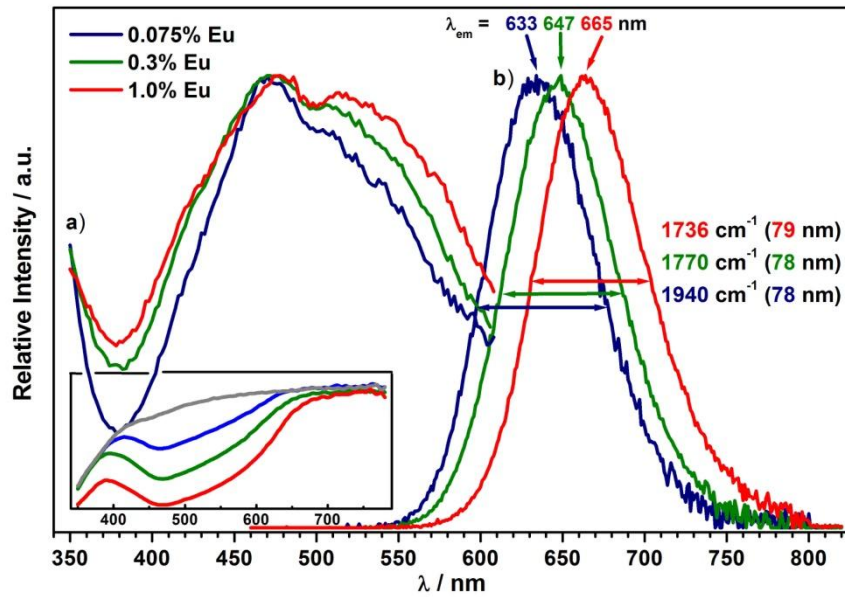


Figure 4.8. Photoluminescence spectra of $\text{Sr}_2[\text{MgAl}_5\text{N}_7]:\text{Eu}^{2+}$ with different activator concentrations. (a) Excitation spectra ($\lambda_{\text{obs}} = 620\text{--}660$ nm). (b) Emission spectra ($\lambda_{\text{exc}} = 440$ nm). Inset: Reflectance spectra; gray line: undoped sample.

Effects of different activator concentrations on the luminescence properties of $\text{Sr}_8[\text{LiMg}_2\text{Al}_{21}\text{N}_{28}]:\text{Eu}^{2+}$ are not presented here due to their qualitative similarity to α - $\text{Sr}_2[\text{MgAl}_5\text{N}_7]:\text{Eu}^{2+}$ based on their identical crystal structure. Emission and reflectance spectra are shown in Figure 4.9. Emission fwhm remain virtually unchanged by the different Li contents.

Compared to other red emitting nitridometallates like $\text{Ca}[\text{LiAl}_3\text{N}_4]:\text{Eu}^{2+}$ ($\lambda_{\text{em}} = 668$ nm, $\text{fwhm} = 1333$ cm^{-1} , 60 nm),¹⁰ $\text{Sr}[\text{LiAl}_3\text{N}_4]:\text{Eu}^{2+}$ ($\lambda_{\text{em}} = 650$ nm, $\text{fwhm} = 1180$ cm^{-1} , 50 nm),⁴ and $\text{Sr}[\text{Mg}_3\text{SiN}_4]:\text{Eu}^{2+}$ ($\lambda_{\text{em}} = 615$ nm, $\text{fwhm} = 1170$ cm^{-1} , 43 nm),¹⁵ $\text{Sr}_2[\text{MgAl}_5\text{N}_7]:\text{Eu}^{2+}$ and $\text{Sr}_8[\text{LiMg}_2\text{Al}_{21}\text{N}_{28}]:\text{Eu}^{2+}$ exhibit significantly broader emission bands, although the activator-site coordination sphere is virtually identically cube-like. This line broadening may be explained by structural details: In $\text{Ca}[\text{LiAl}_3\text{N}_4]:\text{Eu}^{2+}$, $\text{Sr}[\text{LiAl}_3\text{N}_4]:\text{Eu}^{2+}$, and $\text{Sr}[\text{Mg}_3\text{SiN}_4]:\text{Eu}^{2+}$, the network cations exclusively occupy element specific sites, whereas in $\text{Sr}_2[\text{MgAl}_5\text{N}_7]:\text{Eu}^{2+}$ and $\text{Sr}_8[\text{LiMg}_2\text{Al}_{21}\text{N}_{28}]:\text{Eu}^{2+}$, two network cation sites are occupied by Al and Mg with statistical disorder. A similar broadening of the emission can be observed in $M[\text{Mg}_2\text{Al}_2\text{N}_4]:\text{Eu}^{2+}$ ($M = \text{Ca}$,

4. Tunable Red Luminescence in Nitridomagnesoaluminates

α - $\text{Sr}_2[\text{MgAl}_5\text{N}_7]:\text{Eu}^{2+}$, β - $\text{Sr}_2[\text{MgAl}_5\text{N}_7]:\text{Eu}^{2+}$ and $\text{Sr}_8[\text{LiMg}_2\text{Al}_{21}\text{N}_{28}]:\text{Eu}^{2+}$

Sr; $\lambda_{\text{em}}(\text{Ca}) = 607 \text{ nm}$, $\text{fwhm} = 1815 \text{ cm}^{-1}$; $\lambda_{\text{em}}(\text{Sr}) = 612 \text{ nm}$, $\text{fwhm} = 1823 \text{ cm}^{-1}$) where Mg and Al also show statistical disorder and the activator site is coordinated cube-like as well.⁹

Table 4.4. Emission Maxima and Emission fwhm of Representatives of the Solid Solution Series $(\alpha)\text{Sr}_8[\text{Li}_{(2-0.5x)}\text{Mg}_x\text{Al}_{(22-0.5x)}\text{N}_{28}]:\text{Eu}^{2+}$

composition	$\lambda_{\text{em}}/\text{nm}$	$\text{fwhm}/\text{cm}^{-1}$ (/nm)
x = 4 0.075 atom-% Eu^{2+}	633	1940 (78)
x = 4 0.3 atom-% Eu^{2+}	647	1770 (78)
x = 4 1 atom-% Eu^{2+}	665	1736 (79)
x = 2 0.075 atom-% Eu^{2+}	645	1964 (82)
x = 0 0.4 atom-% Eu^{2+}	670	1880 (85) ¹⁴

The larger fwhm here consequently are attributed to inhomogeneous line broadening due to the varying crystal fields around each activator ion resulting from the statistical disorder on one or more network cation positions.

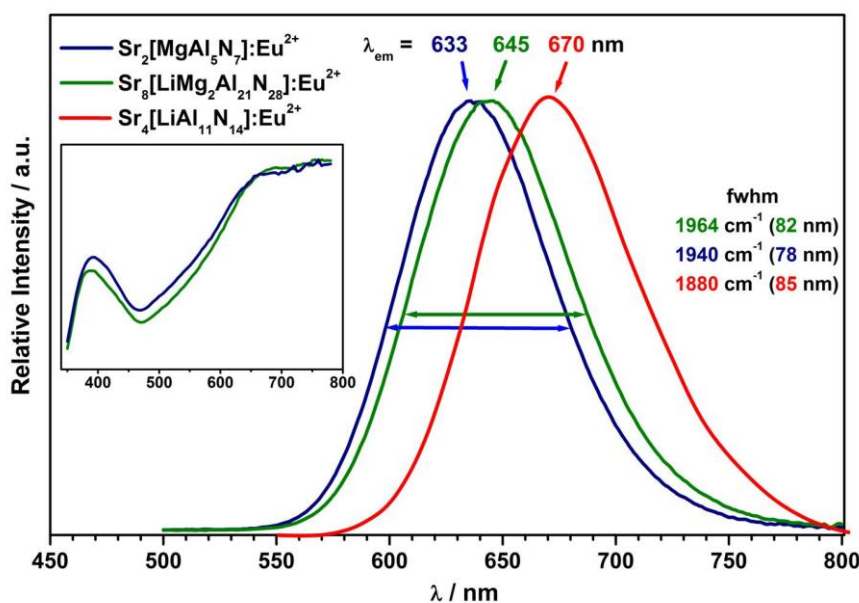


Figure 4.9. Photoluminescence spectra of $\text{Sr}_2[\text{MgAl}_5\text{N}_7]:\text{Eu}^{2+}$, $\text{Sr}_8[\text{LiMg}_2\text{Al}_{21}\text{N}_{28}]:\text{Eu}^{2+}$, and $\text{Sr}_4[\text{LiAl}_{11}\text{N}_{14}]:\text{Eu}^{2+}$. Data for $\text{Sr}_4[\text{LiAl}_{11}\text{N}_{14}]:\text{Eu}^{2+}$ adapted from the literature.¹⁴ Inset: Reflectance spectra.

The thermal behavior of the emission quantum efficiency of both $(\alpha)\text{Sr}_2[\text{MgAl}_5\text{N}_7]:\text{Eu}^{2+}$ and $\text{Sr}_8[\text{LiMg}_2\text{Al}_{21}\text{N}_{28}]:\text{Eu}^{2+}$ is shown in Figure 4.10. Compared to the emission intensity at room temperature, both materials exhibit moderate thermal quenching. At 200 °C, QE_{rel} drops to

66% for $x = 4$ and 84% for $x = 2$. Postsynthetic heat treatment of samples with $x = 2$ at 250 °C shows no significant impact on the thermal properties.

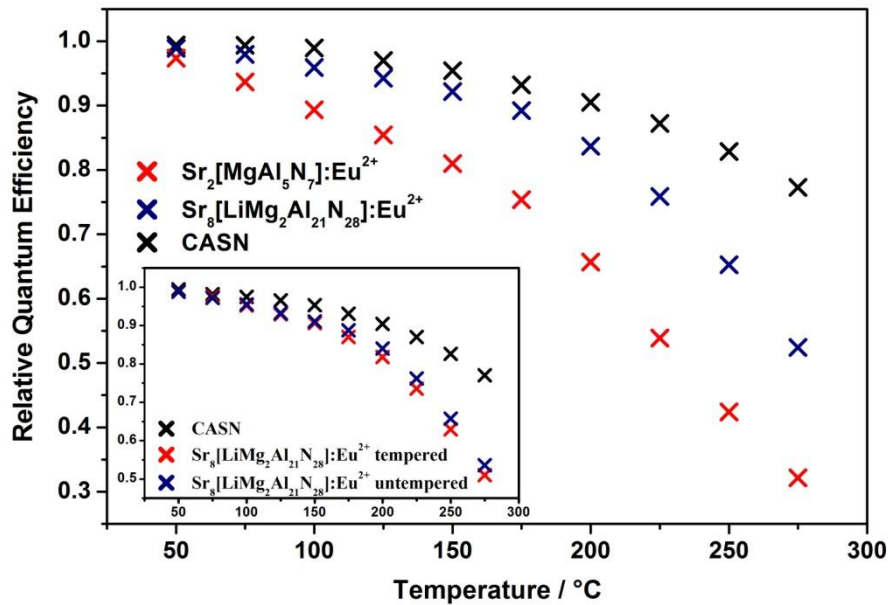


Figure 4.10. Thermal behavior of the emission quantum efficiency of $\text{Sr}_2[\text{MgAl}_5\text{N}_7]:\text{Eu}^{2+}$ and $\text{Sr}_8[\text{LiMg}_2\text{Al}_{21}\text{N}_{28}]:\text{Eu}^{2+}$ with a dopant concentration of 0.075% and a commercial red nitride phosphor (CASN BR101, Mitsubishi Chemical) as reference. Inset: Thermal quenching of samples ($x = 2$) with (red) or without (blue) postsynthetic annealing.

The more pronounced thermal quenching of the emission intensity of α - $\text{Sr}_2[\text{MgAl}_5\text{N}_7]:\text{Eu}^{2+}$ compared to $\text{Sr}_8[\text{LiMg}_2\text{Al}_{21}\text{N}_{28}]:\text{Eu}^{2+}$ results from the smaller band gap of the more Mg containing material. Therefore, the energetic separation of the lowest lying excited $5d$ state of the activator and the host lattice conduction band is reduced, and nonradiative relaxation through photoionization processes becomes more probable.

Conclusion

In this contribution, we report on novel nitridomagnesoaluminates with the general sum formula $\text{Sr}_8[\text{Li}_{(2-0.5x)}\text{Mg}_x\text{Al}_{(22-0.5x)}\text{N}_{28}]:\text{Eu}^{2+}$ ($x = 2$ and 4). Synthesis was carried out by a heterogeneous high-pressure/high-temperature reaction in a hot isostatic press. The crystal structures of isotypic α - $\text{Sr}_2[\text{MgAl}_5\text{N}_7]:\text{Eu}^{2+}$ and $\text{Sr}_8[\text{LiMg}_2\text{Al}_{21}\text{N}_{28}]:\text{Eu}^{2+}$ were refined from powder X-ray diffraction data based on a model adapted from $\text{Sr}_4[\text{LiAl}_{11}\text{N}_{14}]:\text{Eu}^{2+}$.¹⁴ The crystal structure of β - $\text{Sr}_2[\text{MgAl}_5\text{N}_7]:\text{Eu}^{2+}$ was solved and refined from powder X-ray

4. Tunable Red Luminescence in Nitridomagnesoaluminates

α -Sr₂[MgAl₅N₇]:Eu²⁺, β -Sr₂[MgAl₅N₇]:Eu²⁺ and Sr₈[LiMg₂Al₂₁N₂₈]:Eu²⁺

diffraction data. All compounds possess highly condensed, rigid networks favorable for efficient conversion. Eu²⁺-doped samples show intense red luminescence upon irradiation with blue–green light. The emission maximum is tunable over a wide range in the red spectral region by adjusting the activator concentration and by substituting the network cations Al³⁺ and Mg²⁺ with Li⁺. Similar to extremely narrow emitting Sr[Mg₃SiN₄]:Eu²⁺ and Sr[LiAl₃N₄]:Eu²⁺, the activator position of α - and β -Sr₂[MgAl₅N₇]:Eu²⁺ and Sr₈[LiMg₂Al₂₁N₂₈]:Eu²⁺ is coordinated cube-like by eight N atoms.^{4,15} Here, the emission fwhm is at $\approx 1850 \pm 100 \text{ cm}^{-1}$ due to statistical disorder on some network-cation sites comparable to (Ca/Sr)[Mg₂Al₂N₄]:Eu²⁺.⁹

On the basis of the crystal structure providing a rigid host lattice and the intriguing luminescence properties, materials of the mixed crystal series Sr₈[Li_(2-0.5x)Mg_xAl_(22-0.5x)N₂₈]:Eu²⁺ have the potential for application as red phosphors in illumination grade white LEDs.

Associated Content

Supporting Information

The Supporting Information is available free of charge on the ACS Publications website at DOI: 10.1021/acs.chemmater.8b00106.

X-ray crystallographic information file of β -Sr₂[MgAl₅N₇]:Eu²⁺ from powder X-ray diffraction data (CIF)

Author Information

Corresponding Author

*E-mail: wolfgang.schnick@uni-muenchen.de.

ORCID

Wolfgang Schnick: 0000-0003-4571-8035

Notes

The authors declare no competing financial interest.

Acknowledgements

The authors thank Christian Maak (Department of Chemistry, LMU) for EDX measurements and SEM imaging.

References

- (1) Uheda, K.; Hirosaki, N.; Yamamoto, H. Host lattice materials in the system Ca₃N₂-AlN-Si₃N₄ for white light emitting diode. *Phys. Status Solidi A* **2006**, *203*, 2712–2717.
- (2) Uheda, K.; Hirosaki, N.; Yamamoto, Y.; Naito, A.; Nakajima, T.; Yamamoto, H. Luminescence properties of a red phosphor, CaAlSiN₃:Eu²⁺, for white light-emitting diodes. *Electrochem. Solid-State Lett.* **2006**, *9*, H22–H25.
- (3) Pust, P.; Schnick, W.; Schmidt, P. J. A revolution in lighting. *Nat. Mater.* **2015**, *14*, 454–458.
- (4) Pust, P.; Weiler, V.; Hecht, C.; Tücks, A.; Wochnik, A. S.; Henss, A.-K.; Wiechert, D.; Scheu, C.; Schmidt, P. J.; Schnick, W. Narrow-band red-emitting Sr[LiAl₃N₄]:Eu²⁺ as a next-generation LED-phosphor material. *Nat. Mater.* **2014**, *13*, 891–896.
- (5) Blase, W.; Cordier, G.; Ludwig, M.; Kniep, R. Sr₃[Al₂N₄]: A Nitridoaluminate with Corrugated Tetrahedral Chains ∞ [AlN_{4/2}³⁻]. *Z. Naturforsch., B: J. Chem. Sci.* **1994**, *49*, 501–505.
- (6) Ludwig, M.; Jäger, J.; Niewa, R.; Kniep, R. Crystal Structures of Two Polymorphs of Ca₃[Al₂N₄]. *Inorg. Chem.* **2000**, *39*, 5909–5911.
- (7) Ludwig, M.; Niewa, R.; Kniep, R. Dimers [Al₂N₆]¹²⁻ and chains ∞ [AlN_{4/2}³⁻] in the crystal structures of Ca₆[Al₂N₆] and Ba₃[Al₂N₄]. *Z. Naturforsch., B: J. Chem. Sci.* **1999**, *54*, 461–465.
- (8) Pust, P.; Pagano, S.; Schnick, W. Ca[LiAlN₂]: A Quaternary Nitridoaluminate. *Eur. J. Inorg. Chem.* **2013**, *2013*, 1157–1160.
- (9) Pust, P.; Hintze, F.; Hecht, C.; Weiler, V.; Locher, A.; Zitnanska, D.; Harm, S.; Wiechert, D.; Schmidt, P. J.; Schnick, W. Group (III) Nitrides M[Mg₂Al₂N₄] (M = Ca, Sr, Ba, Eu) and Ba[Mg₂Ga₂N₄]-Structural Relation and Nontypical Luminescence Properties of Eu²⁺ Doped Samples. *Chem. Mater.* **2014**, *26*, 6113–6119.
- (10) Pust, P.; Wochnik, A. S.; Baumann, E.; Schmidt, P. J.; Wiechert, D.; Scheu, C.; Schnick, W. Ca[LiAl₃N₄]:Eu²⁺-A Narrow-Band Red-Emitting Nitridolithoaluminate. *Chem. Mater.* **2014**, *26*, 3544–3549.
- (11) Kubus, M.; Levin, K.; Kroeker, S.; Ensling, D.; Juestel, T.; Meyer, H. J. Structural and luminescence studies of the new nitridomagnesoaluminate CaMg₂AlN₃. *Dalton Trans.* **2015**, *44*, 2819–2826.
- (12) Wagatha, P.; Pust, P.; Weiler, V.; Wochnik, A. S.; Schmidt, P. J.; Scheu, C.; Schnick, W. Ca_{18.75}Li_{10.5}[Al₃₉N₅₅]:Eu²⁺-Supertetrahedron Phosphor for Solid-State Lighting. *Chem. Mater.* **2016**, *28*, 1220–1226.
- (13) Schmidt, R.; Stroebale, M.; Eichele, K.; Meyer, H.-J. Crystal Structure and Luminescence Investigations of the Nitridomagnesoaluminates Mg₃Al_nN_{n+2} with n = 1, 2, 3. *Eur. J. Inorg. Chem.* **2017**, *2017*, 2727–2735.
- (14) Wilhelm, D.; Baumann, D.; Seibald, M.; Wurst, K.; Heymann, G.; Huppertz, H. Narrow-Band Red Emission in the Nitridolithoaluminate Sr₄[LiAl₁₁N₁₄]:Eu²⁺. *Chem. Mater.* **2017**, *29*, 1204–1209.

4. Tunable Red Luminescence in Nitridomagnesoaluminates

α -Sr₂[MgAl₅N₇]:Eu²⁺, β -Sr₂[MgAl₅N₇]:Eu²⁺ and Sr₈[LiMg₂Al₂₁N₂₈]:Eu²⁺

(15) Schmiechen, S.; Schneider, H.; Wagatha, P.; Hecht, C.; Schmidt, P. J.; Schnick, W. Toward New Phosphors for Application in Illumination-Grade White pc-LEDs: The Nitridomagnesosilicates Ca[Mg₃SiN₄]:Ce³⁺, Sr[Mg₃SiN₄]:Eu²⁺, and Eu[Mg₃SiN₄]. *Chem. Mater.* **2014**, *26*, 2712–2719.

(16) Coelho, A. *TOPAS-Academic*; Coelho Software: Brisbane, 2007.

(17) Cheary, R. W.; Coelho, A. A.; Cline, J. P. Fundamental Parameters Line Profile Fitting in Laboratory Diffractometers. *J. Res. Natl. Inst. Stand. Technol.* **2004**, *109*, 1–25.

(18) Rietveld, H. M. Profile Refinement Method for Nuclear and Magnetic Structures. *J. Appl. Crystallogr.* **1969**, *2*, 65–71.

(19) Bergmann, J.; Kleeberg, R.; Haase, A.; Breidenstein, B. Advanced Fundamental Parameters Model for Improved Profile Analysis. *Mater. Sci. Forum* **2000**, *347–349*, 303–308.

(20) Wambach, K. R.; Hoppe, R. Die Koordinationszahl 3 bei Zn²⁺ Zur Kenntnis von K₂[Zn₆O₇]. *Z. Anorg. Allg. Chem.* **1978**, *445*, 91–101.

(21) Liebau established the terms *einer*, *zweier*, *dreier*, *vierer*, and *fünfer*. Thereby, a *vierer* ring can be described as four polyhedra connected to each other by common vertices forming a ring. The terms derive from the German numerals *eins* (1), *zwei* (2), *drei* (3), *vier* (4), *fünf* (5), ..., *acht* (8), etc. by adding the suffix “er” to the numeral; Liebau, F. *Structural Chemistry of Silicates*; Springer: Berlin, 1985.

(22) Schultz-Coulon, V.; Schnick, W. CaMg₂N₂ - a Mixed Alkaline-Earth Metal Nitride with anti-La₂O₃ Structure. *Z. Naturforsch., B: J. Chem. Sci.* **1995**, *50*, 619–622.

(23) Bachmann, V.; Ronda, C.; Oeckler, O.; Schnick, W.; Meijerink, A. Color Point Tuning for (Sr,Ca,Ba)Si₂O₂N₂:Eu²⁺ for White Light LEDs. *Chem. Mater.* **2009**, *21*, 316–325.

(24) Shchekin, O. B.; Schmidt, P. J.; Jin, F.; Lawrence, N.; Vampola, K. J.; Bechtel, H.; Chamberlin, D. R.; Mueller-Mach, R.; Mueller, G. O. Excitation dependent quenching of luminescence in LED phosphors. *Phys. Status Solidi RRL* **2016**, *10*, 310–314.

5. Narrow-Band Red Luminescence in Nitridolithoaluminate $\text{CaBa}[\text{Li}_2\text{Al}_6\text{N}_8]:\text{Eu}^{2+}$

published in: *Chem. Mater.* **2018**, *30*, 7885–7891

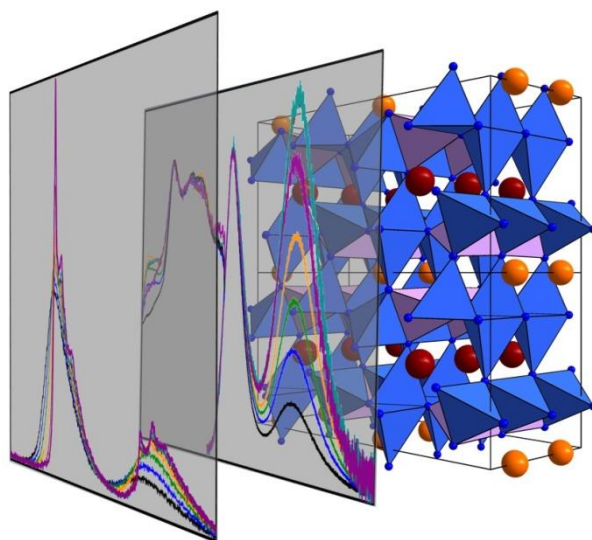
authors: Peter Wagatha, Volker Weiler, Peter J. Schmidt and Wolfgang Schnick

DOI: 10.1021/acs.chemmater.8b03485

Reprinted with permission from American Chemical Society, Copyright © 2018

Abstract

Narrow-band red-emitting luminescent $\text{CaBa}[\text{Li}_2\text{Al}_6\text{N}_8]:\text{Eu}^{2+}$ for potential application in illumination-grade white-light-emitting diodes (WLEDs) was synthesized by reaction of the metal hydrides and nitrides in molybdenum crucibles in a hot isostatic press. Upon irradiation with high-energy visible light (444 nm), the material exhibits intense red and infrared luminescence (emission maxima, 636–639 nm, 790 nm; full width at half-maximum (fwhm), $1095\text{--}1266\text{ cm}^{-1}$ (48–57 nm), $\approx 1450\text{ cm}^{-1}$ (89 nm)). The red emission from Eu occupying the Ba site is nearly optimal for use in WLEDs combining outstanding color rendition and excellent luminous efficacy and the most narrow-band Eu^{2+} emission observed to date. The infrared emission intensity from Eu occupying the Ca site can be limited by reducing the activator concentration (here, 0.02–5 atom % Eu). $\text{CaBa}[\text{Li}_2\text{Al}_6\text{N}_8]:\text{Eu}^{2+}$ crystallizes isotypically with $\text{RbNaLi}_6\text{Si}_2\text{O}_8$ in the monoclinic space group $C2/m$ (no. 12) with unit cell parameters $a = 16.0851(2)$, $b = 6.46738(4)$, $c = 8.04242(13)$ Å, $\beta = 90.004(2)^\circ$, and $Z = 4$. The material is obtained almost phase pure with <4 wt % AlN as side phase. The crystal structure consists of a network of vertex- and edge-sharing AlN_4 and



LiN_4 tetrahedra with differently sized four-membered ring channels along [010] occupied by either cubelike coordinated Ca or Ba atoms or left empty.

Introduction

On the road to decelerating global energy consumption, solid-state lighting (SSL) technology is playing an important part. At an anticipated 86% market penetration within the United States, SSL is expected to enable a 75% reduction in lighting-specific energy consumption compared with a conventional lighting scenario, according to the US Department of Energy (DOE).¹

Crucial for achieving a high market penetration with white-light-emitting diodes (WLEDs) is high consumer acceptance by a market-specific correlated color temperature (CCT), natural color rendition (i.e., high color rendering index, CRI), and long service life as well as adequate initial and operating costs. Initially, WLEDs comprised a blue-emitting primary LED and the yellow-emitting luminescent material $\text{YAG}:\text{Ce}$. This combination allows for high luminous efficacies, but its at most mediocre color rendition ($\text{CRI} < 70$) due to lack of emission in the red spectral region limits applications. Development of efficient red-emitting phosphor materials like $\text{Sr}_{1-x}\text{Ca}_x\text{AlSiN}_3:\text{Eu}^{2+}$ (SCASN) first made high-CRI illumination-grade WLEDs possible. While the use of SCASN closes the red gap, it simultaneously limits the device's luminous efficacy because of its relatively broad emission band ($\text{fwhm} \approx 2100\text{--}2500 \text{ cm}^{-1}$).²⁻⁴ The combination of high chromatic saturation in the red spectral region for excellent color rendition and high luminous efficacy for highly efficient devices is only made possible by narrow-band emission, resulting in little to, ideally, no IR spillover.⁵

Aside from the widely used SCASN, only few narrow-band red-emitting nitridic phosphor materials have yet been identified and found their way to industrial application.^{6,7} Most relevantly, that is the nitridolithoaluminate $\text{Sr}[\text{LiAl}_3\text{N}_4]:\text{Eu}^{2+}$ (SLA). Prototype high-CRI WLEDs equipped with the advantages of this phosphor's emission at $\lambda_{\text{em}} = 650 \text{ nm}$ and $\text{fwhm} = 1180 \text{ cm}^{-1}$ exhibit luminous efficacies increased by 14% compared to commercially available products.⁸ The discovery of extremely narrow-band red Eu^{2+} emission in SLA—and the related material $\text{Sr}[\text{Mg}_3\text{SiN}_4]:\text{Eu}^{2+}$ with $\lambda_{\text{em}} = 615 \text{ nm}$ and $\text{fwhm} = 1170 \text{ cm}^{-1}$ —renewed scientific interest in the compound class of nitridoaluminates.⁹ Prior to this decade, only few nitridoaluminates were known, and no optical properties have been reported.¹⁰⁻¹² Likewise,

$\text{Ca}[\text{LiAlN}_2]:\text{Eu}^{2+}$ exhibits no luminescence, but $M[\text{Mg}_2\text{Al}_2\text{N}_4](:\text{Eu}^{2+})$ with $M = \text{Ca}, \text{Sr}, \text{Ba}$ (Eu) (MMA) and $\text{Ca}[\text{LiAl}_3\text{N}_4]:\text{Eu}^{2+}$ (CLA), both structurally closely related to SLA, show red luminescence.^{13–15} Other red-emitting nitridoaluminate materials include $\text{Ca}_{18.75}\text{Li}_{10.5}[\text{Al}_{39}\text{N}_{55}]:\text{Eu}^{2+}$ with an unusual supertetrahedron-containing crystal structure, $\text{Sr}_4[\text{LiAl}_{11}\text{N}_{14}]:\text{Eu}^{2+}$,¹⁶ isotopic with $\text{Sr}_2[\text{MgAl}_5\text{N}_7]:\text{Eu}^{2+}$ and their solid solutions with tunable emission characteristics,¹⁷ and most recently the oxonitridolithoaluminate $\text{Sr}[\text{Li}_2\text{Al}_2\text{O}_2\text{N}_2]:\text{Eu}^{2+}$ with $\lambda_{\text{em}} \approx 614 \text{ nm}$ and roughly estimated fwhm $\approx 1500 \text{ cm}^{-1}$ ($>55 \text{ nm}$).¹⁸ Although these optical properties allow for greatly increased luminous efficacy by virtually eliminating IR spillover, the blue-shifted emission wavelength hampers excellent color rendition because of a lack of deeper-red spectral components.

Luminous efficacies of high-CRI WLEDs could be further increased by 22% by using red luminescent materials with fwhm $\approx 30 \text{ nm}$.¹⁹ One possible strategy for blue-shifting the emission of SLA toward the desired emission wavelength is utilizing the heavier homologue Ba instead of Sr to form isostructural $\text{Ba}[\text{LiAl}_3\text{N}_4]:\text{Eu}^{2+}$ (BLA). In this case, the longer Eu–N bond lengths would lead to a higher energetic emission. Unfortunately, the synthesis of BLA has not been successful, yet. Alternatively, the alkaline earth (AE) element Sr in SLA could be partially substituted by another AE metal in a total atomic ratio of 1:1, so that each of the two heavy-atom sites are fully occupied by one element resulting in tailored emission characteristics. Consequently, here we present the novel nitridolithoaluminate phosphor $\text{CaBa}[\text{Li}_2\text{Al}_6\text{N}_8]:\text{Eu}^{2+}$ and give insight into its preparation, crystal structure, and photoluminescence properties. The potential for application in high-CRI WLEDs and its impact on the understanding and conception of narrow-band red emission are discussed.

Experimental Section

Synthesis

All reagents and reaction products were handled in Ar atmosphere under exclusion of oxygen and moisture in a glovebox (Unilab, MBraun, Garching, $\text{O}_2 < 1 \text{ ppm}$, $\text{H}_2\text{O} < 1 \text{ ppm}$). Products of the composition $\text{CaBa}[\text{Li}_2\text{Al}_6\text{N}_8]:\text{Eu}^{2+}$ (nominal Eu concentration: 0.02–5 mol %) were obtained by reacting the starting materials CaH_2 (Materion, 99.5%), BaH_2 (Materion, 99.5%), Li_3N (Materion, 99.5%), AlN (H.C. Starck, grade B), and Eu_2O_3 (Neo, 99.99%) in molybdenum crucibles in a hot isostatic press. The reagents were mixed in stoichiometric

5. Narrow-Band Red Luminescence in Nitridolithoaluminate $\text{CaBa}[\text{Li}_2\text{Al}_6\text{N}_8]:\text{Eu}^{2+}$

amounts by ball milling, filled into crucibles, and subsequently heated to 1050 °C for 5 h at a N_2 pressure of 51.7 MPa. $\text{CaBa}[\text{Li}_2\text{Al}_6\text{N}_8]:\text{Eu}^{2+}$ was obtained as a finely crystalline powder with purple body color. The material exhibits intense red luminescence upon irradiation with blue–green light.

Powder X-Ray Diffraction

Powder X-ray diffraction data were collected with a STOE Stadi P diffractometer with $\text{Mo K}\alpha_1$ radiation ($\lambda = 0.70932 \text{ \AA}$) with a Ge(111) monochromator and a Mythen 1K (Dectris, Baden-Dättwil, Switzerland) detector in parafocusing Debye–Scherrer geometry. Samples were filled into glass capillaries (Hilgenberg, Malsfeld, Germany) with 0.3 mm diameter and 0.01 mm wall thickness. Rietveld refinement was conducted using the TOPAS-Academic V4.1 software package applying the fundamental parameters approach (direct convolution of source emission profiles, axial instrument contributions, crystallite size, and microstrain effects).^{20–23} Absorption correction was done using the calculated absorption coefficient. Preferred orientation of crystallites was handled with the spherical harmonics model of fourth order. Details on the structure investigation may be obtained from the Cambridge Crystallographic Data Centre on quoting the depository no. CCDC 1860700.

Electron Microscopy

A Dualbeam Helios Nanolab G3 UC (FEI) scanning electron microscope (SEM), equipped with an X-Max 80 SDD (Oxford Instruments) energy-dispersive X-ray (EDX) detector was used for scanning electron investigations.

EDX Spectroscopy

The chemical composition of the samples and individual crystallites was determined by EDX spectroscopy at an acceleration voltage of 5 kV.

Luminescence

Emission spectra were measured on powder samples in PTFE sample holders on an in-house built system based on a 5.3 in. integrating sphere and a spectrofluorimeter equipped with a 150 W Xe lamp, two 500 mm Czerny–Turner monochromators, 1800 1/mm lattices and 2500/500 nm lamps with the spectral range 230–820 nm. Excitation spectra were measured

on powder samples using a blue primary LED (444 nm) without monochromators and an AvaSpec-2048-TEC-USB2 (Avantes, spectral range 580–1100 nm) with fiber optics of the light source and detector each mounted at a 45° angle with respect to the sample surface.

Results and Discussion

Synthesis and Chemical Analysis

The synthesis described above enabled access to the luminescent material $\text{CaBa}[\text{Li}_2\text{Al}_6\text{N}_8]:\text{Eu}^{2+}$. Samples were obtained as finely crystalline powders with purple body color and intense red photoluminescence upon irradiation with blue–red light. SEM images showing the typical crystal morphology and crystallite size are presented in Figure 5.1. Atomic ratios of Ca:Ba:Al:N were determined to be 1:1:7:9 by EDX spectroscopy on multiple crystallites. These values correspond well with the proposed sum formula, taking into consideration the finely dispersed side phase AlN ($\text{CaBa}[\text{Li}_2\text{Al}_6\text{N}_8]\cdot\text{AlN}$).

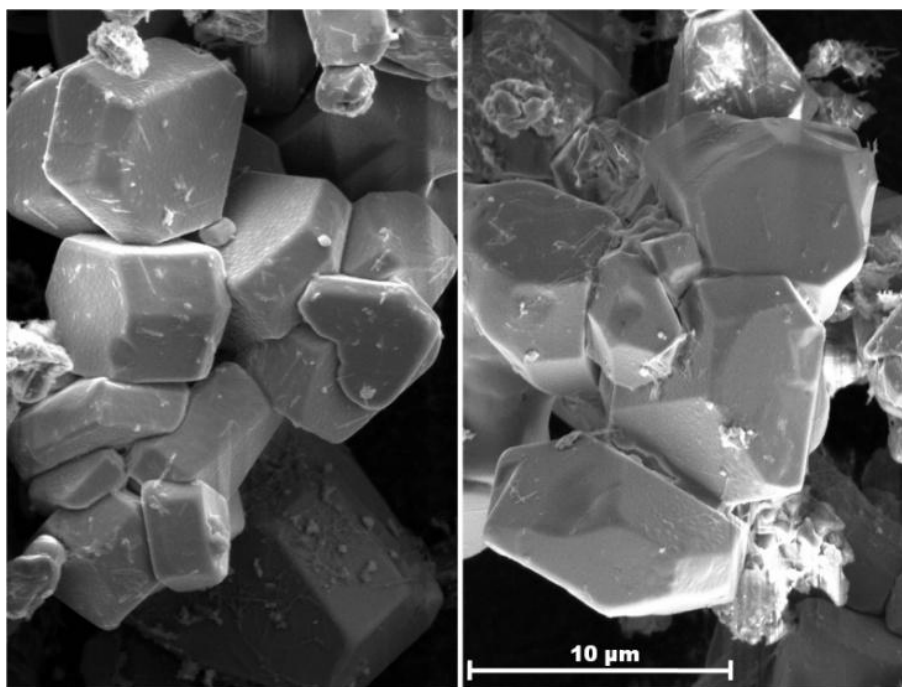


Figure 5.1. SEM image of crystals of $\text{CaBa}[\text{Li}_2\text{Al}_6\text{N}_8]:\text{Eu}^{2+}$. The crystal morphology is nearly spherical with well-developed faces. The narrow crystallite size distribution peaks at approximately 5–10 μm.

Crystal Structure

$\text{CaBa}[\text{Li}_2\text{Al}_6\text{N}_8]$ crystallizes isotypically with $\text{RbNaLi}_6\text{Si}_2\text{O}_8$ in the monoclinic space group $C2/m$ (no. 12) with unit cell parameters $a = 16.0851(2)$, $b = 6.46738(4)$, $c = 8.04242(13)$ Å,

5. Narrow-Band Red Luminescence in Nitridolithoaluminate $\text{CaBa}[\text{Li}_2\text{Al}_6\text{N}_8]:\text{Eu}^{2+}$

$\beta = 90.004(2)^\circ$, $Z = 4$, and $V = 836.64(2) \text{ \AA}^3$. The crystal structure of the title compound indicates pseudotetragonal symmetry with a halved unit cell volume, that is broken by the arrangement of the light elements' atom positions. A modified structural model of $\text{RbNaLi}_6\text{Si}_2\text{O}_8$ obtained from single-crystal X-ray diffraction data by Hofmann et al. was used for Rietveld refinement.²⁴ Only negligible contribution to the scattering power of the Ca and Ba sites partially occupied by Eu is to be expected because of the low dopant concentration of ≤ 1 mol %. Therefore, Eu was disregarded during the Rietveld refinement. Crystallographic data from the Rietveld refinement are given in Table 5.1. Atomic coordinates, isotropic displacement parameters, and site occupancy factors (SOFs) are presented in Table 5.2.

Table 5.1. Crystallographic Data of the Rietveld Refinement of $\text{CaBa}[\text{Li}_2\text{Al}_6\text{N}_8]:\text{Eu}^{2+}$

sum formula	$\text{CaBa}[\text{Li}_2\text{Al}_6\text{N}_8]$
crystal system	moniclinic
space group	$C2/m$ (no. 12)
lattice parameters	
$a / \text{ \AA}$	16.0851(2)
$b / \text{ \AA}$	6.46738(4)
$c / \text{ \AA}$	8.04242(13)
$\beta / ^\circ$	90.004(2)
$V / \text{ \AA}^3$	836.64(2)
formula units / cell	4
calculated density / $\text{g}\cdot\text{cm}^{-3}$	3.694
T / K	293
diffractometer	STOE Stadi P
radiation	$\text{Mo K}\alpha_1$ ($\lambda = 0.70932 \text{ \AA}$)
range / $^\circ$	$2.0 \leq 2\theta \leq 70.325$
background function	Chebychev polynomial (21 parameters)
R values	$R_p = 0.0422$ $R_{wp} = 0.0583$ $R_{exp} = 0.0174$ $R_{Bragg} = 0.0254$
goodness of fit	3.347

Like in $\text{RbNaLi}_6\text{Si}_2\text{O}_8$, where the different tetrahedrally coordinated network ions Si and Li occupy separate crystallographic sites, an ordered distribution of Al and Li is observed in

$\text{CaBa}[\text{Li}_2\text{Al}_6\text{N}_8]$. A plot of the Rietveld refinement of $\text{CaBa}[\text{Li}_2\text{Al}_6\text{N}_8]:\text{Eu}^{2+}$ is shown in Figure 5.2. The material is obtained with a yield of 96 wt % and 4 wt % AlN side phase.

The crystal structure is closely related to that of UCr_4C_4 ,²⁵ which can be considered as the aristotype, and consequently is closely related to the crystal structure of $\text{Sr}[\text{LiAl}_3\text{N}_4]:\text{Eu}^{2+}$ as well.⁸ The unit cell of $\text{CaBa}[\text{Li}_2\text{Al}_6\text{N}_8]$ is a $2 \times 2 \times 1$ supercell of the UCr_4C_4 unit cell, if only the cell metrics are taken into consideration. It consists of a three-dimensional network of AlN_4 and LiN_4 tetrahedra connected by common vertices and edges with three different kinds of vierer ring channels in the [010] direction. Liebau established the terms einer, zweier, dreier, vierer. A vierer ring therefore is a four-membered ring of vertex-sharing tetrahedra. The terms derive from the German numerals eins (1), zwei (2), drei (3), vier (4), etc. by adding the suffix “er”.²⁶ The crystal structure is illustrated in Figure 5.3. The AlN_4 (and LiN_4) tetrahedra form gapless double chains along [010] by edge-sharing.

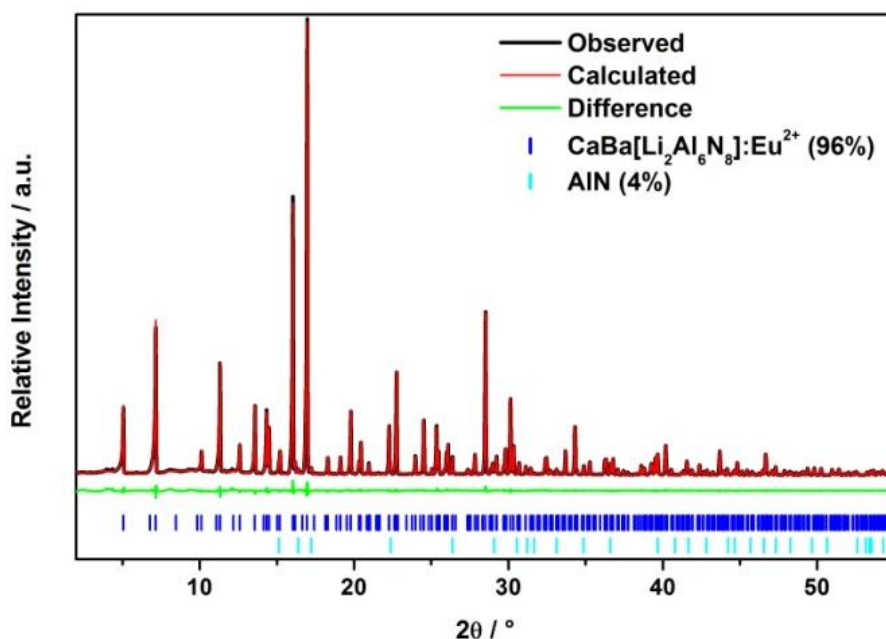


Figure 5.2. Rietveld fit of PXRD data of $\text{CaBa}[\text{Li}_2\text{Al}_6\text{N}_8]:\text{Eu}^{2+}$ ($\text{Mo K}\alpha_1$, $\lambda = 0.70932 \text{ \AA}$). The side phase AlN was quantified to 4 wt %.

Formally, these double chains can be described as two condensed einer single chains where each tetrahedron of one chain shares two edges with two tetrahedra of the other chain. Consequently, the vertically aligned faces of tetrahedra of both einer single chains adjacent to the shared edge are coplanar, but the tetrahedra themselves oriented antiparallel.

Table 5.2. Atomic Coordinates and Isotropic Displacement Parameters of $\text{CaBa}[\text{Li}_2\text{Al}_6\text{N}_8]:\text{Eu}^{2+}$

atom	Wyckoff position	x	y	z	$U_{\text{iso}}/\text{\AA}^2$
Ba1	4i	0.7504(3)	0	0.5000(5)	0.0077(2)
Ca1	4g	0	0.246(2)	0	0.0046(5)
Al1	4i	0.4334(8)	0	0.710(2)	0.003(4)
Al2	4i	0.1524(9)	0	0.875(2)	0.003(4)
Al3	4i	0.3472(9)	0	0.144(2)	0.003(4)
Al4	4i	0.5743(8)	1/2	0.296(2)	0.003(4)
Al5	8j	0.4220(2)	0.7502(3)	0.3631(9)	0.0065(9)
Li1	8j	0.1761(10)	0.250(11)	0.188(3)	0.003(5)
N1	8j	0.4003(6)	0.261(6)	0.58504(12)	0.014(3)
N2	4i	0.4584(2)	1/2	0.2444(4)	0.003(8)
N3	4i	0.3727(3)	0	0.9026(3)	0.005(8)
N4	4i	0.0443(2)	1/2	0.7586(3)	0.003(8)
N5	8j	0.3100(6)	0.7624(5)	0.2352(10)	0.003(3)
N6	4i	0.3725(3)	1/2	0.9126(3)	0.003(9)

^aEstimated standard deviations in parentheses

Accordingly, like in SLA, only 4-fold bound $\text{N}^{[4]}$ atoms occur in the crystal structure. The outward facing N atoms of the tetrahedra simultaneously are part of the common edge of tetrahedra of the next double chains. Two different double chains can be distinguished: one composed solely of AlN_4 tetrahedra and one composed of one single chain of AlN_4 tetrahedra and one single chain of LiN_4 tetrahedra. The AE counterions Ba^{2+} and Ca^{2+} are located within the aforementioned channels along [010]. The largest-diameter channel is occupied by Ba atoms coordinated cubelike by eight N atoms. One of the smaller-diameter channels is occupied by Ca atoms coordinated cubelike by eight N atoms, while the third channel remains empty. The AEN_8 polyhedra themselves are displayed in Figure 5.4 with the corresponding AE–N bond lengths and share common faces forming strands in the [010] direction.

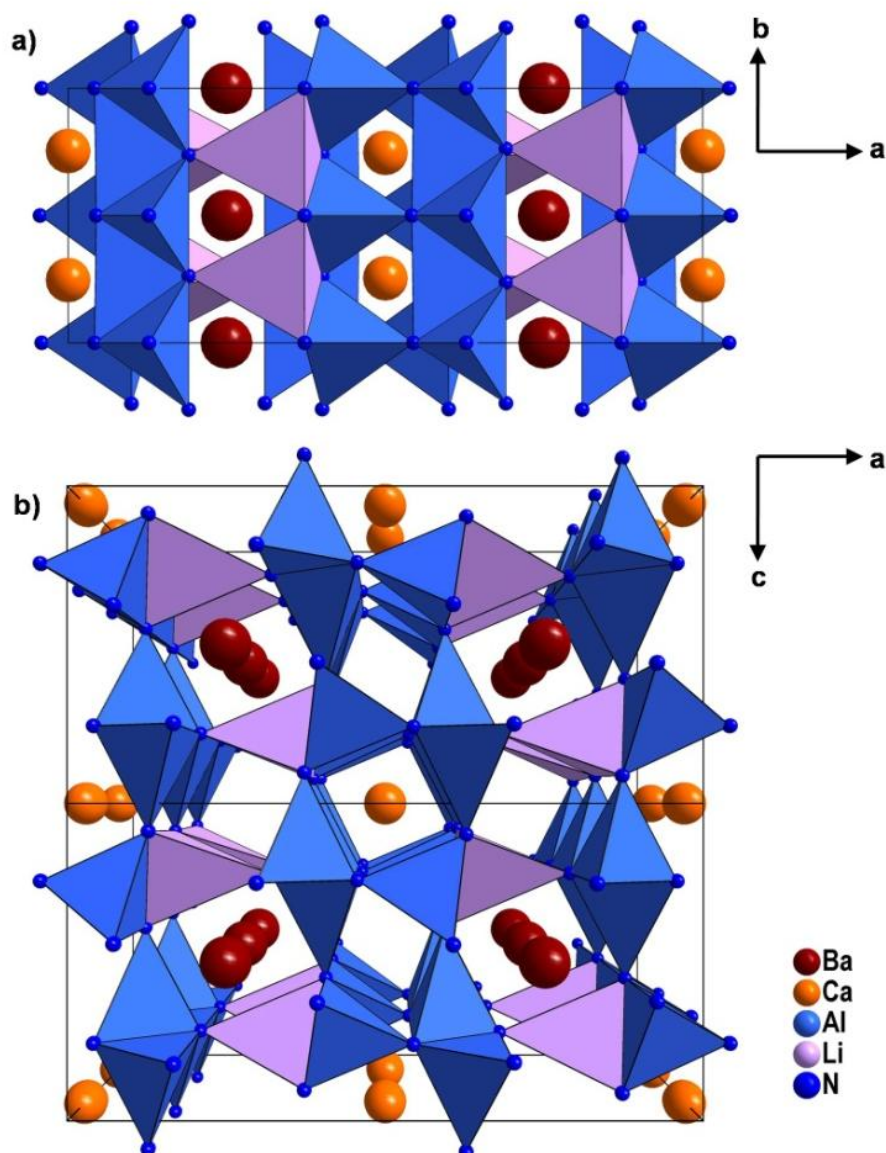


Figure 5.3. Crystal structure of $\text{CaBa}[\text{Li}_2\text{Al}_6\text{N}_8]:\text{Eu}^{2+}$. AlN_4 tetrahedra rendered blue, $(\text{Al/Li})\text{N}_4$ tetrahedra rendered turquoise. (a) View along $[001]$, (b) view along $[010]$.

The bond lengths of the AlN_4 polyhedra as well as AlN_4 and $(\text{Al/Li})\text{N}_4$ tetrahedra correspond well with other known nitrido(litho)aluminates. Al-N bond lengths are in the range 1.755(13)–2.08(9) Å and are therefore comparable to the bond length range given in the literature (e.g., $\text{Sr}[\text{LiAl}_3\text{N}_4]$, 1.87–2.00 Å;⁸ $\text{Ca}_{18.75}\text{Li}_{10.5}[\text{Al}_{39}\text{N}_{55}]$, 1.8086(14)–1.9805(14) Å;²⁷ $\alpha\text{-Ca}_3[\text{Al}_2\text{N}_4]$, 1.822(2)–1.981(2) Å).¹¹ Observed Li-N distances are 1.94(6)–2.20(2) Å, close to reports in the literature (e.g., $\text{Ca}[\text{LiAl}_3\text{N}_4]$, 1.9680(2)–2.2788(3) Å;¹⁵ $\text{Ca}[\text{LiAlN}_2]$, 2.043(3)–2.278(7) Å).¹³ Ca-N bond lengths range from 2.616(8) to 2.74(1) Å with reports for similar

5. Narrow-Band Red Luminescence in Nitridolithoaluminate $\text{CaBa}[\text{Li}_2\text{Al}_6\text{N}_8]:\text{Eu}^{2+}$

coordination geometries from 2.5202(3) to 2.9075(3) Å in $\text{Ca}[\text{LiAl}_3\text{N}_4]^{15}$ and 2.763(3) Å in $\text{Ca}[\text{Mg}_2\text{Al}_2\text{N}_4]^{14}$.

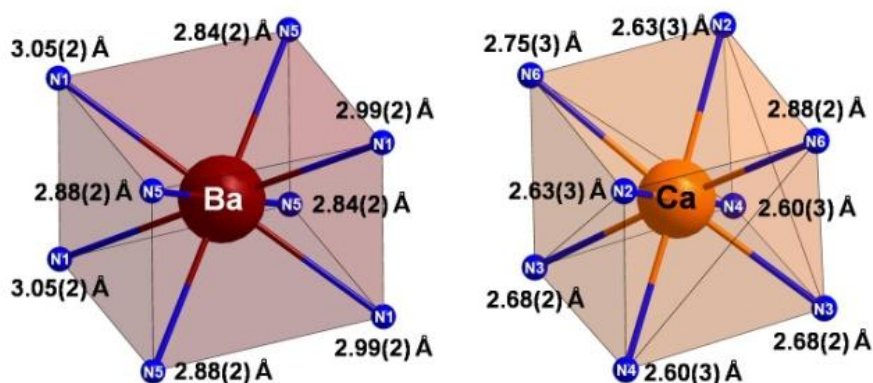


Figure 5.4. Coordination polyhedra of the AE atoms and bond lengths of the AE–N bonds in $\text{CaBa}[\text{Li}_2\text{Al}_6\text{N}_8]:\text{Eu}^{2+}$.

Upon direct comparison of the crystal structures of $\text{Sr}[\text{LiAl}_3\text{N}_4]:\text{Eu}^{2+}$ and $\text{CaBa}[\text{Li}_2\text{Al}_6\text{N}_8]:\text{Eu}^{2+}$, the close similarities quickly become apparent: Both crystal structures derive from the UCr_4C_4 structure type, with highly condensed tetrahedra networks (cation/anion ratio $\kappa = 1$) and vierer-ring channels partially occupied by cubelike coordinated heavy-atom sites. In both structures two of these heavy-atom sites exist, which are both occupied by Sr in SLA, while in $\text{CaBa}[\text{Li}_2\text{Al}_6\text{N}_8]:\text{Eu}^{2+}$ one site is fully occupied with Ba and the other with Ca. Both structures exhibit lower symmetry than the tetragonal UCr_4C_4 crystal structure, due to ordering of the network cations Li and Al that would not be possible with the single network cation site in UCr_4C_4 . The main distinguishing feature, other than the different counterions, is the differing order of Al and Li in the respective compounds.

Luminescence

Upon doping with Eu, the title material shows intense red luminescence when irradiated with blue–green light. Photoluminescence and excitation spectra at different activator concentrations were investigated on bulk powder samples in PTFE sample holders and are shown in Figure 5.5. The material features two emission maxima at 636–639 nm and approximately 790 nm, respectively. The relative intensities of the two emission peaks depend on the activator concentration with the IR emission gaining intensity with increasing Eu content up to a saturation concentration at ≈ 0.4 mol % Eu. At very high Eu concentrations, the IR emission peak intensity again decreases compared to the emission at

637 nm. The two discrete emission bands are assigned to Eu^{2+} occupying either the Ba ($\lambda_{\text{em}} = 637 \text{ nm}$) or the Ca site ($\lambda_{\text{em}} = 790 \text{ nm}$) in the crystal structure. As a result of the differing respective ionic radii, Eu preferably occupies Ba sites at very low concentrations and more extensively occupies Ca sites only at higher concentrations. Consequently, the relative infrared emission intensity initially increases with the activator concentration.

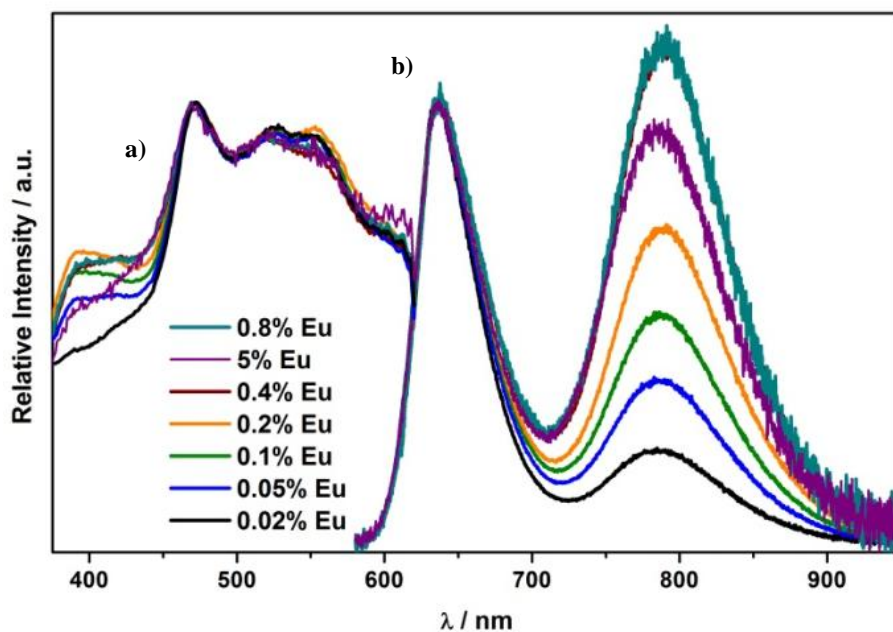


Figure 5.5. Photoluminescence spectra of $\text{CaBa}[\text{Li}_2\text{Al}_6\text{N}_8]:\text{Eu}^{2+}$ at different activator concentrations. (a) Excitation spectra ($\lambda_{\text{obs}} = 635\text{--}950 \text{ nm}$). (b) Emission spectra ($\lambda_{\text{exc}} = 444 \text{ nm}$).

The assignment of $\lambda_{\text{em}} = 637 \text{ nm}$ to emission of Eu^{2+} from a Ba site is corroborated by the emission band resolved excitation spectra shown in Figure 5.6. Here, the lowest-lying absorption band with a maximum at 541 nm, indicating the shortest Eu–N contacts, that is Eu^{2+} occupying the Ca site, is clearly associated with the deep-red/infrared emission centered at 790 nm. The absorption band centered at 470 nm vice versa corresponds to emission from Eu occupying the Ba site. The observed stagnation and eventual decrease of the infrared emission relative to the red emission intensity at high activator concentrations may be due to relaxation mechanisms competing with photoemission, like resonant energy transfer between activator centers at high activator concentrations. Because of the shorter Ca–Ca contacts in this crystal structure compared to Ba–Ba contacts, concentration quenching is expected to be more pronounced for emission from the Ca site than from the Ba site. Compared to the emission of Eu^{2+} occupying the Ca site in $\text{CaBa}[\text{Li}_2\text{Al}_6\text{N}_8]:\text{Eu}^{2+}$ the emission of $\text{Ca}[\text{LiAl}_3\text{N}_4]:\text{Eu}^{2+}$ with $\lambda_{\text{em}} = 668 \text{ nm}$ is strongly blue-shifted.¹⁵

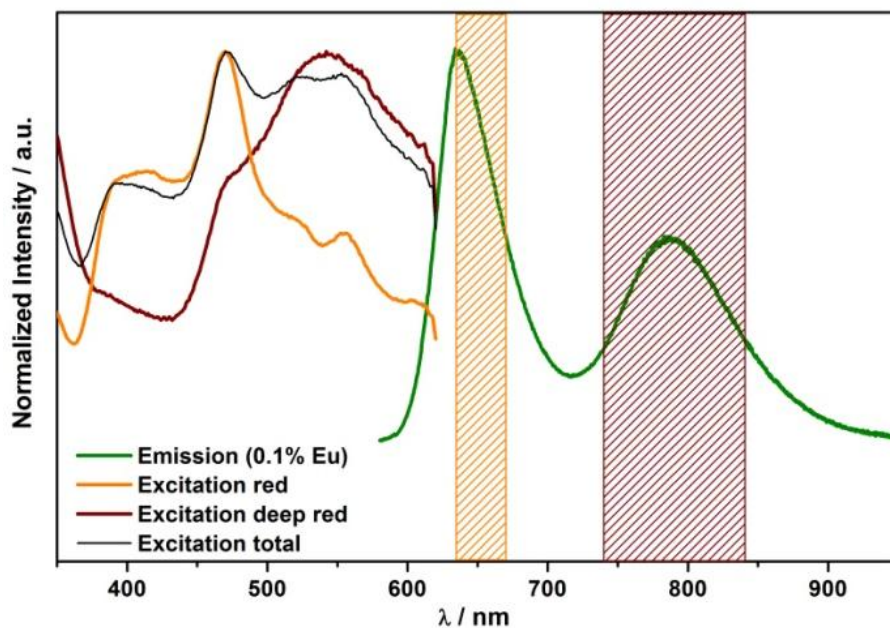


Figure 5.6. Photoluminescence spectra of $\text{CaBa}[\text{Li}_2\text{Al}_6\text{N}_8]:\text{Eu}^{2+}$ (0.1 mol % Eu). Green: emission spectrum, $\lambda_{\text{exc}} = 444$ nm; yellow, excitation spectrum, $\lambda_{\text{obs}} = 630\text{--}670$ nm; red, excitation spectrum, $\lambda_{\text{obs}} = 740\text{--}840$ nm; black, excitation spectrum, $\lambda_{\text{obs}} = 635\text{--}950$ nm.

The different emission wavelengths for topologically identical materials and activator positions can be explained by the significantly shorter average $\text{Ca}(\text{Eu})\text{--N}$ distances in $\text{CaBa}[\text{Li}_2\text{Al}_6\text{N}_8]:\text{Eu}^{2+}$ (2.6714 Å) than in $\text{Ca}[\text{LiAl}_3\text{N}_4]:\text{Eu}^{2+}$ (2.7263 Å). Because of the weaker crystal field splitting associated with longer activator–ligand contacts, the emission of $\text{Ca}[\text{LiAl}_3\text{N}_4]:\text{Eu}^{2+}$ is blue-shifted.

While the infrared emission band is already relatively narrow ($\text{fwhm} \approx 1450 \text{ cm}^{-1}$) the emission band at 636–639 nm exhibits an exceptionally small fwhm of 1095–1266 cm^{-1} depending on the activator concentration (see Table 5.3). Emission fwhm of the emission band centered at 637 nm is comparable to that of other narrow-band red-emitting materials like $\text{Sr}[\text{LiAl}_3\text{N}_4]:\text{Eu}^{2+}$ ($\text{fwhm} = 1180 \text{ cm}^{-1}$),⁸ $\text{Sr}[\text{Mg}_3\text{SiN}_4]:\text{Eu}^{2+}$ ($\text{fwhm} = 1170 \text{ cm}^{-1}$),⁹ or $\text{Ca}_{18.75}\text{Li}_{10.5}[\text{Al}_{39}\text{N}_{55}]:\text{Eu}^{2+}$ ($\text{fwhm} = 1280 \text{ cm}^{-1}$).²⁷ In the first two just-mentioned materials, the *AE* sites occupied by Eu are coordinated more or less distorted cubelike by N atoms, just like in $\text{CaBa}[\text{Li}_2\text{Al}_6\text{N}_8]:\text{Eu}^{2+}$. Additionally, the $\text{Al}/\text{Li}(\text{Mg}/\text{Si})\text{N}_4$ tetrahedra of the *AE* second sphere coordination show no disorder and consequently cause only minor, if any, anisotropic line broadening, resulting in the narrow emission observed here. The broadening of the emission band with increasing activator content is accompanied by a marginal shift of the emission toward longer wavelengths. This red-shift is due to increased reabsorption on the high

energy side of the emission spectrum, which in turn simultaneously limits the increase of the emission fwhm. The strong absorption in the red spectral region, as shown by the excitation spectra in Figures 5.5 and 5.6, is largely on account of Eu occupying the Ca site. Red light emitted by Eu occupying the Ba site therefore can easily be reabsorbed by Eu occupying the Ca site and re-emitted as infrared light.

Table 5.3. Emission Maxima and fwhm of Red Emission of $\text{CaBa}[\text{Li}_2\text{Al}_6\text{N}_8]:\text{Eu}^{2+}$ at Different Activator Concentrations

Eu concentration / mol %	$\lambda_{\text{em}} / \text{nm}$	fwhm / cm^{-1}	IQE
0.02	636	1095	12
0.05	637	1163	19
0.1	637	1207	18
0.2	638	1226	7
0.4	639	1266	4
0.8	639	–	2

Internal quantum efficiencies measured at an excitation wavelength of $\lambda_{\text{exc}} = 440 \text{ nm}$ are in the range 2–19% at room temperature, depending on the activator concentration (see Table 5.3). Temperature-dependent relative quantum efficiencies of the total emission and resolved for emission from Eu^{2+} occupying the Ba and Ca site are presented in Figure 5.7. While the Ba-site emission is largely comparable to that of SLA with $\text{QE}_{\text{rel}}(500 \text{ K}) \approx 95\%$,⁸ the Ca-site emission rapidly decreases with increasing temperatures. The total thermal behavior composed of the extremely high thermal stability Ba-site emission and the strongly quenching Ca-site emission lies in between the two extremes at $\text{QE}_{\text{rel}}^{\text{total}}(500 \text{ K}) \approx 58\%$. Thus, the Ca-site emission is more susceptible not only to concentration quenching but also to thermal quenching.

Low-temperature photoluminescence spectra shown in Figure 5.8 reveal that the mean phonon energy (approximated by $\Gamma(T) = \Gamma(0) \sqrt{\coth(\hbar\omega/2kT)}$ ²⁸ of the Ba site ($\approx 40 \text{ cm}^{-1}$) is significantly smaller than that of the Ca site ($\approx 160 \text{ cm}^{-1}$), corresponding with weaker electron–phonon coupling according to the broadening of the individual lines with increasing temperatures.²⁹ Additional information can be derived from the relative intensities of the respective vibrational replicas, i.e., the additional peaks at higher respective wavelengths.

5. Narrow-Band Red Luminescence in Nitridolithoaluminate $\text{CaBa}[\text{Li}_2\text{Al}_6\text{N}_8]:\text{Eu}^{2+}$

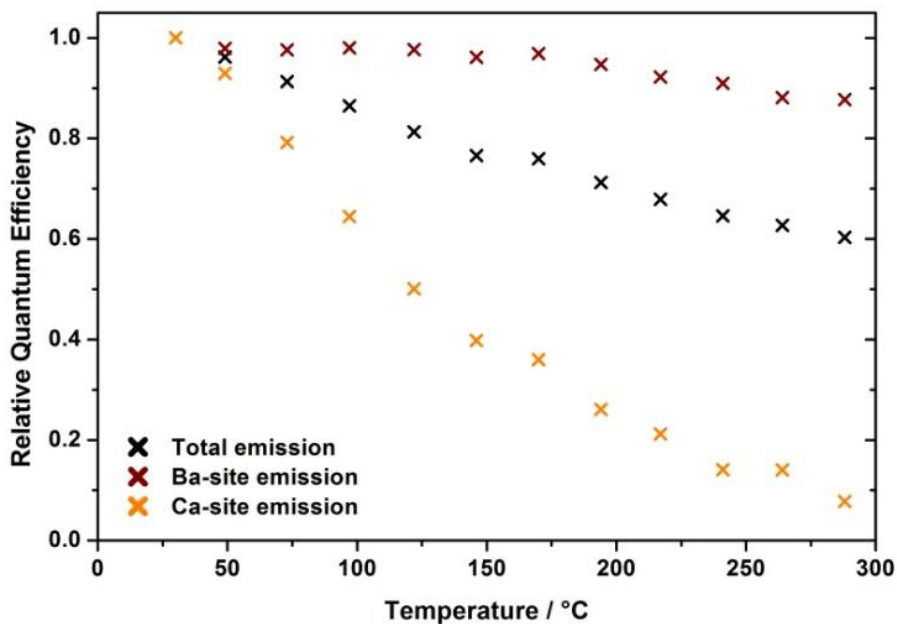


Figure 5.7: Thermal behavior of the emission of $\text{CaBa}[\text{Li}_2\text{Al}_6\text{N}_8]:\text{Eu}^{2+}$. The relative quantum efficiencies of the total emission (black) as well as that of the emissions corresponding to the respective alkaline-earth metal atom sites (red, Ba; orange, Ca) are given.

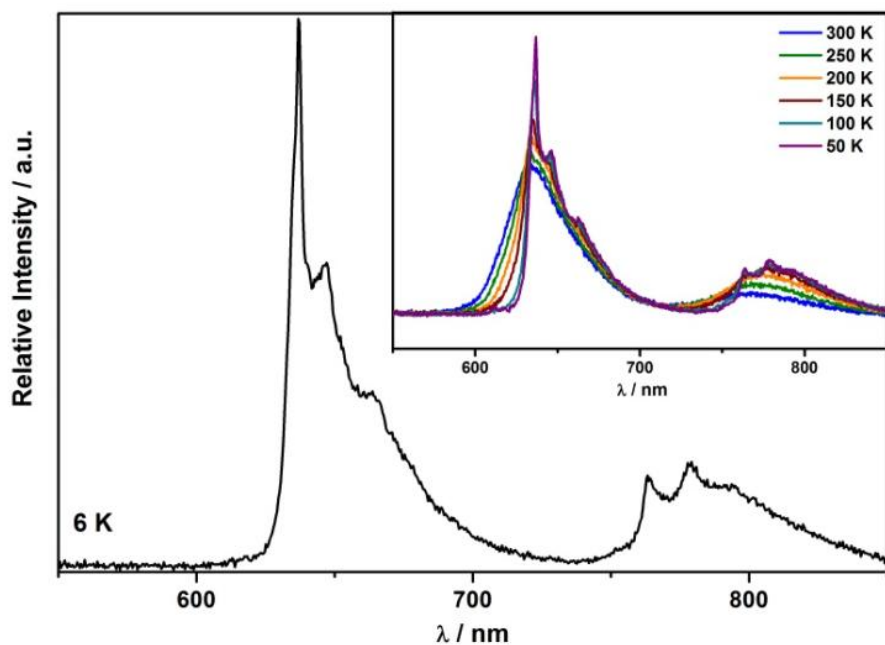


Figure 5.8. Low-temperature photoluminescence spectrum of $\text{CaBa}[\text{Li}_2\text{Al}_6\text{N}_8]:\text{Eu}^{2+}$ at 6 K. Inset: photoluminescence spectra at different temperatures from 50 to 300 K.

The zero-phonon line of emission from Eu occupying the Ba site seems to be the most intense transition, with higher vibronic replica at at most half of the zero-phonon line

intensity indicating a Huang–Rhys factor <1 . Emission from Eu occupying the Ca site exhibits higher transition intensities for higher vibrational replicas, indicating a Huang–Rhys factor ≈ 1.5 – 2 .³⁰ These differences in Huang–Rhys factors are due to the stronger relaxation in the $4f^65d$ excited state of the Eu^{2+} ion occupying the smaller Ca site.³¹

Conclusion

Here, we reported on the novel red-/infrared-emitting nitridolithoaluminate $\text{CaBa}[\text{Li}_2\text{Al}_6\text{N}_8]:\text{Eu}^{2+}$. The material was obtained by reacting the nitrides and hydrides in a heterogeneous high-pressure/high-temperature reaction in a hot isostatic press. The crystal structure was refined from powder X-ray diffraction data on the basis of the isotopic compound $\text{RbNaLi}_6\text{Si}_2\text{O}_8$. Derived from the related compound $\text{Sr}[\text{LiAl}_3\text{N}_4]:\text{Eu}^{2+}$ with remarkable optical properties, its highly condensed and rigid network of LiN_4 and AlN_4 tetrahedra and their well-ordered arrangement combined with channels occupied by the alkaline earth counterions in cubelike coordination provide optimum conditions for efficient conversion and narrow-band emission.

Red luminescence upon doping with Eu and irradiation with blue–green light is observed with two distinct emission maxima at $\lambda \approx 638$ nm and $\lambda \approx 790$ nm, corresponding with emission from Eu occupying the Ba and Ca site, respectively. The ratio of red/infrared emission is tunable by adjusting the dopant concentration in the range 0.02–5%. Very small Eu contents effectively suppress the infrared emission. The remaining emission from the Ba site with a minimum fwhm of 1095 cm^{-1} is the most narrow-band red emission of any known Eu^{2+} -activated phosphor material to date.

On the basis of the rigid network structure and the material's outstanding luminescence properties, $\text{CaBa}[\text{Li}_2\text{Al}_6\text{N}_8]:\text{Eu}^{2+}$ could play a key role in the development of nearly optimal narrow-band phosphors, e.g., by substituting Ca by Mg and thus constraining Eu^{2+} to occupying solely the Ba site for eliminating IR emission, and their application in illumination-grade WLEDs.

Associated Content

Supporting Information

The Supporting Information is available free of charge on the ACS Publications website at DOI: 10.1021/acs.chemmater.8b03485.

X-ray crystallographic information file of $\text{CaBa}[\text{Li}_2\text{Al}_6\text{N}_8]:\text{Eu}^{2+}$ from powder X-ray diffraction data (CIF)

Author Information

Corresponding Author

*E-mail: wolfgang.schnick@uni-muenchen.de

ORCID

Wolfgang Schnick: 0000-0003-4571-8035

Notes

The authors declare no competing financial interest.

Acknowledgements

The authors thank Christian Maak (Department of Chemistry, University of Munich) for EDX measurements and SEM imaging.

References

- (1) Energy Savings Forecast of Solid-State Lighting in General Illumination Applications; U.S. Department of Energy: Washington, D.C., 2016.
- (2) Uheda, K.; Hirosaki, N.; Yamamoto, H. Host lattice materials in the system $\text{Ca}_3\text{N}_2\text{-AlN-Si}_3\text{N}_4$ for white light emitting diode. *Phys. Status Solidi A* **2006**, *203*, 2712–2717.
- (3) Uheda, K.; Hirosaki, N.; Yamamoto, Y.; Naito, A.; Nakajima, T.; Yamamoto, H. Luminescence properties of a red phosphor, $\text{CaAlSiN}_3:\text{Eu}^{2+}$, for white light-emitting diodes. *Electrochem. Solid-State Lett.* **2006**, *9*, H22–H25.
- (4) Wang, L.; Xie, R.-J.; Li, Y.; Wang, X.; Ma, C.-G.; Luo, D.; Takeda, T.; Tsai, Y.-T.; Liu, R.-S.; Hirosaki, N. $\text{Ca}_{1-x}\text{Li}_x\text{Al}_{1-x}\text{Si}_{1+x}\text{N}_3:\text{Eu}^{2+}$ solid solutions as broadband, color-tunable and thermally robust red phosphors for superior color rendition white light-emitting diodes. *Light: Sci. Appl.* **2016**, *5*, e16155.
- (5) Pust, P.; Schnick, W.; Schmidt, P. J. A revolution in lighting. *Nat. Mater.* **2015**, *14*, 454–458.

5. Narrow-Band Red Luminescence in Nitridolithoaluminate $\text{CaBa}[\text{Li}_2\text{Al}_6\text{N}_8]:\text{Eu}^{2+}$

- (6) Wang, L.; Xie, R.-J.; Suehiro, T.; Takeda, T.; Hirosaki, N. Down-Conversion Nitride Materials for Solid State Lighting: Recent Advances and Perspectives. *Chem. Rev.* **2018**, *118*, 1951–2009.
- (7) Li, S.; Xie, R.-J.; Takeda, T.; Hirosaki, N. Critical Review-Narrow-Band Nitride Phosphors for Wide Color-Gamut White LED Backlighting. *ECS J. Solid State Sci. Technol.* **2018**, *7*, R3064–R3078.
- (8) Pust, P.; Weiler, V.; Hecht, C.; Tücks, A.; Wochnik, A. S.; Henss, A.-K.; Wiechert, D.; Scheu, C.; Schmidt, P. J.; Schnick, W. Narrow-band red-emitting $\text{Sr}[\text{LiAl}_3\text{N}_4]:\text{Eu}^{2+}$ as a next-generation LED-phosphor material. *Nat. Mater.* **2014**, *13*, 891–896.
- (9) Schmiechen, S.; Schneider, H.; Wagatha, P.; Hecht, C.; Schmidt, P. J.; Schnick, W. Toward New Phosphors for Application in Illumination-Grade White pc-LEDs: The Nitridomagnesosilicates $\text{Ca}[\text{Mg}_3\text{SiN}_4]:\text{Ce}^{3+}$, $\text{Sr}[\text{Mg}_3\text{SiN}_4]:\text{Eu}^{2+}$, and $\text{Eu}[\text{Mg}_3\text{SiN}_4]$. *Chem. Mater.* **2014**, *26*, 2712–2719.
- (10) Blase, W.; Cordier, G.; Ludwig, M.; Kniep, R. $\text{Sr}_3[\text{Al}_2\text{N}_4]$: A Nitridoaluminate with Corrugated Tetrahedral Chains ${}^1[\text{AlN}_{4/2}{}^{3-}]$. *Z. Naturforsch., B: J. Chem. Sci.* **1994**, *49*, 501–505.
- (11) Ludwig, M.; Jäger, J.; Niewa, R.; Kniep, R. Crystal Structures of Two Polymorphs of $\text{Ca}_3[\text{Al}_2\text{N}_4]$. *Inorg. Chem.* **2000**, *39*, 5909–5911.
- (12) Ludwig, M.; Niewa, R.; Kniep, R. Dimers $[\text{Al}_2\text{N}_6]^{12-}$ and chains ${}^1[\text{AlN}_{4/2}{}^{3-}]$ in the crystal structures of $\text{Ca}_6[\text{Al}_2\text{N}_6]$ and $\text{Ba}_3[\text{Al}_2\text{N}_4]$. *Z. Naturforsch., B: J. Chem. Sci.* **1999**, *54*, 461–465.
- (13) Pust, P.; Pagano, S.; Schnick, W. $\text{Ca}[\text{LiAlN}_2]$: A Quaternary Nitridoaluminate. *Eur. J. Inorg. Chem.* **2013**, *2013*, 1157–1160.
- (14) Pust, P.; Hintze, F.; Hecht, C.; Weiler, V.; Locher, A.; Zitnanska, D.; Harm, S.; Wiechert, D.; Schmidt, P. J.; Schnick, W. Group (III) Nitrides $M[\text{Mg}_2\text{Al}_2\text{N}_4]$ ($M = \text{Ca}, \text{Sr}, \text{Ba}, \text{Eu}$) and $\text{Ba}[\text{Mg}_2\text{Ga}_2\text{N}_4]$ —Structural Relation and Nontypical Luminescence Properties of Eu^{2+} Doped Samples. *Chem. Mater.* **2014**, *26*, 6113–6119.
- (15) Pust, P.; Wochnik, A. S.; Baumann, E.; Schmidt, P. J.; Wiechert, D.; Scheu, C.; Schnick, W. $\text{Ca}[\text{LiAl}_3\text{N}_4]:\text{Eu}^{2+}$ -A Narrow-Band Red-Emitting Nitridolithoaluminate. *Chem. Mater.* **2014**, *26*, 3544–3549.
- (16) Wilhelm, D.; Baumann, D.; Seibald, M.; Wurst, K.; Heymann, G.; Huppertz, H. Narrow-Band Red Emission in the Nitridolithoaluminate $\text{Sr}_4[\text{LiAl}_{11}\text{N}_{14}]:\text{Eu}^{2+}$. *Chem. Mater.* **2017**, *29*, 1204–1209.
- (17) Wagatha, P.; Weiler, V.; Schmidt, P. J.; Schnick, W. Tunable Red Luminescence in Nitridomagnesoaluminates $\alpha\text{-Sr}_2[\text{MgAl}_5\text{N}_7]:\text{Eu}^{2+}$, $\beta\text{-Sr}_2[\text{MgAl}_5\text{N}_7]:\text{Eu}^{2+}$, and $\text{Sr}_8[\text{LiMg}_2\text{Al}_{21}\text{N}_{28}]:\text{Eu}^{2+}$. *Chem. Mater.* **2018**, *30*, 1755–1761.
- (18) Seibald, M.; Baumann, D.; Schroeder, T.; Lange, S.; Hoerder, G.; Achrainger, G. M.; Huppertz, H.; Peschke, S.; Marchuk, A.; Schmid, P.; Hummel, F.; Dirksmeyer, S. OSRAM GmbH. Oxynitride phosphors, lighting devices using the phosphors, and their use as backlights, Patent WO2018087304A1, 2018
- (19) Narrow Red Phosphor Technology White Paper 2016. Lumileds. www.lumileds.com/support/documentation/white-papers (accessed Oct 12, 2018).
- (20) Bergmann, J.; Kleeberg, R.; Haase, A.; Breidenstein, B. Advanced Fundamental Parameters Model for Improved Profile Analysis. *Mater. Sci. Forum* **2000**, *347–349*, 303–308.
- (21) Cheary, R. W.; Coelho, A. A.; Cline, J. P. Fundamental Parameters Line Profile Fitting in Laboratory Diffractometers. *J. Res. Natl. Inst. Stand. Technol.* **2004**, *109*, 1–25.
- (22) Coelho, A. *TOPAS—Academic 2007*; Coelho Software, Brisbane.

5. Narrow-Band Red Luminescence in Nitridolithoaluminate $\text{CaBa}[\text{Li}_2\text{Al}_6\text{N}_8]:\text{Eu}^{2+}$

- (23) Rietveld, H. M. Profile Refinement Method for Nuclear and Magnetic Structures. *J. Appl. Crystallogr.* **1969**, *2*, 65–71.
- (24) Hoffmann, J.; Brandes, R.; Hoppe, R. Neue Silicate mit „Stuffed Pyrgoms“: $\text{CsKNaLi}_9\{\text{Li}[\text{SiO}_4]\}_4$, $\text{CsKNa}_2\text{Li}_8\{\text{Li}[\text{SiO}_4]\}_4$, $\text{RbNa}_3\text{Li}_8\{\text{Li}[\text{SiO}_4]\}_4$ [1] und $\text{RbNaLi}_4\{\text{Li}[\text{SiO}_4]\}_2$ [2]. *Z. Anorg. Allg. Chem.* **1994**, *620*, 1495–1508.
- (25) Behrens, R. K.; Jeitschko, W. Uranium Chromium Carbide (UCr_4C_4) with Filled Molybdenum-Nickel (MoNi_4) Type Structure. *Monatsh. Chem.* **1987**, *118*, 43–50.
- (26) Liebau, F. *Structural Chemistry of Silicates*; Springer: Berlin, 1985.
- (27) Wagatha, P.; Pust, P.; Weiler, V.; Wochnik, A. S.; Schmidt, P. J.; Scheu, C.; Schnick, W. $\text{Ca}_{18.75}\text{Li}_{10.5}[\text{Al}_{39}\text{N}_{55}]:\text{Eu}^{2+}$ -Supertetrahedron Phosphor for Solid-State Lighting. *Chem. Mater.* **2016**, *28*, 1220–1226.
- (28) Curie, D. Absorption and Emission Spectra. In *Optical Properties of Ions in Solids*; Di Bartolo, B., Ed.; Springer: Boston, Ma, 1975; Vol. 8.
- (29) Kunkel, N.; Meijerink, A.; Kohlmann, H. Bright Yellow and Green Eu(II) Luminescence and Vibronic Fine Structures in LiSrH_3 , LiBaH_3 and their Corresponding Deuterides. *Phys. Chem. Chem. Phys.* **2014**, *16*, 4807–4813.
- (30) de Jong, M.; Seijo, L.; Meijerink, A.; Rabouw, F. T. Resolving the Ambiguity in the Relation Between Stokes Shift and Huang-Rhys Parameter. *Phys. Chem. Chem. Phys.* **2015**, *17*, 16959–16969.
- (31) Meijerink, A.; Blasse, G. Luminescence Properties of Europium(2+)-Activated Alkaline Earth Haloborates. *J. Lumin.* **1989**, *43*, 283–289

6. Conclusion and Outlook

Phosphors for lighting in general and pc-LEDs in particular have come a long way. Since the development of a highly-efficient blue LED and the initial use of a single yellow phosphor (e.g. YAG:Ce), illumination-grade solid-state lighting evolved to multi-phosphor devices for excellent color rendition. The development of red-emitting materials received special attention because of the significant impact of the red component on the luminous efficacy and color rendering index of a white LED. Naturally, Eu^{2+} doped materials are well suited as phosphors due to the parity allowed and therefore intense $f-d$ transition. While the energy of this transition is too high to produce red emission in an oxidic environment, the nephelauxetic effect resulting from a nitridic environment can effectively reduce emission energy to the red spectral region. Several red-emitting Eu^{2+} -doped nitride materials have found their way to industrial application over the last decade, namely SCASN ($\text{Sr}_x\text{Ca}_{1-x}\text{AlSiN}_3:\text{Eu}^{2+}$), BSSNE ($\text{Ba}_x\text{Sr}_{1-x}\text{Si}_5\text{N}_8:\text{Eu}^{2+}$) and most recently SLA ($\text{Sr}[\text{LiAl}_3\text{N}_4]:\text{Eu}^{2+}$).¹⁻⁴ Nitridoaluminates like SLA as a material class had not received much attention in neither academic research communities nor in the phosphors industry prior to our group intensifying investigation efforts less than ten years ago.⁵⁻⁷ As a consequence, several novel nitridoaluminates and nitridoaluminate phosphors were discovered and their physical properties probed.⁸⁻¹⁰ Other research groups contributed various additional nitridoaluminate materials to our knowledge base over the course of this work.¹¹⁻¹⁴

Major challenges in the synthesis of novel nitridoaluminates are not only the limited range of possible aluminum precursors and the thermodynamic stability of binary AlN, but also the tendency of again and again obtaining the same few phases that just a short while ago had been both most elusive and desirable simultaneously. Classical synthesis strategies like high-temperature approaches or flux methods yielded predominantly the UCr_4C_4 -type and related materials first described by Philipp Pust^{2, 9-10} or reached their limitations with Mg-containing materials due to the relatively high vapor pressure of Mg and Mg_3N_2 . One possible answer to prevent the evaporation of magnesium species from the reaction mixture and circumvent the formation of already known phases, was the introduction of the reaction parameter gas pressure to the equation. Consequently, the acquisition of a hot isostatic press was pursued.

6. Conclusion and Outlook

Hot isostatic presses originate from ceramics production, where they are mainly used for sintering closed porous ceramic green bodies. In our application the high obtainable N₂-pressures are favorable for both preventing reagent evaporation and for additional reactivity of thermally activated nitrogen.

The so realizable heterogenous high-temperature/high-pressure reaction yielded access to four previously unknown nitridoaluminates and phosphor materials, Ca_{20-x}Li_{8+2x}[Al₃₉N₅₅]:Eu²⁺ ($x = 0-2$), (α -)Sr₈[Li_{2-0.5x}Mg_xAl_{22-0.5x}N₂₈]:Eu²⁺ ($x = 0-4$) and β -Sr₂[MgAl₅N₇] and CaBa[Li₂Al₆N₈]:Eu²⁺ by reacting the respective metal nitrides and/or metal hydrides in molybdenum crucibles at around 1000–1500 °C. These materials represent a significant advance in the research of narrow-band red emitting phosphors for solid-state lighting.

Pure nitridoaluminate Ca_{18.75}Li_{10.5}[Al₃₉N₅₅]:Eu²⁺ and other representatives of the solid solution series Ca_{20-x}Li_{8+2x}[Al₃₉N₅₅]:Eu²⁺ ($x = 0-2$) combine intense narrow-band red luminescence with a very unusual crystal structure. Crystallizing homeotypically with the oxomanganate Na₂₆Mn₃₉O₅₅ in the cubic space group $Fd\bar{3}m$ (no. 227) with $a = 22.415(3)$ Å,¹⁵ two interpenetrating diamond-type networks of vertex-sharing T₅ supertetrahedra—each consisting of 35 individual AlN₄ tetrahedra and representing sections of a sphalerite-type cubic AlN network—ultimately form a hierarchical variant of the NaTl structure type with a degree of condensation $\kappa = 0.71$.¹⁶ The structural motif of supertetrahedra is quite rare in nitride chemistry and prior to Ca_{18.75}Li_{10.5}[Al₃₉N₅₅]:Eu²⁺ was observed only twice in Li₂SiN₂ and Li₁₀P₄N₁₀.¹⁷⁻¹⁸ More recently nitridophosphates Li₁₃P₄N₁₀X₃ (X = Cl, Br) and Li₄₇B₃P₁₂N₄₂, also exhibiting supertetrahedra, were reported on.¹⁹⁻²⁰

Emission maxima $\lambda_{\max} = 640-648$ nm (fwhm = 56–61 nm; ≈ 1280 cm⁻¹) depending on the compositional variable x show internal quantum efficiencies from 9–24% at a nominal Eu²⁺ dopant concentration of 0.5% and pronounced thermal quenching of emission. While in most other narrow-band red emitting materials the alkaline earth counterions, and consequently the activator ions occupying these atom sites as well, are coordinated cube like, the Ca atoms are coordinated distorted trigonal antiprismatically and trigonal prismatically in Ca_{18.75}Li_{10.5}[Al₃₉N₅₅]:Eu²⁺. Despite this coordination geometry not being as clearly associated with narrow-band emission as cube-like coordination, the material's rigid structure with no disorder in the anionic network still provides a suitable environment for small fwhms.²¹

Representatives of the narrow-band red emitting solid-solution series $\text{Sr}_8[\text{Li}_{2-0.5x}\text{Mg}_x\text{Al}_{22-0.5x}\text{N}_{28}]:\text{Eu}^{2+}$ ($x = (0), 2, 4$) crystallize homeotypically with the oxozincate $\text{K}_2\text{Zn}_6\text{O}_7$ in the orthorhombic space group $Pn\bar{n}m$ (no. 58) with unit cell parameters $a = 10.4291(7)/10.51818(5)/10.54878(6)$, $b = 10.4309(7)/10.44513(5)/10.48253(6)$, $c = 3.2349(2)/3.25704(1)/3.27275(2)$ Å and $V = 351.9(2)/357.831(3)/361.894(3)$ Å³ ($x = 0/2/4$) and were first reported as nitridolithoaluminate with $x = 0$ and the sum formula $\text{Sr}_4[\text{LiAl}_{11}\text{N}_{14}]:\text{Eu}^{2+}$.^{12, 22} Depending on the Eu content of $\text{Sr}_2[\text{MgAl}_5\text{N}_7]:\text{Eu}^{2+}$ ($x = 4$), the emission maximum can be shifted from $\lambda_{\text{em}} = 633$ nm (0.075% Eu) to $\lambda_{\text{em}} = 665$ nm (1% Eu) with a correspondingly decreasing fwhm from 1940–1736 cm⁻¹ due to increasing reabsorption on the high-energy side of the spectrum. The incorporation of Mg^{2+} as network cation in addition to Li^+ and Al^{3+} leads to a significantly blue-shifted emission with $\lambda_{\text{em}} = 633$ nm for $x = 4$ and $\lambda_{\text{em}} = 645$ nm for $x = 2$, compared to $\lambda_{\text{em}} = 670$ nm for $x = 0$. Here, the relatively broad emission is caused by statistical disorder on some of the network-cation sites like in $(\text{Ca}/\text{Sr})[\text{Mg}_2\text{Al}_2\text{N}_4]:\text{Eu}^{2+}$.⁹

A β -polymorph of α - $\text{Sr}_2[\text{MgAl}_5\text{N}_7]:\text{Eu}^{2+}$ was obtained as side phase with up to 40 wt %. It crystallizes in the monoclinic space group $C2/m$ (no. 12) with unit cell parameters $a = 11.12874(11)$, $b = 3.27289(3)$, $c = 10.54530(11)$ Å, $\beta = 109.8939(7)^\circ$ and $V = 361.173(7)$ Å³. Its crystal structure exhibits similar building units as the α polymorph in a slightly different arrangement. In both compounds the anionic network is highly condensed with $\kappa = 0.857$, promising the necessary rigidity for efficient light conversion. The alkaline-earth counterions are coordinated cube-like by eight N atoms—with a ninth N atom capping one polyhedron face at a significantly longer AE -N distance—forming strands in either the $[001]$ direction for the α polymorph or the $[010]$ direction for the β polymorph. Of the β - $\text{Sr}_2[\text{MgAl}_5\text{N}_7]$ no luminescence properties could be determined, due to the material being a side-phase to the always present α - $\text{Sr}_2[\text{MgAl}_5\text{N}_7]$.²³

$\text{CaBa}[\text{Li}_2\text{Al}_6\text{N}_8]:\text{Eu}^{2+}$ is the material closest to optimum narrow-band red phosphors for solid state lighting. Obtainable by a heterogenous high-temperature/high pressure reaction at 1050 °C and 51.7 MPa N_2 pressure, the compound crystallizes isotypically with $\text{RbNaLi}_6\text{Si}_2\text{O}_8$ in the monoclinic space group $C2/m$ (no. 12) with unit cell parameters $a = 16.0851(2)$ Å, $b = 6.46738(4)$ Å, $c = 8.04242(13)$ Å, $\beta = 90.004(2)^\circ$ and $V = 836.64(2)$ Å³, exhibiting a $2 \times 2 \times 1$ supercell of the UCr_4C_4 unit cell regarding only the metrics and is therefore related to MMA, CLA and SLA with an identically high degree of condensation $\kappa = 1$.²⁴ $\text{CaBa}[\text{Li}_2\text{Al}_6\text{N}_8]:\text{Eu}^{2+}$

6. Conclusion and Outlook

shows intense red luminescence when irradiated with blue–green light and altogether extremely favorable luminescence properties. Its main emission at $\lambda_{em} = 636\text{--}639\text{ nm}$ is close to the optimal position at $\lambda_{em} \approx 630\text{ nm}$. With its extremely narrow emission with $fwhm = 1095\text{--}1266\text{ cm}^{-1}$

CBLA is the most narrowly red emitting Eu^{2+} luminescent material known today. Like in SLA, the network cations Li and Al show ordering, and consequently only minor anisotropic line broadening of the emission occurs. The two heavy atom sites are coordinated cube-like and are occupied by Ca and Ba, respectively, resulting in two distinct emission maxima after doping with Eu^{2+} . Apart from emission in the far deep-red/near infrared spectral region at $\lambda_{em} \approx 790\text{ nm}$, that can effectively be suppressed by reducing the activator concentration, CBLA would be the optimal red-emitting component for pcLEDs. The two observed emission bands can be attributed to the two different crystallographic alkaline-earth atom sites, with the red emission band corresponding to Eu occupying the Ba site and the infrared emission to Eu occupying the Ca site. Thermal behavior of the red emission is on par with SLA at $Q_{rel}(500\text{ K}) \approx 95\%$. Low-temperature photoluminescence spectra allow for approximation of Huang-Rhys factors and mean phonon energies for both the Ba and Ca sites respectively. A much lower Huang-Rhys factor <1 for Eu on the Ba site than $\approx 1.5\text{--}2$ for Eu on the Ca site and significantly weaker electron-phonon coupling on the Ba site are revealed.

Excellent thermal properties of especially the Ba-site emission coupled with the low phonon energies and consequently low electron-phonon coupling make $\text{CaBa}[\text{Li}_2\text{Al}_6\text{N}_8]:\text{Eu}^{2+}$ a strong contender for the development of nearly optimal narrow-band red phosphors.²⁵

Final Remarks

The here presented luminescent materials clearly show the importance of providing suitable reaction parameters for nitridoaluminate chemistry. Synthesis of these compounds was made possible by the HIP that was put into service in May 2017. Physical properties of the respective materials exhibit a clear correlation between the degree of condensation and the thermal behavior of the luminescence. From $\text{Ca}_{20-x}\text{Li}_{8+2x}[\text{Al}_{39}\text{N}_{55}]:\text{Eu}^{2+}$ ($x = 0\text{--}2$) to $\text{Sr}_8[\text{Li}_{2-0.5x}\text{Mg}_x\text{Al}_{22-0.5x}\text{N}_{28}]:\text{Eu}^{2+}$ ($x = (0), 2, 4$) to $\text{CaBa}[\text{Li}_2\text{Al}_6\text{N}_8]:\text{Eu}^{2+}$ the degree of condensation of the tetrahedron network increases from $\kappa = 0.71$ to $\kappa = 0.857$ to $\kappa = 1$.

Relative quantum efficiencies at 500 K likewise increase from >5% to 55–75% to >95% for the respective materials.

Further investigations on these materials could include substitution of either counterions of network cations for better performance. In analogy to $\text{Sr}_8[\text{Li}_{2-0.5x}\text{Mg}_x\text{Al}_{22-0.5x}\text{N}_{28}]:\text{Eu}^{2+}$ ($x = (0), 2, 4$), where a higher Li content is associated with higher relative quantum efficiencies due to the then larger band gap, Ca could be substituted by Sr in $\text{Ca}_{20-x}\text{Li}_{8+2x}[\text{Al}_{39}\text{N}_{55}]:\text{Eu}^{2+}$ ($x = 0-2$) for the same effect. In that case, a larger band gap would lead to an increased energetic separation between the excited electronic state of Eu^{2+} within the band gap and the conduction band. The consequently reduced tendency towards photoionization of the excited electron into the conduction band and subsequent nonradiative relaxation would effectively increase conversion efficiency of the material.

A similar approach for $\text{CaBa}[\text{Li}_2\text{Al}_6\text{N}_8]:\text{Eu}^{2+}$, where substitution of Ca by Mg could reduce the size of the second heavy atom site, possibly results in Eu^{2+} not occupying that site altogether due to size restraints. The resulting hypothetical material " $\text{MgBa}[\text{Li}_2\text{Al}_6\text{N}_8]:\text{Eu}^{2+}$ " therefore could exhibit only the desired emission band from Eu^{2+} occupying the Ba site at $\lambda = 636-639$ nm. Such a material, should it be accessible, would indeed be close to *the* optimum narrow-band red phosphor the solid state lighting industry is looking for.

References

- (1) Höpfe, H. A.; Lutz, H.; Morys, P.; Schnick, W.; Seilmeier, A., Luminescence in Eu^{2+} -doped $\text{Ba}_2\text{Si}_5\text{N}_8$: fluorescence, thermoluminescence, and upconversion. *J. Phys. Chem. Solids* **2000**, *61*, 2001–2006.
- (2) Pust, P.; Weiler, V.; Hecht, C.; Tücks, A.; Wochnik, A. S.; Henss, A.-K.; Wiechert, D.; Scheu, C.; Schmidt, P. J.; Schnick, W., Narrow-band red-emitting $\text{Sr}[\text{LiAl}_3\text{N}_4]:\text{Eu}^{2+}$ as a next-generation LED-phosphor material. *Nat. Mater.* **2014**, *13*, 891–896.
- (3) Uheda, K.; Hirosaki, N.; Yamamoto, H., Host lattice materials in the system $\text{Ca}_3\text{N}_2\text{-AlN-Si}_3\text{N}_4$ for white light emitting diode. *Phys. Status Solidi A* **2006**, *203*, 2712–2717.
- (4) Uheda, K.; Hirosaki, N.; Yamamoto, Y.; Naito, A.; Nakajima, T.; Yamamoto, H., Luminescence properties of a red phosphor, $\text{CaAlSiN}_3:\text{Eu}^{2+}$, for white light-emitting diodes. *Electrochem. Solid-State Lett.* **2006**, *9*, H22–H25.
- (5) Blase, W.; Cordier, G.; Ludwig, M.; Kniep, R., $\text{Sr}_3[\text{Al}_2\text{N}_4]$: A Nitrodoaluminate with Corrugated Tetrahedral Chains $\infty^1[\text{AlN}_{4/2}^{3-}]$. *Z. Naturforsch., B: Chem. Sci.* **1994**, *49*, 501–505.
- (6) Ludwig, M.; Niewa, R.; Kniep, R., Dimers $[\text{Al}_2\text{N}_6]^{12-}$ and chains $\infty^1[\text{AlN}_{4/2}^{3-}]$ in the crystal structures of $\text{Ca}_6[\text{Al}_2\text{N}_6]$ and $\text{Ba}_3[\text{Al}_2\text{N}_4]$. *Z. Naturforsch., B: Chem. Sci.* **1999**, *54*, 461–465.

6. Conclusion and Outlook

- (7) Ludwig, M.; Jäger, J.; Niewa, R.; Kniep, R., Crystal Structures of Two Polymorphs of $\text{Ca}_3[\text{Al}_2\text{N}_4]$. *Inorg. Chem.* **2000**, *39*, 5909–5911.
- (8) Pust, P.; Pagano, S.; Schnick, W., $\text{Ca}[\text{LiAlN}_2]$: A Quaternary Nitridoaluminate. *Eur. J. Inorg. Chem.* **2013**, 1157–1160.
- (9) Pust, P.; Hintze, F.; Hecht, C.; Weiler, V.; Locher, A.; Zitnanska, D.; Harm, S.; Wiechert, D.; Schmidt, P. J.; Schnick, W., Group (III) Nitrides $M[\text{Mg}_2\text{Al}_2\text{N}_4]$ ($M = \text{Ca}, \text{Sr}, \text{Ba}, \text{Eu}$) and $\text{Ba}[\text{Mg}_2\text{Ga}_2\text{N}_4]$ -Structural Relation and Nontypical Luminescence Properties of Eu^{2+} Doped Samples. *Chem. Mater.* **2014**, *26*, 6113–6119.
- (10) Pust, P.; Wochnik, A. S.; Baumann, E.; Schmidt, P. J.; Wiechert, D.; Scheu, C.; Schnick, W., $\text{Ca}[\text{LiAl}_3\text{N}_4]:\text{Eu}^{2+}$ -A Narrow-Band Red-Emitting Nitridolithoaluminate. *Chem. Mater.* **2014**, *26*, 3544–3549.
- (11) Schmidt, R.; Stroebele, M.; Eichele, K.; Meyer, H.-J., Crystal Structure and Luminescence Investigations of the Nitridomagnesoaluminates $\text{Mg}_3\text{Al}_n\text{N}_{n+2}$ with $n = 1, 2, 3$. *Eur. J. Inorg. Chem.* **2017**, *2017*, 2727–2735.
- (12) Wilhelm, D.; Baumann, D.; Seibald, M.; Wurst, K.; Heymann, G.; Huppertz, H., Narrow-Band Red Emission in the Nitridolithoaluminate $\text{Sr}_4[\text{LiAl}_{11}\text{N}_{14}]:\text{Eu}^{2+}$. *Chem. Mater.* **2017**, *29*, 1204–1209.
- (13) Seibald, M.; Baumann, D.; Schroeder, T.; Lange, S.; Hoerder, G.; Achrainger, G. M.; Huppertz, H.; Peschke, S.; Marchuk, A.; Schmid, P.; Hummel, F.; Dirksmeyer, S. Oxynitride phosphors, lighting devices using the phosphors, and their use as backlights. *Appl., P. I.* **2018**, WO2018087304A1, OSRAM GmbH
- (14) Kubus, M.; Levin, K.; Kroeker, S.; Enseling, D.; Juestel, T.; Meyer, H. J., Structural and luminescence studies of the new nitridomagnesoaluminate $\text{CaMg}_2\text{AlN}_3$. *Dalton Trans.* **2015**, *44*, 2819–2826.
- (15) Möller, A.; Amann, P.; Kataev, V.; Schittner, N., The First T_5 -Supertetrahedron in Oxide Chemistry: $\text{Na}_{26}\text{Mn}_{39}\text{O}_{55}$. *Z. Anorg. Allg. Chem.* **2004**, *630*, 890–894.
- (16) Zintl, E.; Dullenkopf, W., Metals and Alloys. IV. Lattice Structure of Sodium Thallide and its Relation to Structures of the beta-Brass Type. *Z. Phys. Chem. B* **1932**, *16*, 195–205.
- (17) Pagano, S.; Zeuner, M.; Hug, S.; Schnick, W., Single-Crystal Structure Determination and Solid-State NMR Investigations of Lithium Nitridosilicate Li_2SiN_2 Synthesized by a Precursor Approach Employing Amorphous “ $\text{Si}(\text{CN}_2)_2$ ”. *Eur. J. Inorg. Chem.* **2009**, 1579–1584.
- (18) Schnick, W.; Berger, U., $\text{Li}_{10}\text{P}_4\text{N}_{10}$ – A Lithium Phosphorous(V) Nitride Containing the New Complex Anion $\text{P}_4\text{N}_{10}^{10-}$. *Angew. Chem.* **1991**, *103*, 857–858; *Angew. Chem. Int. Ed.* **1991**, *30*, 830–831.
- (19) Bertschler, E.-M.; Dietrich, C.; Leichtweiss, T.; Janek, J.; Schnick, W., Li^+ Ion Conductors with Adamantane-Type Nitridophosphate Anions $\beta\text{-Li}_{10}\text{P}_4\text{N}_{10}$ and $\text{Li}_{13}\text{P}_4\text{N}_{10}\text{X}_3$ with $\text{X} = \text{Cl}, \text{Br}$. *Chem. Eur. J.* **2018**, *24*, 196–205.
- (20) Bertschler, E.-M.; Bräuniger, T.; Dietrich, C.; Janek, J.; Schnick, W., $\text{Li}_{47}\text{B}_3\text{P}_{14}\text{N}_{42}$ -A Lithium Nitridoborophosphate with $[\text{P}_3\text{N}_9]^{12-}$, $[\text{P}_4\text{N}_{10}]^{10-}$, and the Unprecedented $[\text{B}_3\text{P}_3\text{N}_{13}]^{15-}$ Ion. *Angew. Chem.* **2017**, *129*, 4884–4887; *Angew. Chem. Int. Ed.* **2017**, *56*, 4806–4809.
- (21) Wagatha, P.; Pust, P.; Weiler, V.; Wochnik, A. S.; Schmidt, P. J.; Scheu, C.; Schnick, W., $\text{Ca}_{18.75}\text{Li}_{10.5}[\text{Al}_{39}\text{N}_{55}]:\text{Eu}^{2+}$ -Supertetrahedron Phosphor for Solid-State Lighting. *Chem. Mater.* **2016**, *28*, 1220–1226.
- (22) Wambach, K. R.; Hoppe, R., Die Koordinationszahl 3 bei Zn^{2+} Zur Kenntnis von $\text{K}_2[\text{Zn}_6\text{O}_7]$. *Z. Anorg. Allg. Chem.* **1978**, *445*, 91–101.

- (23) Wagatha, P.; Weiler, V.; Schmidt, P. J.; Schnick, W., Tunable Red Luminescence in Nitridomagnesoaluminates α - $\text{Sr}_2[\text{MgAl}_5\text{N}_7]:\text{Eu}^{2+}$, β - $\text{Sr}_2[\text{MgAl}_5\text{N}_7]:\text{Eu}^{2+}$, and $\text{Sr}_8[\text{LiMg}_2\text{Al}_{21}\text{N}_{28}]:\text{Eu}^{2+}$. *Chem. Mater.* **2018**, *30*, 1755–1761.
- (24) Hofmann, J.; Brandes, R.; Hoppe, R., Neue Silicate mit „Stuffed Pyrgoms“: $\text{CsKNaLi}_9\{\text{Li}[\text{SiO}_4]\}_4$, $\text{CsKNa}_2\text{Li}_8\{\text{Li}[\text{SiO}_4]\}_4$, $\text{RbNa}_3\text{Li}_8\{\text{Li}[\text{SiO}_4]\}_4$ [1] und $\text{RbNaLi}_4\{\text{Li}[\text{SiO}_4]\}_2$ [2]. *Z. Anorg. Allg. Chem.* **1994**, *620*, 1495–1508.
- (25) Wagatha, P.; Weiler, V.; Schmidt, P. J.; Schnick, W., Tailoring Emission Characteristics: Narrow-Band Red Luminescence from SLA to $\text{CaBa}[\text{Li}_2\text{Al}_6\text{N}_8]:\text{Eu}^{2+}$. *Chem. Mater.* **2018**, *30*, 7885–7891.

7. Summary

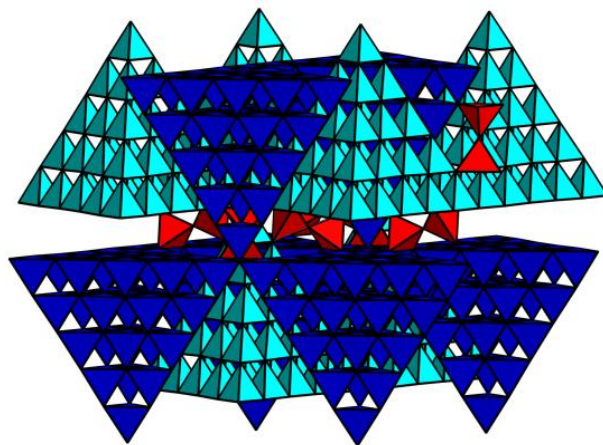
Central objective of research behind this dissertation was the discovery of novel narrow-band red emitting phosphors for potential application in solid-state lighting devices. Of special interest in this context was the materials class of nitridoaluminates, representatives of which had previously shown highly promising properties. In the line of this work, three further novel nitridoaluminate phosphors were discovered and thoroughly investigated.

$\text{Ca}_{18.75}\text{Li}_{10.5}[\text{Al}_{39}\text{N}_{55}]:\text{Eu}^{2+}$ —Supertetrahedron Phosphor for Solid-State Lighting

Peter Wagatha, Philipp Pust, Volker Weiler, Angela S. Wochnik, Peter J. Schmidt, Christina Scheu and Wolfgang Schnick

Chem. Mater. **2016**, *28*, 1220–1226

Representatives of the solid solution series $\text{Ca}_{(20-x)}\text{Li}_{(8+2x)}[\text{Al}_{39}\text{N}_{55}]:\text{Eu}^{2+}$ are presented in this research article. The title compound's characterization regarding its chemical composition, crystal structure and morphology as well as its physical properties is reported on. Materials with the compositions $\text{Ca}_{20}\text{Li}_8[\text{Al}_{39}\text{N}_{55}]:\text{Eu}^{2+}$



($x = 0$), $\text{Ca}_{18.75}\text{Li}_{10.5}\text{Al}_{39}\text{N}_{55}:\text{Eu}^{2+}$ ($x = 1.25$) and $\text{Ca}_{18}\text{Li}_{12}[\text{Al}_{39}\text{N}_{55}]:\text{Eu}^{2+}$ ($x = 2$) were obtained by a novel heterogenous high-temperature/high-pressure reaction in a hot isostatic press. Here, the metal hydrides and nitrides with EuF_3 as dopant in the respective stoichiometric amounts were reacted for 5 hours at a temperature of 1250 °C and a nitrogen pressure of 51.7 MPa. The compound crystallizes homeotypically with the oxomanganate $\text{Na}_{26}\text{Mn}_{39}\text{O}_{55}$ in the cubic space group $Fd\bar{3}m$ (no. 227) with $a = 22.415(3)$ Å and $V = 11263(2)$ Å³. Optical luminescence properties of different representatives of the solid solution are correlated with

7. Summary

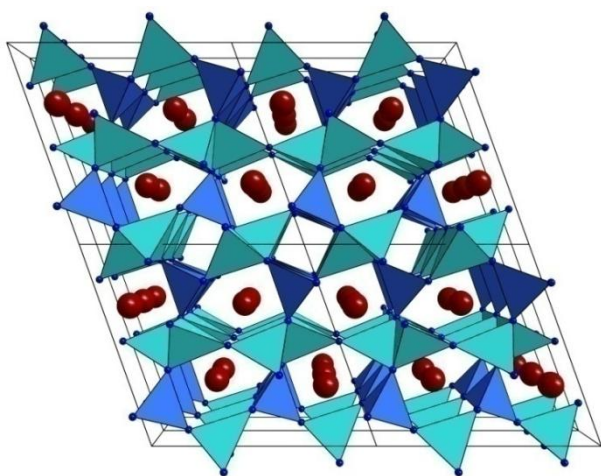
motifs of the T_5 supertetrahedra containing crystal structure and compared to other nitridic phosphors. $\text{Ca}_{(20-x)}\text{Li}_{(8+2x)}[\text{Al}_{39}\text{N}_{55}]:\text{Eu}^{2+}$ exhibits exceptional narrow-band red luminescence ($\lambda_{\text{max}} = 640\text{--}648\text{ nm}$; $\text{fwhm} \approx 1280\text{ cm}^{-1}$) despite multiple activator sites and two distinct excitation bands in the near UV and blue–green spectral region, respectively. Thermal behavior of the emission exhibits slight improvements with increasing Li content of the samples. In consequence, narrow-band red luminescence is shown not to be limited to UCr_4C_4 -type phases, and $\text{Ca}_{(20-x)}\text{Li}_{(8+x)}[\text{Al}_{39}\text{N}_{55}]:\text{Eu}^{2+}$ could be a key material to comprehending the principles of narrow-band Eu^{2+} luminescence.

Tunable Red Luminescence in Nitridomagnesoaluminates

$\alpha\text{-Sr}_2[\text{MgAl}_5\text{N}_7]:\text{Eu}^{2+}$, $\beta\text{-Sr}_2[\text{MgAl}_5\text{N}_7]:\text{Eu}^{2+}$, and $\text{Sr}_8[\text{LiMg}_2\text{Al}_{21}\text{N}_{28}]:\text{Eu}^{2+}$

Peter Wagatha, Volker Weiler, Peter J. Schmidt and Wolfgang Schnick

Chem. Mater. **2018**, *30*, 1755–1761



Solid-state lighting phosphors $\text{Sr}_8[\text{Li}_{(2-0.5x)}\text{Mg}_x\text{Al}_{(22-0.5x)}\text{N}_{28}]:\text{Eu}^{2+}$ ($x = 0\text{--}4$) of the class of nitrido(litho)-magnesoaluminates crystallizing homeotypic with oxozincate $\text{K}_2\text{Zn}_6\text{O}_7$ in orthorhombic space group $Pn\bar{m}$ (no. 58) with unit cell parameters $a = 10.4291(7)\text{--}10.54878(6)$, $b = 10.4309(7)\text{--}10.48253(6)$, $c = 3.2349(2)\text{--}3.27275(2)\text{ \AA}$ and

$V = 351.9(2)\text{--}361.894(3)$ were obtained by a newly established heterogenous high-temperature/high-pressure reaction in a hot isostatic press. Starting from the metals, hydrides and nitrides in the respective stoichiometric amounts with Eu_2O_3 as dopant, representatives of the title solid solution series $\alpha\text{-Sr}_2[\text{MgAl}_5\text{N}_7]:\text{Eu}^{2+}$, ($x = 4$) and $\text{Sr}_8[\text{LiMg}_2\text{Al}_{21}\text{N}_{28}]:\text{Eu}^{2+}$ ($x = 2$) were investigated. The narrow-band red luminescence of these materials is tunable in the range of $\lambda_{\text{max}} = 633\text{--}665\text{ nm}$ and $\text{fwhm} = 1736\text{--}1964\text{ cm}^{-1}$ by adjusting the composition as well as the activator concentration. Partial disorder on the

network cation sites impacts the band width of the emission compared to other narrow-band red emitting nitridoaluminates or -silicates. Thermal behavior of the emission is promising with only moderate thermal quenching that can additionally be influenced by adjusting the band gap of the material via the chemical composition. A second polytype β - $\text{Sr}_2[\text{MgAl}_5\text{N}_7]:\text{Eu}^{2+}$ crystallizing in monoclinic space group $C2/m$ (no. 12) with unit cell parameters $a = 11.12874(11)$, $b = 3.27289(3)$, $c = 10.54530(11)$ Å, $\beta = 109.8939(7)^\circ$ and $V = 361.173(7)$ Å³ was observed for $x = 4$ with a phase fraction of ≈ 40 wt % and its crystal structure solved and refined from powder X-ray diffraction data. Luminescence of the β -phase was either not observed, or is identical to the α -phase. Similar to ultra-narrow emitting $\text{Sr}[\text{LiAl}_3\text{N}_4]:\text{Eu}^{2+}$ the title compounds' activator position is coordinated cube-like, with the emission fwhm here broadened due to statistical disorder on some network cation sites comparable to $(\text{Ca}/\text{Sr})[\text{Mg}_2\text{Al}_2\text{N}_4]\text{Eu}^{2+}$. It's overall luminescence properties make the solid-solution series $\text{Sr}_8[\text{Li}_{(2-0.5x)}\text{Mg}_x\text{Al}_{(22-0.5x)}\text{N}_{28}]:\text{Eu}^{2+}$ ($x = 0-4$) a highly promising material for application in illumination grade white LEDs.

Narrow-Band Red Luminescence in Nitridolithoaluminate $\text{CaBa}[\text{Li}_2\text{Al}_6\text{N}_8]:\text{Eu}^{2+}$

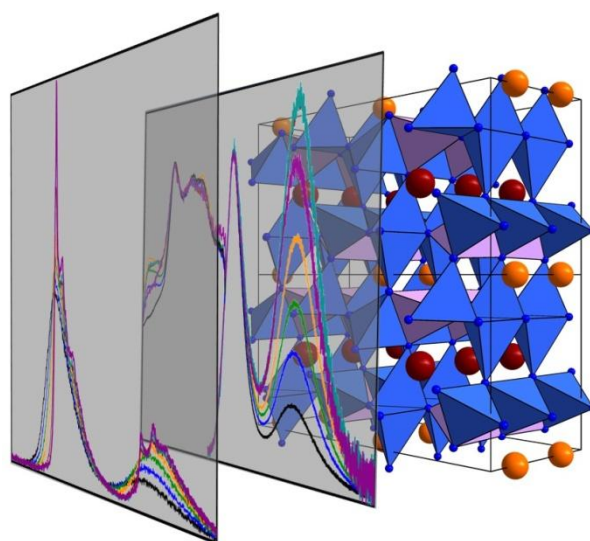
Peter Wagatha, Volker Weiler, Peter J. Schmidt and Wolfgang Schnick

Chem. Mater. **2018**, *30*, 7885–7891

Tunable narrow-band red emitting $\text{CaBa}[\text{Li}_2\text{Al}_6\text{N}_8]:\text{Eu}^{2+}$ was synthesized by reaction of the metal hydrides and nitrides in a hot isostatic press via a heterogenous high-temperature/high-pressure reaction. The compound crystallizes in the monoclinic space group $C2/m$ (no. 12) with unit cell parameters

$$a = 16.0851(2) \text{ \AA},$$

$$b = 6.46738(4) \text{ \AA},$$

$$c = 8.04242(13) \text{ \AA},$$


7. Summary

$\beta = 90.004(2)^\circ$ and $V = 836.64(2) \text{ \AA}^3$ and exhibits intense luminescence upon irradiation with blue light. Two emission maxima at $\lambda_{\text{max}}(1) \approx 637 \text{ nm}$ and $\lambda_{\text{max}}(2) \approx 790 \text{ nm}$ can be observed and assigned to emission of Eu^{2+} occupying the cube-like coordinated Ba- and Ca-sites, respectively. Both emission bands are extremely narrow with $\text{fwhm}(1) = 1095\text{--}1266 \text{ cm}^{-1}$ being the narrowest red Eu^{2+} emission observed to date and $\text{fwhm}(2) \approx 1450 \text{ cm}^{-1}$. The red emission from Eu occupying the Ba site is nearly optimal for use in WLEDs combining outstanding color rendition, excellent luminous efficacy and extraordinary thermal stability. Its thermal quenching behavior with $\text{QE}_{\text{rel}}(500 \text{ K}) \approx 95 \%$ rivals that of $\text{Sr}[\text{LiAl}_3\text{N}_4]:\text{Eu}^{2+}$. The infrared emission intensity from Eu occupying the Ca site can be limited by reducing the activator concentration. Low-temperature luminescence spectra reveal a significantly smaller mean phonon energy on the Ba site, correlated with weaker electron-phonon coupling. Huang-Rhys factors < 1 for the Ba site and $\approx 1.5\text{--}2$ for the Ca site indicate a strong relaxation of the $\text{Eu}^{2+} 4f^65d$ excited state on the smaller Ca site. On the basis of the rigid network structure of LiN_4 and AlN_4 tetrahedra and the material's outstanding luminescence properties, $\text{CaBa}[\text{Li}_2\text{Al}_6\text{N}_8]:\text{Eu}^{2+}$ could play a key role in the development of nearly optimal narrow-band phosphors.

8. Appendix

Supporting Information for $\text{Ca}_{18.75}\text{Li}_{10.5}[\text{Al}_{39}\text{N}_{55}]:\text{Eu}^{2+}$ — Supertetrahedron Phosphor for Solid-State Lighting

Table S8.1: Atomic Coordinates and Isotropic Displacement Parameters of $\text{Ca}_{18.75}\text{Li}_{10.5}[\text{Al}_{39}\text{N}_{55}]^a$

atom	Wyckoff	x	y	z	$U_{\text{eq}} / \text{\AA}^2$	sof
Ca1	96h	0.101327(18)	0.398673(18)	0	0.01111(14)	1
Ca2	48f	0.20520(3)	3/8	-1/8	0.01019(16)	1
Ca3	16d	0	1/2	0	0.0140(7)	0.38
Al1	8b	1/8	5/8	1/8	0.0070(5)	1
Al2	96g	0.02747(2)	0.52747(2)	0.12590(4)	0.00701(17)	1
Al3	32e	0.32399(4)	0.42601(4)	-0.07399(4)	0.0071(3)	1
Al4	48f	0.06975(5)	3/8	-1/8	0.0075(2)	1
Al5	96g	0.07175(4)	0.27368(2)	-0.02368(2)	0.00713(18)	1
Al6	32e	0.29658(3)	0.29658(3)	-0.04658(3)	0.0071(3)	1
N1	16c	1/4	1/4	0	0.0088(11)	1
N2	32e	0.07637(10)	0.57637(10)	0.17363(10)	0.0068(7)	1
N3	8a	3/8	3/8	-1/8	0.0091(15)	1
N4	96g	0.02257(10)	0.42525(7)	-0.07475(7)	0.0082(4)	1
N5	96g	0.02342(7)	0.22658(7)	-0.07569(10)	0.0078(4)	1
N6	96g	0.27561(7)	0.47439(7)	-0.12321(10)	0.0084(4)	1
N7	96g	0.11970(10)	0.32479(7)	-0.07479(7)	0.0084(4)	1
Li1	96g	0.3152(6)	1/4	0.0652(6)	0.026(6)	0.44(3)
Li2	192i	0.3226(13)	0.2322(14)	0.0438(11)	0.026(6)	0.218(13)

^a e.s.d.s in parentheses

8. Appendix

Table S8.2: Anisotropic Displacement Parameters (\AA^2) of $\text{Ca}_{18.75}\text{Li}_{10.5}[\text{Al}_{39}\text{N}_{55}]^a$

atom	U11	U22	U33	U12	U13	U23
Ca1	0.01160(18)	0.01160(18)	0.0101(3)	-0.00062(13)	-0.00062(13)	-0.0019(2)
Ca2	0.0065(3)	0.0120(2)	0.0120(2)	0.0037(3)	0	0
Ca3	0.0140(7)	0.0140(7)	0.0140(7)	0.0003(8)	0.0003(8)	0.0003(8)
Al1	0.0070(5)	0.0070(5)	0.0070(5)	0	0	0
Al2	0.0072(2)	0.0072(2)	0.0067(4)	0.0000(2)	0.0000(2)	0.0001(3)
Al3	0.0071(3)	0.0071(3)	0.0071(3)	-0.0001(3)	0.0001(3)	0.0001(3)
Al4	0.0075(5)	0.0075(3)	0.0075(3)	-0.0004(4)	0	0
Al5	0.0075(4)	0.0070(2)	0.0070(2)	-0.0004(3)	0.0001(2)	-0.0001(2)
Al6	0.0071(3)	0.0071(3)	0.0071(3)	0.0002(3)	0.0002(3)	-0.0002(3)
N1	0.0088(11)	0.0088(11)	0.0088(11)	0.0026(11)	0.0026(11)	-0.0026(11)
N2	0.0068(7)	0.0068(7)	0.0068(7)	0.0002(8)	0.0002(8)	-0.0002(8)
N3	0.0091(15)	0.0091(15)	0.0091(15)	0	0	0
N4	0.0090(11)	0.0078(6)	0.0078(6)	0.0010(8)	-0.0002(6)	-0.0002(6)
N5	0.0079(6)	0.0079(6)	0.0076(10)	-0.0001(6)	0.0001(6)	-0.0001(8)
N6	0.0090(7)	0.0090(7)	0.0072(11)	-0.0004(6)	0.0004(6)	0.0017(8)
N7	0.0085(10)	0.0085(6)	0.0085(6)	0.0024(8)	0.0003(6)	-0.0003(6)
Li1	0.019(6)	0.042(15)	0.019(6)	0.000(7)	-0.008(8)	0.000(7)
Li2	0.019(6)	0.042(15)	0.019(6)	0.000(7)	-0.008(8)	0.000(7)

^a e.s.d.s in parentheses

Table S8.3: Selected Bond Lengths (Å) in $\text{Ca}_{18.75}\text{Li}_{10.5}[\text{Al}_{39}\text{N}_{55}]^{\text{a}}$

bond name	bond length / Å
Ca1–N7	2.3923(6)
Ca1–N4	2.5057(18)
Ca2–N7	2.491(2)
Ca2–N6	2.7305(7)
Ca3–N4	2.423(2)
Al1–N2	1.888(4)
Al2–N4	1.9226(15)
Al2–N5	1.944(2)
Al3–N6	1.889(2)
Al3–N3	1.9805(14)
Al4–N4	1.912(2)
Al4–N7	1.946(2)
Al5–N5	1.9098(15)
Al5–N7	1.944(2)
Al6–N1	1.8086(14)
Al6–N6	1.917(2)
Li1–N6	2.526(4)
Li1–N7	2.233(10)
Li2–N1	1.94(3)
Li2–N6	2.20(3)
Li2–N7	1.95(3)
Ca1–Li1	2.646(19)
Ca1–Li2	2.93(3)
Ca1–Al5	2.9277(7)
Ca2–Al3	3.1152(8)
Ca3–Al2	2.9535(9)
Al5–Li1	2.751(8)
Al5–Li2	2.42(3)
Al6–Li2	2.55(3)

^a e.s.d.s in parentheses

Table S8.4: Crystallographic Data of the Rietveld Refinement of $\text{Ca}_{18.75}\text{Li}_{10.5}[\text{Al}_{39}\text{N}_{55}]^{\text{a}}$

Formula	$\text{Ca}_{18.75}\text{Li}_{10.5}[\text{Al}_{39}\text{N}_{55}]^{\text{a}}$
crystal system	cubic
space group	$Fd\bar{3}m$ (no. 227)
lattice parameters / Å	$a = 22.3611(2)$
cell volume / Å ³	11180(1)
formula units / unit cell	8
density / g·cm ⁻³	3.147
linear absorption coefficient / mm ⁻¹	40
radiation	Cu-K _α ($\lambda = 1.540596$ nm)
monochromator	Ge(111)
diffractometer	Huber G670
detector	imaging plate
program used	TOPAS academic
profile function	fundamental parameters
background function	shifted Chebyshev (30 parameters)
R_{wp}	3.390
R_{p}	2.375
χ^2	1.641

^a e.s.d.s in parentheses

9. Publications

List of Publications within this Thesis

Ca_{18.75}Li_{10.5}[Al₃₉N₅₅]:Eu²⁺—Supertetrahedron Phosphor for Solid-State Lighting

Peter Wagatha, Philipp Pust, Volker Weiler, Angela S. Wochnik, Peter J. Schmidt, Christina Scheu and Wolfgang Schnick

Chem. Mater. **2016**, 28, 1220–1226, DOI: 10.1021/acs.chemmater.5b04929

In this article high-pressure / high-temperature syntheses, structure elucidation from single-crystal X-ray diffraction data and Rietveld refinement of powder X-ray diffraction data were carried out by Philipp Pust and partly Peter Wagatha. Literature research and writing of the main part of the manuscript was done by Peter Wagatha and partly Philipp Pust. Luminescence excitation- and emission spectra as well as temperature dependent emission spectra were carried out by Volker Weiler and supervised by Peter J. Schmidt. EELS measurements were carried out by Angela S. Wochnik and supervised by Christina Scheu. Graphical material was created by Philipp Pust and Peter Wagatha. Wolfgang Schnick supervised and directed the research project. Peter J. Schmidt and Peter Wagatha revised the manuscript.

Tunable Red Luminescence in Nitridomagnesoaluminates α -Sr₂[MgAl₅N₇]:Eu²⁺, β -Sr₂[MgAl₅N₇]:Eu²⁺, and Sr₈[LiMg₂Al₂₁N₂₈]:Eu²⁺

Peter Wagatha, Volker Weiler, Peter J. Schmidt and Wolfgang Schnick

Chem. Mater. **2018**, 30, 1755–1761, DOI: 10.1021/acs.chemmater.8b00106

The manuscript of this contribution was written by Peter Wagatha, also responsible for literature screening, crystal structure elucidation from powder X-ray diffraction data, Rietveld refinement, REM/EDX measurements and graphical materials. Relevant syntheses of the title compounds, as well as luminescence measurements were carried out by Volker Weiler and supervised by Peter J. Schmidt. The research project was directed and supervised by Wolfgang Schnick. Peter J. Schmidt and Peter Wagatha revised the manuscript.

9. Publications

Tailoring Emission Characteristics: Narrow-Band Red Luminescence from SLA to CaBa[Li₂Al₆N₈]:Eu²⁺

Peter Wagatha, Volker Weiler, Peter J. Schmidt and Wolfgang Schnick

Chem. Mater. **2018**, *30*, 7885–7891, DOI: 10.1021/acs.chemmater.8b03485

For this contribution Peter Wagatha wrote the manuscript and performed the crystal structure determination from powder X-ray diffraction data, Rietveld refinement, REM/EDX measurements as well as literature research and graphical materials. Relevant syntheses of the title compound were done by Volker Weiler who also carried out luminescence measurements under the supervision of Peter J. Schmidt. Wolfgang Schnick directed and overall supervised the research project. The manuscript was revised by Peter J. Schmidt and Peter Wagatha.

Other Publications

Toward New Phosphors for Application in Illumination-Grade White pc-LEDs: The Nitridomagnesosilicates Ca[Mg₃SiN₄]:Ce³⁺, Sr[Mg₃SiN₄]:Eu²⁺, and Eu[Mg₃SiN₄]

Sebastian Schmiechen, Hajnalka Schneider, Peter Wagatha, Cora Hecht, Peter J. Schmidt, Wolfgang Schnick

Chem. Mater. **2014**, *26*, 2712–2719

Model for Hydrothermal Growth of Rutile Wires and the Associated Development of Defect Structures

Andreas Wisnet, Sophia B. Betzler, Rachel V. Zucker, James A. Dorman, Peter Wagatha, Sonja Matich, Eiji Okunishi, Lukas Schmidt-Mende, Christina Scheu

Cryst. Growth Des. **2014**, *14*, 4658–4663

Structural Features and Physical Properties of InBi₂Se₄I, and BiSeI

Tobias Rosenthal, Markus Döblinger, Peter Wagatha, Christian Gold, Ernst-Wilhelm Scheidt, Wolfgang Scherer, Oliver Oeckler

Z. Anorg. Allg. Chem. **2011**, *637*, 2239–2245

Conference Contributions

Luminescent Materials—Light Conversion for pc-LEDs (talk)

Peter Wagatha and Wolfgang Schnick

1. Obergurgl-Seminar Festkörperchemie, Obergurgl (Austria), January 28–31, 2014

HIP to be Square Cubic—The Rocky Road to Nitridoaluminates (talk)

Peter Wagatha and Wolfgang Schnick

2. Obergurgl-Seminar Festkörperchemie, Obergurgl (Austria), January 26–29, 2016

Investigations of the Luminescence Properties of SLA:Eu codoped with Cu (poster presentation)

Martin Obermeier, Peter Wagatha and Wolfgang Schnick

Undergraduate Research Conference on Molecular Science (URCUP), Kloster Irsee (Germany), July 2–3, 2016

Structure and Luminescence Properties of $\text{Ca}_{(20-x)}\text{Li}_{(8+2x)}[\text{Al}_{39}\text{N}_{55}]:\text{Eu}^{2+}$ (poster presentation)

Peter Wagatha, Philipp Pust, Peter J. Schmidt and Wolfgang Schnick

18. Vortragstagung Fachgruppe Festkörperchemie und Materialforschung, Innsbruck (Austria), September 19–21, 2016

Deposited Crystallographic Data

Material	Deposition Number
$\text{Ca}_{18.75}\text{Li}_{10.5}[\text{Al}_{39}\text{N}_{55}]:\text{Eu}^{2+}$	CSD-430639
$\beta\text{-Sr}_2[\text{MgAl}_5\text{N}_7]:\text{Eu}^{2+}$	CCDC-1813230
$\text{CaBa}[\text{Li}_2\text{Al}_6\text{N}_8]:\text{Eu}^{2+}$	CCDC-1860700